Cross-reactivity between tumor MHC class I-restricted antigens and an enterococcal bacteriophage

Aurélie Fluckiger, Romain Daillere, Mohamed Sassi, Barbara S Sixt, Peng Liu, Friedemann Loos, Corentin Richard, Catherine Rabu, Maryam Tidjani, Anne-Gaëlle Goubet, et al.

Title: Crossreactivity between MHC class I-restricted antigens from cancer cells and an enterococcal bacteriophage.

Authors: Aurélie Fluckiger[1-3], Romain Daillère[1-3], Mohamed Sassi[4], Barbara Susanne Sixt[5,6-10], Peng Liu[6-10], Friedemann Loos[6-10], Corentin Richard[11-13], Catherine Rabu[17,18], Maryam Tidjani Alou[1,2,14], Anne-Gaëlle Goubet[1,2], Fabien Lemaitre[1], Gladys Ferrere[1,2] , Lisa Derosa[1,2,14], Connie PM Duong[1,2], Meriem Messaoudene[15], Andréanne Gagné[15], Philippe Joubert[15], Luisa De Sordi[16], Laurent Debarbieux[16], Sylvain Simon[17,18], Clara-Maria Scarlata[19], Maha Ayyoub[19], Belinda Palermo[20], Francesco Facciolo[21], Romain Boidot[22], Richard Wheeler[23], Ivo Gomperts Boneca[23], Zsofia Sztupinszki[24], Krisztian Papp[25], Istvan Csabai[25], Edoardo Pasolli[26], Nicola Segata[27], Carlos Lopez-Otin[7-10,28], Zoltan Szallasi[24,29-31], Fabrice Andre[32,33], Valerio Iebba[34], Valentin Quiniou[35,36], David Klatzmann[35,36], Jacques Boukhalil[37], Saber Khelaifia[37], Didier Raoult[37], Laurence Albiges[1,14,38], Bernard Escudier[1,38,39], Alexander Eggermont[1-14], Fathia Mami-Chouaib[40], Paola Nistico[20], François Ghiringhelli[41], Bertrand Routy[15,42], Nathalie Labarrière[17,18], Vincent Cattoir[4,43,44], Guido Kroemer[6-10,45,46,47]*, and Laurence Zitvogel[1-3,14,47]*

Affiliations:

[1] Gustave Roussy Cancer Campus (GRCC), Villejuif, France.

[2] Institut National de la Santé et de la Recherche Médicale, U1015, Institut Gustave Roussy, Villejuif, France

[14] Université Paris-Saclay, Villejuif, F-94805, France.

[3] Center of Clinical Investigations in Biotherapies of Cancer (CICBT) 1428, Villejuif, France.

[4] Université Rennes 1, Laboratoire de Biochimie Pharmaceutique, Inserm U1230 - UPRES EA 2311, Rennes, France.

[5] Laboratory for Molecular Infection Medicine Sweden, Umeå Centre for Microbial Research, Department of Molecular Biology, Umeå University, 90187, Umeå, Sweden.

[6] Cell Biology and Metabolomics Platforms, Gustave Roussy Cancer Campus, Villejuif, France.

[7] Equipe 11 labellisée Ligue contre le Cancer, Centre de Recherche des Cordeliers, Paris, France

[8] INSERM U1138, Paris, France.

[9] Université de Paris, Paris, France

[10] Sorbonne Université, Paris, France.

[11] Research Platform in Biological Oncology, Dijon, France.

[12] GIMI Genetic and Immunology Medical Institute, Dijon, France.

[13] University of Burgundy-Franche Comté, Dijon, France.

[15] Centre de recherche du centre hospitalier de l'université de Montréal (CRCHUM), 900 rue Saint-Denis, H2X 3H8 Montréal, Québec, Canada.

[16] Department of Microbiology, Institut Pasteur, F-75015 Paris, France

[17] CRCINA, INSERM, Université d'Angers, Université de Nantes, Nantes, France.

[18] LabEx IGO "Immunotherapy, Graft, Oncology," Nantes, France.

[19] Cancer Research Centre of Toulouse, INSERM UMR 1037, 31037 Toulouse, France; Université Toulouse III Paul Sabatier, 31330 Toulouse, France; Institut Universitaire du Cancer de Toulouse-Oncopole, 31100 Toulouse, France.

[20] Unit of Tumor Immunology and Immunotherapy, Department of Research, Advanced Diagnostics and Technological Innovation, IRCCS Regina Elena National Cancer Institute, Rome, Italy.

[21] Thoracic Surgery Unit, Department of Surgical Oncology, IRCCS Regina Elena National Cancer Institute, Rome, Italy.
[22] Unit of Molecular Biology - Department of Biology and Pathology of Tumors - Georges-François Leclerc anticancer center - UNICANCER - Dijon – France
[23] Institut Pasteur, Unit Biology and genetics of the bacterial cell wall, Paris, France
[24] Computational Health Informatics Program (CHIP), Boston Children's Hospital, Boston, MA, USA.
[25] Department of Physics of Complex Systems, ELTE Eötvös Loránd University, Budapest, Hungary.
[26] Department of Agricultural Sciences, University of Naples Federico II, Naples, Italy
[27] Department CIBIO, University of Trento, Trento, Italy.
[28] Dpto. de Bioquímica y Biología Molecular, Instituto Universitario de Oncología (IUOPA), Universidad de Oviedo, Oviedo, Spain.
[29] Harvard Medical School, Boston, MA, USA.
[30] Danish Cancer Society Research Center, Copenhagen, Denmark.
[31] MTA-SE-NAP, Brain Metastasis Research Group, 2nd Department of Pathology, Semmelweis University, Budapest, Hungary.
[32] Department of Cancer Medicine, Breast Cancer Committee, Gustave Roussy, Villejuif, France.
[33] INSERM Unit 981, Gustave Roussy, Villejuif, France.
[34] Department of Public Health and Infectious Diseases, Section of Microbiology, Sapienza University of Rome, Rome 00185, Italy.
[35] AP-HP, Hôpital Pitié-Salpêtrière, Clinical Investigation Center in Biotherapy (CIC-BTi) and Immunology-Inflammation-Infectiology and Dermatology Department (3iD), F-75651, Paris, France
[36] Sorbonne Université, INSERM, Immunology-Immunopathology-Immunotherapy (i3), F-75651,Paris, France
[37] URMITE, Aix Marseille Université, UM63, CNRS 7278, IRD 198, INSERM 1095, IHU-Méditerranée Infection, 13005 Marseille, France.
[38] Department of Medical Oncology, Gustave Roussy, Villejuif, France.
[39] INSERM U981, GRCC, Villejuif, France.
[40] INSERM UMR 1186, Integrative Tumour Immunology and Genetic Oncology, Gustave Roussy, EPHE, PSL, Faculté de Médecine, Université Paris-Sud, Université Paris-Saclay, Villejuif, France.
[41] Department of Medical Oncology, Center GF Leclerc, Dijon, France.
[42] Division d'hémato-oncologie, département de médicine, centre hospitalier de l'université de Montréal (CHUM), Montréal, Québec, Canada.
[43] CHU de Rennes - Hôpital Ponchaillou, Service de Bactériologie-Hygiène hospitalière, Rennes, France.
[44] CNR de la Résistance aux Antibiotiques (laboratoire associé 'Entérocoques'), Rennes, France.
[45] Pôle de Biologie, Hôpital Européen Georges Pompidou, Assistance Publique–Hôpitaux de Paris, Paris, France
[46] Department of Women's and Children's Health, Karolinska University Hospital, 1 Stockholm, Sweden.
[47] Suzhou Institute for Systems Biology, Chinese Academy of Medical Sciences, Suzhou, China

*Correspondence to: laurence.zitvogel@gustaveroussy.fr; kroemer@orange.fr

One sentence summary:

Cytotoxic T lymphocytes that recognize antigens from a prophage of a commensal enterococcus can mediate anticancer immunosurveillance by recognizing cross-reactive tumor-associated antigens.

Abstract:

It has been speculated that the intestinal microbiota induces commensal-specific memory T cells that then cross-react with tumor-associated antigens. Here, we identified MHC class I-binding epitopes within the tail length tape measure protein (TMP) of a prophage found in the genome of *Enterococcus hirae*. Mice bearing *E. hirae* strains harboring this prophage mounted a TMP-specific H-2K^{b} restricted CD8^{+} T lymphocyte response upon immunotherapy with cyclophosphamide or anti-PD1 antibodies. Such TMP-specific T cells also recognized a 78%-identical H-2K^{b}-binding peptide derived from the proteasome (20S) subunit beta type-4 (PSMB4), allowing them to control mouse tumors expressing this oncogenic driver. Administration of bacterial strains engineered to express the TMP epitope improved the outcome of immunotherapy. Tumors bearing PSMB4 knock-in mutations that abolish crossreactivity with TMP became immunotherapy-resistant. In renal and lung cancer patients, the presence of the enterococcal prophage in stools, as well as the expression of a TMP-cross reactive antigen by tumors, predicted the long-term benefit of PD-1 blockade. In melanoma patients, we detected T cell clones recognizing naturally processed cancer antigens that are cross-reactive with microbial peptides. Altogether, these results support the idea that intestinal microbe-specific T cell responses contribute to anticancer immunosurveillance.

Main Text:

Unleashing immune responses against tumor-associated antigens through chemotherapy, radiotherapy, targeted therapies or immune checkpoint inhibitors has become the mainstay of successful cancer treatments (*1, 2*). The recent discovery that the gut microbiota determines the cancer-immune set point, thus influencing the clinical outcome of antineoplastic therapies, has rekindled the concept that microbes or their products modulate not only intestinal but also systemic immunity (*3, 4*). Indeed, memory responses by interferon-γ (IFNγ) secreting $CD4^+$ and $CD8^+$ T cells specific for *Enterococcus hirae, Bacteroides fragilis,* and *Akkermansia muciniphila* are associated with favorable clinical outcome in cancer patients (*5–8*), suggesting that microbe-specific T lymphocytes may contribute to antitumor immune responses. The mechanisms through which microbes trigger chronic intestinal inflammation and systemic autoimmune disease have not been resolved (*9*). The theory of molecular mimicry (*10–14*) posits that T cells elicited by bacteria or viruses accidentally recognize autoantigens as they 'escape' from self-tolerance inducing mechanisms (such as clonal deletion or inactivation). While MHC class I and class II binding epitopes encoded by bacterial genomes may be immunogenic (*10–14*), very few reports have demonstrated that microbe-specific $CD4^+$ or $CD8^+$ T lymphocytes attack normal or neoplastic tissues (*15–17*).

Cyclophosphamide (CTX) induces the translocation of *E. hirae* from the gut lumen to the mesenteric and splenic immune tissues, thereby eliciting specific $CD4^+$ and $CD8^+$ T lymphocytes producing interleukin-17 (IL17) and interferon-γ (IFNγ), correlating with therapeutically effective anticancer immune responses (*6, 18*). Broad-spectrum antibiotics abolished the therapeutic efficacy of CTX unless *E. hirae* was supplied by oral gavage (*6*). When comparing a panel of distinct *E. hirae* strains (Table S1, Figure S1A) for their capacity to restore the antibiotic-perturbed anticancer effects of CTX, we found that only a few *E. hirae* isolates (such as 13144 and IGR11) were efficient (Figure 1A-B, Ref. (*6*)). Given that the therapeutic efficacy of the combination of CTX and *E. hirae* 13144 is abrogated by the depletion of $CD8^+$ T cells or the neutralization of IFNγ (*6*), we screened the differential capacity of *E. hirae* strains to elicit memory T cell responses after priming of the host, measured as the *ex vivo* recall response (IFNγ secretion) of splenic $CD8^+$ T cells against various *E. hirae* strains loaded onto dendritic cells

(DC) (Figure S2A). While *E. hirae* 13144 triggered specific $CD8^+$ T cell responses (that were not cross-reactive against irrelevant enterococci), *E. hirae* 708 and 13344 (two prototypic inefficient strains) (*6*) failed to do so (Figure S2A).

To identify relevant T cell epitopes, we aligned the sequences of bacterial genes encoding putative cell wall and secreted proteins for immunogenic (13144) *versus* non-immunogenic (708 and 13344) *E. hirae* strains, followed by the in silico identification of 13144-specific nonapeptides with strong affinity (<50 nM) for the MHC class I H-$2K^b$ protein (Table S2). Subsequently, we recovered splenic $CD8^+$ T cells from mice that had been exposed to *E. hirae* 13144 and CTX (Figure 1C), restimulated them *in vitro* with pools of potentially immunogenic nonapeptides from *E. hirae* 13144 to measure IFNγ production (Table S2, Figure S2B) and finally split the most efficient pool (No. 7) into individual peptides (Figure 1D). This approach led to the identification of one dominant epitope (one-letter amino acid [aa] code: TSLARFANI, abbreviation TMP1) in position 187 to 197 of the aa sequence of the phage tail length tape measure protein (TMP, 1506 aa) from a 39.2 kb prophage of *E. hirae* 13144 (Figure 1D, Figure S3, Tables S2-S3). The 39.2kb prophage encodes 65 genes, including one shared between all 18 *E. hirae* genomes and 38 unique to *E. hirae* 13144 (Figure S1B), encoding capsid, portal and tail structures characteristic of *Siphoviridae* phages. Importantly, the TMP1 epitope of the 39.2kb prophage from *E. hirae* 13144 and the prophage fragment contained in *E. hirae* IGR11 showed 100% sequence identity (Figure S3 and S4A). Accordingly, *E. hirae* IGR11 was as efficient as *E. hirae* 13144 in reducing the growth of MCA205 sarcomas treated with CTX (Figure 1A-B). In contrast, the absence of a *bona fide* TMP1 epitope (observed in *E. hirae* 708 and 13344, Figure S1B) and a mutation in position 3 of the TSLARFANI peptide (L→F observed in *E. hirae* ATCC9790, Figure S4A) correlated with the lack of anticancer effects of these *E. hirae* strains (Figure 1B and Ref. (*6*)). ELIspot assays designed to detect peptide-specific IFNγ-producing T cells revealed that mice gavaged with *E. hirae* 13144 or IGR11 mounted a $CD8^+$ T cell response against TMP1 (but not against the control peptides TMP2 and TMP3), while mice receiving *E. hirae* strains lacking TMP1 (strains 708, 13344) or a strain possessing a mutated TMP1 (strain ATCC9790) were unable to do so (Figure 1D). We used a fluorescent H-$2K^b$/TSLARFANI tetrameric complex (and its negative control H-$2K^b$/SIINFEKL binding to ovalbumine (OVA) specific $CD8^+$ T cells) to detect the frequency and distribution of TMP1-specific cytotoxic T

lymphocytes (CTLs) in naive and MCA205 sarcoma bearing C57BL/6 mice. We observed a specific increase in splenic $CD8^+$ T cells that recognized the TMP1 peptide (but not the OVA peptide SIINFEKL) at day 7 following treatment with CTX and gavage with *E. hirae* 13144 (Figure 1E), as well as in tumor draining lymph nodes (LN) of tumor bearers at day 14 after treatment with CTX and gavage with *E. hirae* 13144 (Figure S2C-D). Splenic TMP1 (but not OVA)-specific (H-$2K^b$/TSLARFANI tetramer-positive) CTLs also increased in their frequency after gavage with *E. hirae* IGR11 (but not 13344 nor ATCC9790) (Figure 1E). The H-$2K^b$/TSLARFANI tetramer-positive CTLs were specifically enriched in the $CXCR3^+CCR9^+$ fraction of $CD8^+$ T cells from secondary lymphoid organs (Figure S2C). Even in mice colonized with human fecal materials, CTX administration and oral gavage with *E. hirae* 13144 induced an anticancer effect (Figure S2E) and an expansion of H-$2K^b$/TSLARFANI tetramer-positive CTL in tumor draining LN at day 7 and in tumor beds at day 17 while vanishing from mesenteric LN (Figure S2F-H). Hence, immunogenic *E. hirae* elicits a H-$2K^b$ restricted CTL response against the TMP-derived peptide TMP1/TSLARFANI.

To explore the capacity of TMP1-specific H-$2K^b$ restricted T cells to control the growth of MCA205 cancers, we subcutaneously (s.c.) immunized naive C57BL/6 mice with dendritic cells (DC) loaded with heat-inactivated *E. hirae* 13144 (positive control), the naturally occurring TMP1/TSLARFANI peptide from 13144 and IGR11, its L→F mutant from *E. hirae* ATCC9790 ('mut3', Figure 2A, Figure S4A) or other non-immunogenic bacterial peptides (group 1, Figure S2B). In this prophylactic setting, DC pulsed with TMP1 (but not mut3) were as efficient as the whole *E. hirae* extract in reducing tumor growth (Figure 2B-C). Next, we explored whether the TMP1 peptide would be able to confer immunogenicity to the usually inefficient bacterium *Escherichia coli* strain DH5α in the therapeutic setting, in which antibiotic treatment is followed by gavage with different bacterial strains and CTX-based chemotherapy (Figure 1A and Ref. (*6*)). *E. coli* engineered to express TMP1 (Figure S5) was as efficient as *E. hirae* 13144 in restraining MCA205 tumor growth (Figure S4B, Figure 2D) and eliciting tetramer binding CTL in the spleen (Figure 2E). In contrast, *E. coli* expressing an irrelevant sequence (encoding mouse EGFP protein), mut3 or or mutant TMP1 bearing a S→A exchange in the anchor position 2 ('mut2') (Figure 2A) failed to induce such a cancer-protective immune response (Figure 2D-E).

To explore the mechanism by which TMP1 exerts its anticancer activity against MCA205 tumors in C57BL/6 mice, we investigated whether H-2K^b-restricted mouse tumor antigens with high identity to the TMP1 peptide (TSLARFANI) exist. Using the NCBI BLASTP suite, we found that the peptide (GSLARFRNI) belonging to the proteasome subunit beta type-4 (PSMB4) located at amino acid positions 76-84 shared a strong homology (7 out of 9 amino acids with identical amino acids at the MHC Class I anchoring positions 2 and 9) with TMP1 (Figure 3A). We queried for potential neoepitopes of MCA205 but found no significant homology with TMP1, prompting us to focus on the non-mutated PSMB4 peptide. In fact, some mouse tumors (such as MCA205 sarcomas and TC1 lung cancers) overexpress the PSMB4 antigen compared with their normal tissues of origin, while others (such as MC38 colon cancers) failed to do so (Figure 3B). This correlates with the fact that MCA205 and TC1 tumors respond to the treatment with CTX+*E. hirae* 13144, while MC38 cancer does not (Figure S6A-B). PSMB4 is an oncogenic driver involved in proliferation and invasion (*19*) in a variety of malignancies such as glioblastoma (*20*), melanoma (*21*) and breast cancers (*22*), associated with dismal prognosis (*19*, *20*, *22*). CRISPR/Cas9-mediated genomic knock-in of the PSMB4 sequence replacing GSLARFRNI by GALARFRNI (with an S→A exchange in position 2) or GSFARFRNI (with an L→F exchange in position 3 equivalent to mut 3 of TSLARFANI) in MCA205 cells (Figure S7) significantly affected tumor growth kinetics (Figure S6C-D), suggesting that this PSMB4 epitope contributes to the oncogenic activity of PSMB4. While these knock-in mutations did not interfere with the efficacy of CTX treatment alone, they drastically blunted the anticancer effects of *E. hirae* 13144 (Figure 3C-D). We extended these findings to a second tumor model where the anticancer effects of the combination of CTX+*E. hirae* 13144 were additive even in the absence of antibiotic-induced dysbiosis. Introducing a knock-in mutation in position 3 of PSMB4 into TC1 lung cancer cells again compromised the antitumor effects of CTX (Figure 3E). Moreover, in the setting of PD-1 blockade, administration of E. *hirae* 13144 without prior conditioning with antibiotics reduced the growth of parental but not PSMB4-mutated MCA205 cancers (Figure S6E). These results support the idea that the TSLARFANI TMP1 peptide encoded by *E. hirae* 13144 indeed induces T cell responses against the PSMB4-derived GSLARFRNI peptide across different tumor types and therapy modalities.

Reenforcing the notion of molecular mimicry between phage-encoded and cancer antigens, flow cytometric analyses using fluorescent-labelled tetramers H-2K^b/TSLARFANI (from TMP1) and H-2K^b/GSLARFRNI (from PSMB4) identified a subset of double-positive CTLs that infiltrate MCA205 tumors from CTX/*E. hirae 13144*-treated mice (Figure S6F) and that was as frequent as CTLs recognizing the PSMB4 peptide only (Figure 4A). We purified the splenic CD8$^+$ T cells using either the TMP1-H-2K^b or PSMB4-H-2K^b specific tetramers and stimulated them with irrelevant (OVA-derived-SIINFEKL) *versus* relevant (TMP-derived TSLARFANI or PSMB4-derived GSLARFRNI) peptides (Figure 4B). CD8$^+$ T cells binding H-2K^b-TMP1 tetramers produced IFNγ not only in response to TMP1 (up to 5-fold increase in IFNγ secreting T cells) but also in response to the PSMB4 epitope (2-fold increase, as much as with heat-killed *E. hirae* 13144 processed by DC) (Figure 4C, Figure S6G). Similarly, CD8$^+$ T cells binding H-2K^b-PSMB4 tetramers functionally recognized TMP1, albeit less efficiently than the PSMB4 epitope (Figure S6G). We analyzed the T cell receptor (TCR) repertoire of these two tetramer-reactive CD8$^+$ T cell subsets. In accordance with the functional data, half of the CD8$^+$ T cells labelled with PSMB4-H-2K^b tetramers shared clonotypes with the much wider TCR repertoire of T cells labelled with the TMP1-H-2K^b specific tetramers (Figure 4D, Table S4-S5) (but not with the negative fraction, Figure S6H). In sum, T cells recognizing the TMP1 epitope of immunogenic *E. hirae* can crossreact with a peptide contained in the oncogenic driver PSMB4 and *vice versa*.

Temperate bacteriophages are bacterial viruses that can transfer virulence, antimicrobial resistance genes, and immunogenic sequences to new bacterial hosts (*23*). The TMP protein, which contains a variable number of tandem repeats with highly conserved tryptophan and phenylalanine residues at fixed positions is encoded by the genome of *Siphoviridae* phages (*24*, *25*). To investigate the capacity of the *E. hirae 13144* phage to lysogenize other bacterial species *in vivo*, we performed culturomic analyses of the ileal content from C57BL/6 mice subjected to oral gavage with *E. hirae* 13144 and systemic CTX therapy, followed by PCR analyses seeking TMP sequences (Figure S8A-B). We tested 7 to 18 bacterial colonies from each animal and a total of 76 colonies. We only found lysogenic conversion of *E. gallinarum* by the *E. hirae*-temperate phage *in vivo*, as confirmed by sequencing of the phage genome in the second host (Figure 4E, Figure S8B-C). In contrast, none of the 90 colonies (mostly of *E. gallinarum)* isolated from naive mice harbored the TMP sequence (Figure S8A). Similarly, *in vitro* coculture

of TMP^+ *E. hirae* 13144 together with TMP^- *E. gallinarum spp*. at a 1:1 ratio uncovered a significant (~15%) rate of lysogenic conversion (Figure S8D). Examination of a preparation admixing *E. hirae* 13144 and *E. gallinarum* at a 1:10 ratio by means of transmission electron microscopy revealed numerous phages with the typical *Siphoviridae* morphology in the medium, whereas control cultures (bacteria separately) were free of such phages (Figure 4F). Altogether, these results indicate that the TMP1 peptide-encoding *Siphoviridae* phage from *E. hirae* 13144 is a virulent phage.

We next explored the possible pathophysiological relevance of these findings. We first screened a total of 3,027 adult and mother-infant metagenomes (*26*), validated by a second independent metagenomic-assembly based screening of 9,428 metagenomes (*27*) (*28*), to assess the breadth of coverage (BOC) of the *E. hirae* genome and its phages (Figure S9A). *E. hirae* was present with 100% confidence (i.e. BOC > 80%) in less than 150 fecal samples from disparate geography, age and datasets. This phage (and its host) could be vertically transmitted from mothers to infants and then colonizes the neonate. There was an increased prevalence of the phage (57%) in fecal microbiomes from children (representing 16% of all metagenomes, Fisher's test p-value <0.00001). Of note, the *E. hirae* 13144 phage was detectable in many samples lacking the presence of the *E. hirae* core genome, suggesting that other bacteria than *E. hirae* can host this phage. All host genomes belonged to the *Enterococcus* genus (except two assigned to *Coprobacillus*), in particular *E. faecalis* (80 genomes), *E. faecium* (23), and *E. hirae* (15), suggesting that phage 13144 (and its homologues from *E. hirae* 708, and 13344) are genus-specific but not species-specific.

Contrasting with metagenomics that has a low sensitivity to detect poor abundance species, culturomics followed by matrix-assisted laser desorption ionization time-of-flight mass spectrometry (MALDI-TOF) provides a technology for detecting rare *E. hirae* colonies in the stool of healthy individuals (*29*) or cancer patients (*8*). PCR analyses of each single cultivatable enterococcal colony (up to 5 per species and individual) from 76 cancer patients led to the detection of the TMP sequence encompassing the TMP1 peptide in 34% of the patients, only in *E. faecalis* and *E. hirae* (Figure S9B, Figure S10). Advanced renal and lung cancer patients (cohort described in Ref. (16)) with detectable fecal TMP at diagnosis exhibited prolonged

overall survival after therapy with immune checkpoint inhibitors targeting PD-1 (Figure 4G). Therefore, we screened sixteen TMP-derived nonapeptides predicted to bind the human MHC class I HLA-A*0201 with high affinity for their ability to prime naive $CD8^+$ T cells from six healthy volunteers *in vitro*. We found 6 out of 16 epitopes capable of triggering significant peptide-specific IFNγ release that were located in two distinct regions of the TMP protein (504-708 and 1397-1462, Figure S11A-B, Table S6). Using the NCBI BLASTP suite, we searched the human cancer peptidome (of the TCGA database) for a high degree of homology with these 6 HLA-A*0201 -restricted immunogenic nonapeptides. We found that only the TMP-derived peptide KLAKFASVV (aa 631-639) shared significant homology (7 out of 9 aa, with identical residues at the MHC anchoring positions 2 and 9) with a peptide contained in the protein glycerol-3-phosphate dehydrogenase 1-like (GPD1-L) (Figure S11C). GPD1-L reportedly counteracts the oncogenic HIF1α-dependent adaptation to hypoxia, and its expression is associated with favorable prognosis in head and neck squamous cell carcinomas (*30–32*). The TCGA transcriptomics database unveiled that high expression of GPD1-L is associated with improved overall survival in lung adenocarcinoma and kidney cancers (Figure S11D). Moreover, high expression of GPD1-L mRNA by tumors at diagnosis was associated with improved progression-free survival in three independent cohorts of non-small cell lung cancer (NSCLC) patients (n=157, Table S7) treated with anti-PD1 Abs (Figure S11E-F). Expression of GPD-1L failed to correlate with that of PD-L1 in NSCLC (Figure S11G). Of note, mutations in or adjacent to the 631-639 amino acid sequence of GPD-1L gene could rarely be identified in several types of neoplasia (Figure S12).

We derived an HLA-A*0201-restricted, phage peptide (KLAKFASVV)-specific T cell line from peripheral blood mononuclear cells of a human volunteer. Clones from this line also recognized the HLA-A*0201 -restricted, GPD-1L epitope (KLQKFASTV) (Figure S13A-C). Moreover, we detected $CD8^+$ T cells binding HLA-A*0201/KLAKFASVV tetramers exhibiting hallmarks of effector functions after *in vitro* stimulation of PBMC with the KLAKFASVV phage epitope in 3 out of 6 NSCLC patients (Fig. S13D-F). In the reverse attempt searching for molecular mimicry between well known and naturally processed non-mutated melanoma differentiation antigens recognized by human T cell clones (such as HLA-A*0201-binding MART-1 or MELOE epitopes) and gut commensal antigens, we found microbial analogs in the public microbiome data

bases (Figure S14, Table S8-Table S9, Figure S15, Table S8-S10). Some of these microbial peptides are recognized by the corresponding TCR (Tables S9- S10) with similar affinities as the parental (tumoral) epitope.

Altogether the present results demonstrate that microbial genomes code for MHC class I-restricted antigens that induce a memory $CD8^+$ T cell response, which then crossreacts with cancer antigens. Several lines of evidence plead in favor of this interpretation, as exemplified for the TMP1 epitope found within a phage that infects enterococci. First, naturally occurring ('mut3' in *E. hirae* strain ATCC9790) or artificial mutations ('mut2' or 'mut3' *in E.coli*) introduced into the TMP1 epitope suppressed the tumor-prophylactic and therapeutic potential of bacteria expressing TMP1. Second, transfer of the TMP1-encoding gene into *E. coli* conferred immunogenic capacity to this proteobacterium, which acquired the same antitumor properties as TMP1-expressing *E. hirae*. Third, when cancer cells were genetically modified to remove the TMP1-crossreactive peptide within the PSMB4 protein, they formed tumors that could no longer be controlled upon oral gavage with TMP1-expressing *E. hirae*. Fourth, cancer patients carrying the TMP phage sequence in fecal enterococci spp. or the GPD1-L tumoral antigen homologous to TMP epitopes exhibited a better response to PD-1 blockade, suggesting that this type of microbe-cancer cross-reactivity might be clinically relevant.

Recent reports point to the pathological relevance of autoantigen-crossreactive, microbiota-derived peptides for autoimmune disorders such as myocarditis, lupus and rheumatoid arthritis (*34–36*). Given the enormous richness of the commensal proteome (*37*), we expect the existence of other microbial antigens mimicking auto- and tumor antigens. In fact, we extended these findings to naturally processed melanoma-specific antigens that have microbial orthologs recognized by the same TCRs. Global phage numbers have been estimated to reach as high as 10^{31} particles with the potential of 10^{25} phage infections occurring every second (*38, 39*). Thus, the perspective opens that, within the microbiota, bacteriophages may enrich the therapeutic armamentarium for modulating the intestinal flora and for stimulating systemic anticancer immune responses.

References and Notes:

1. P. Sharma, J. P. Allison, Immune checkpoint targeting in cancer therapy: toward combination strategies with curative potential. *Cell*. **161**, 205–214 (2015).

2. L. Galluzzi, A. Buqué, O. Kepp, L. Zitvogel, G. Kroemer, Immunological Effects of Conventional Chemotherapy and Targeted Anticancer Agents. *Cancer Cell*. **28**, 690–714 (2015).

3. L. Zitvogel, Y. Ma, D. Raoult, G. Kroemer, T. F. Gajewski, The microbiome in cancer immunotherapy: Diagnostic tools and therapeutic strategies. *Science*. **359**, 1366–1370 (2018).

4. T. Tanoue, S. Morita, D. R. Plichta, A. N. Skelly, W. Suda, Y. Sugiura, S. Narushima, H. Vlamakis, I. Motoo, K. Sugita, A. Shiota, K. Takeshita, K. Yasuma-Mitobe, D. Riethmacher, T. Kaisho, J. M. Norman, D. Mucida, M. Suematsu, T. Yaguchi, V. Bucci, T. Inoue, Y. Kawakami, B. Olle, B. Roberts, M. Hattori, R. J. Xavier, K. Atarashi, K. Honda, A defined commensal consortium elicits CD8 T cells and anti-cancer immunity. *Nature*. **565**, 600–605 (2019).

5. M. Vétizou, J. M. Pitt, R. Daillère, P. Lepage, N. Waldschmitt, C. Flament, S. Rusakiewicz, B. Routy, M. P. Roberti, C. P. M. Duong, V. Poirier-Colame, A. Roux, S. Becharef, S. Formenti, E. Golden, S. Cording, G. Eberl, A. Schlitzer, F. Ginhoux, S. Mani, T. Yamazaki, N. Jacquelot, D. P. Enot, M. Bérard, J. Nigou, P. Opolon, A. Eggermont, P.-L. Woerther, E. Chachaty, N. Chaput, C. Robert, C. Mateus, G. Kroemer, D. Raoult, I. G. Boneca, F. Carbonnel, M. Chamaillard, L. Zitvogel, Anticancer immunotherapy by CTLA-4 blockade relies on the gut microbiota. *Science*. **350**, 1079–1084 (2015).

6. R. Daillère, M. Vétizou, N. Waldschmitt, T. Yamazaki, C. Isnard, V. Poirier-Colame, C. P. M. Duong, C. Flament, P. Lepage, M. P. Roberti, B. Routy, N. Jacquelot, L. Apetoh, S. Becharef, S. Rusakiewicz, P. Langella, H. Sokol, G. Kroemer, D. Enot, A. Roux, A. Eggermont, E. Tartour, L. Johannes, P.-L. Woerther, E. Chachaty, J.-C. Soria, E. Golden, S. Formenti, M. Plebanski, M. Madondo, P. Rosenstiel, D. Raoult, V. Cattoir, I. G. Boneca, M. Chamaillard, L. Zitvogel, Enterococcus hirae and Barnesiella intestinihominis Facilitate Cyclophosphamide-Induced Therapeutic Immunomodulatory Effects. *Immunity*. **45**, 931–943 (2016).

7. Y. Rong, Z. Dong, Z. Hong, Y. Jin, W. Zhang, B. Zhang, W. Mao, H. Kong, C. Wang, B. Yang, X. Gao, Z. Song, S. E. Green, H. K. Song, H. Wang, Y. Lu, Reactivity toward Bifidobacterium longum and Enterococcus hirae demonstrate robust CD8+ T cell response and better prognosis in HBV-related hepatocellular carcinoma. *Exp. Cell Res.* **358**, 352–359 (2017).

8. B. Routy, E. Le Chatelier, L. Derosa, C. P. M. Duong, M. T. Alou, R. Daillère, A. Fluckiger, M. Messaoudene, C. Rauber, M. P. Roberti, M. Fidelle, C. Flament, V. Poirier-Colame, P. Opolon, C. Klein, K. Iribarren, L. Mondragón, N. Jacquelot, B. Qu, G. Ferrere, C. Clémenson, L. Mezquita, J. R. Masip, C. Naltet, S. Brosseau, C. Kaderbhai, C. Richard,

H. Rizvi, F. Levenez, N. Galleron, B. Quinquis, N. Pons, B. Ryffel, V. Minard-Colin, P. Gonin, J.-C. Soria, E. Deutsch, Y. Loriot, F. Ghiringhelli, G. Zalcman, F. Goldwasser, B. Escudier, M. D. Hellmann, A. Eggermont, D. Raoult, L. Albiges, G. Kroemer, L. Zitvogel, Gut microbiome influences efficacy of PD-1-based immunotherapy against epithelial tumors. *Science*. **359**, 91–97 (2018).

9. N. R. Rose, Negative selection, epitope mimicry and autoimmunity. *Curr. Opin. Immunol.* **49**, 51–55 (2017).

10. V. Rubio-Godoy, V. Dutoit, Y. Zhao, R. Simon, P. Guillaume, R. Houghten, P. Romero, J.-C. Cerottini, C. Pinilla, D. Valmori, Positional scanning-synthetic peptide library-based analysis of self- and pathogen-derived peptide cross-reactivity with tumor-reactive Melan-A-specific CTL. *J. Immunol. Baltim. Md 1950*. **169**, 5696–5707 (2002).

11. L. Vujanovic, M. Mandic, W. C. Olson, J. M. Kirkwood, W. J. Storkus, A mycoplasma peptide elicits heteroclitic CD4+ T cell responses against tumor antigen MAGE-A6. *Clin. Cancer Res. Off. J. Am. Assoc. Cancer Res.* **13**, 6796–6806 (2007).

12. M. E. Perez-Muñoz, P. Joglekar, Y.-J. Shen, Y.-J. Shen, K. Y. Chang, D. A. Peterson, Identification and Phylogeny of the First T Cell Epitope Identified from a Human Gut Bacteroides Species. *PloS One*. **10**, e0144382 (2015).

13. Y. Yang, M. B. Torchinsky, M. Gobert, H. Xiong, M. Xu, J. L. Linehan, F. Alonzo, C. Ng, A. Chen, X. Lin, A. Sczesnak, J.-J. Liao, V. J. Torres, M. K. Jenkins, J. J. Lafaille, D. R. Littman, Focused specificity of intestinal TH17 cells towards commensal bacterial antigens. *Nature*. **510**, 152–156 (2014).

14. J. N. Chai, Y. Peng, S. Rengarajan, B. D. Solomon, T. L. Ai, Z. Shen, J. S. A. Perry, K. A. Knoop, T. Tanoue, S. Narushima, K. Honda, C. O. Elson, R. D. Newberry, T. S. Stappenbeck, A. L. Kau, D. A. Peterson, J. G. Fox, C.-S. Hsieh, Helicobacter species are potent drivers of colonic T cell responses in homeostasis and inflammation. *Sci. Immunol.* **2** (2017), doi:10.1126/sciimmunol.aal5068.

15. Q. Ji, A. Perchellet, J. M. Goverman, Viral infection triggers central nervous system autoimmunity via activation of CD8+ T cells expressing dual TCRs. *Nat. Immunol.* **11**, 628–634 (2010).

16. V. P. Balachandran, M. Łuksza, J. N. Zhao, V. Makarov, J. A. Moral, R. Remark, B. Herbst, G. Askan, U. Bhanot, Y. Senbabaoglu, D. K. Wells, C. I. O. Cary, O. Grbovic-Huezo, M. Attiyeh, B. Medina, J. Zhang, J. Loo, J. Saglimbeni, M. Abu-Akeel, R. Zappasodi, N. Riaz, M. Smoragiewicz, Z. L. Kelley, O. Basturk, Australian Pancreatic Cancer Genome Initiative, Garvan Institute of Medical Research, Prince of Wales Hospital, Royal North Shore Hospital, University of Glasgow, St Vincent's Hospital, QIMR Berghofer Medical Research Institute, University of Melbourne, Centre for Cancer Research, University of Queensland, Institute for Molecular Bioscience, Bankstown Hospital, Liverpool Hospital, Royal Prince Alfred Hospital, Chris O'Brien Lifehouse, Westmead Hospital, Fremantle Hospital, St John of God Healthcare, Royal Adelaide Hospital, Flinders Medical Centre, Envoi Pathology, Princess Alexandria Hospital, Austin Hospital, Johns Hopkins Medical

Institutes, ARC-Net Centre for Applied Research on Cancer, M. Gönen, A. J. Levine, P. J. Allen, D. T. Fearon, M. Merad, S. Gnjatic, C. A. Iacobuzio-Donahue, J. D. Wolchok, R. P. DeMatteo, T. A. Chan, B. D. Greenbaum, T. Merghoub, S. D. Leach, Identification of unique neoantigen qualities in long-term survivors of pancreatic cancer. *Nature*. **551**, 512–516 (2017).

17. C. P. Bradley, F. Teng, K. M. Felix, T. Sano, D. Naskar, K. E. Block, H. Huang, K. S. Knox, D. R. Littman, H.-J. J. Wu, Segmented Filamentous Bacteria Provoke Lung Autoimmunity by Inducing Gut-Lung Axis Th17 Cells Expressing Dual TCRs. *Cell Host Microbe*. **22**, 697-704.e4 (2017).

18. S. Viaud, F. Saccheri, G. Mignot, T. Yamazaki, R. Daillère, D. Hannani, D. P. Enot, C. Pfirschke, C. Engblom, M. J. Pittet, A. Schlitzer, F. Ginhoux, L. Apetoh, E. Chachaty, P.-L. Woerther, G. Eberl, M. Bérard, C. Ecobichon, D. Clermont, C. Bizet, V. Gaboriau-Routhiau, N. Cerf-Bensussan, P. Opolon, N. Yessaad, E. Vivier, B. Ryffel, C. O. Elson, J. Doré, G. Kroemer, P. Lepage, I. G. Boneca, F. Ghiringhelli, L. Zitvogel, The intestinal microbiota modulates the anticancer immune effects of cyclophosphamide. *Science*. **342**, 971–976 (2013).

19. G. Y. Lee, P. M. Haverty, L. Li, N. M. Kljavin, R. Bourgon, J. Lee, H. Stern, Z. Modrusan, S. Seshagiri, Z. Zhang, D. Davis, D. Stokoe, J. Settleman, F. J. de Sauvage, R. M. Neve, Comparative oncogenomics identifies PSMB4 and SHMT2 as potential cancer driver genes. *Cancer Res.* **74**, 3114–3126 (2014).

20. Y.-C. Cheng, W.-C. Tsai, Y.-C. Sung, H.-H. Chang, Y. Chen, Interference with PSMB4 Expression Exerts an Anti-Tumor Effect by Decreasing the Invasion and Proliferation of Human Glioblastoma Cells. *Cell. Physiol. Biochem. Int. J. Exp. Cell. Physiol. Biochem. Pharmacol.* **45**, 819–831 (2018).

21. X. Zhang, D. Lin, Y. Lin, H. Chen, M. Zou, S. Zhong, X. Yi, S. Han, Proteasome beta-4 subunit contributes to the development of melanoma and is regulated by miR-148b. *Tumour Biol. J. Int. Soc. Oncodevelopmental Biol. Med.* **39**, 1010428317705767 (2017).

22. H. Wang, Z. He, L. Xia, W. Zhang, L. Xu, X. Yue, X. Ru, Y. Xu, PSMB4 overexpression enhances the cell growth and viability of breast cancer cells leading to a poor prognosis. *Oncol. Rep.* **40**, 2343–2352 (2018).

23. M. G. Weinbauer, Ecology of prokaryotic viruses. *FEMS Microbiol. Rev.* **28**, 127–181 (2004).

24. M. Piuri, G. F. Hatfull, A peptidoglycan hydrolase motif within the mycobacteriophage TM4 tape measure protein promotes efficient infection of stationary phase cells. *Mol. Microbiol.* **62**, 1569–1585 (2006).

25. M. Belcaid, A. Bergeron, G. Poisson, The evolution of the tape measure protein: units, duplications and losses. *BMC Bioinformatics*. **12 Suppl 9**, S10 (2011).

26. E. Pasolli, L. Schiffer, P. Manghi, A. Renson, V. Obenchain, D. T. Truong, F. Beghini, F. Malik, M. Ramos, J. B. Dowd, C. Huttenhower, M. Morgan, N. Segata, L. Waldron, Accessible, curated metagenomic data through ExperimentHub. *Nat. Methods*. **14**, 1023–1024 (2017).

27. P. Ferretti, E. Pasolli, A. Tett, F. Asnicar, V. Gorfer, S. Fedi, F. Armanini, D. T. Truong, S. Manara, M. Zolfo, F. Beghini, R. Bertorelli, V. De Sanctis, I. Bariletti, R. Canto, R. Clementi, M. Cologna, T. Crifò, G. Cusumano, S. Gottardi, C. Innamorati, C. Masè, D. Postai, D. Savoi, S. Duranti, G. A. Lugli, L. Mancabelli, F. Turroni, C. Ferrario, C. Milani, M. Mangifesta, R. Anzalone, A. Viappiani, M. Yassour, H. Vlamakis, R. Xavier, C. M. Collado, O. Koren, S. Tateo, M. Soffiati, A. Pedrotti, M. Ventura, C. Huttenhower, P. Bork, N. Segata, Mother-to-Infant Microbial Transmission from Different Body Sites Shapes the Developing Infant Gut Microbiome. *Cell Host Microbe*. **24**, 133-145.e5 (2018).

28. E. Pasolli, F. Asnicar, S. Manara, M. Zolfo, N. Karcher, F. Armanini, F. Beghini, P. Manghi, A. Tett, P. Ghensi, M. C. Collado, B. L. Rice, C. DuLong, X. C. Morgan, C. D. Golden, C. Quince, C. Huttenhower, N. Segata, Extensive Unexplored Human Microbiome Diversity Revealed by Over 150,000 Genomes from Metagenomes Spanning Age, Geography, and Lifestyle. *Cell*. **176**, 649-662.e20 (2019).

29. B. Samb-Ba, C. Mazenot, A. Gassama-Sow, G. Dubourg, H. Richet, P. Hugon, J.-C. Lagier, D. Raoult, F. Fenollar, MALDI-TOF identification of the human Gut microbiome in people with and without diarrhea in Senegal. *PloS One*. **9**, e87419 (2014).

30. T. J. Kelly, A. L. Souza, C. B. Clish, P. Puigserver, A hypoxia-induced positive feedback loop promotes hypoxia-inducible factor 1alpha stability through miR-210 suppression of glycerol-3-phosphate dehydrogenase 1-like. *Mol. Cell. Biol.* **31**, 2696–2706 (2011).

31. Z. Feng, J. N. Li, L. Wang, Y. F. Pu, Y. Wang, C. B. Guo, The prognostic value of glycerol-3-phosphate dehydrogenase 1-like expression in head and neck squamous cell carcinoma. *Histopathology*. **64**, 348–355 (2014).

32. S.-C. Liu, S.-M. Chuang, C.-J. Hsu, C.-H. Tsai, S.-W. Wang, C.-H. Tang, CTGF increases vascular endothelial growth factor-dependent angiogenesis in human synovial fibroblasts by increasing miR-210 expression. *Cell Death Dis.* **5**, e1485 (2014).

33. S. Simon, Z. Wu, J. Cruard, V. Vignard, A. Fortun, A. Khammari, B. Dreno, F. Lang, S. J. Rulli, N. Labarriere, TCR Analyses of Two Vast and Shared Melanoma Antigen-Specific T Cell Repertoires: Common and Specific Features. *Front. Immunol.* **9**, 1962 (2018).

34. C. Gil-Cruz, C. Perez-Shibayama, A. De Martin, F. Ronchi, K. van der Borght, R. Niederer, L. Onder, M. Lütge, M. Novkovic, V. Nindl, G. Ramos, M. Arnoldini, E. M. C. Slack, V. Boivin-Jahns, R. Jahns, M. Wyss, C. Mooser, B. N. Lambrecht, M. T. Maeder, H. Rickli, L. Flatz, U. Eriksson, M. B. Geuking, K. D. McCoy, B. Ludewig, Microbiota-derived peptide mimics drive lethal inflammatory cardiomyopathy. *Science*. **366**, 881–886 (2019).

35. T. M. Greiling, C. Dehner, X. Chen, K. Hughes, A. J. Iñiguez, M. Boccitto, D. Z. Ruiz, S. C. Renfroe, S. M. Vieira, W. E. Ruff, S. Sim, C. Kriegel, J. Glanternik, X. Chen, M. Girardi,

P. Degnan, K. H. Costenbader, A. L. Goodman, S. L. Wolin, M. A. Kriegel, Commensal orthologs of the human autoantigen Ro60 as triggers of autoimmunity in lupus. *Sci. Transl. Med.* **10** (2018), doi:10.1126/scitranslmed.aan2306.

36. M. F. Konig, L. Abusleme, J. Reinholdt, R. J. Palmer, R. P. Teles, K. Sampson, A. Rosen, P. A. Nigrovic, J. Sokolove, J. T. Giles, N. M. Moutsopoulos, F. Andrade, Aggregatibacter actinomycetemcomitans-induced hypercitrullination links periodontal infection to autoimmunity in rheumatoid arthritis. *Sci. Transl. Med.* **8**, 369ra176 (2016).

37. J. Li, H. Jia, X. Cai, H. Zhong, Q. Feng, S. Sunagawa, M. Arumugam, J. R. Kultima, E. Prifti, T. Nielsen, A. S. Juncker, C. Manichanh, B. Chen, W. Zhang, F. Levenez, J. Wang, X. Xu, L. Xiao, S. Liang, D. Zhang, Z. Zhang, W. Chen, H. Zhao, J. Y. Al-Aama, S. Edris, H. Yang, J. Wang, T. Hansen, H. B. Nielsen, S. Brunak, K. Kristiansen, F. Guarner, O. Pedersen, J. Doré, S. D. Ehrlich, MetaHIT Consortium, P. Bork, J. Wang, MetaHIT Consortium, An integrated catalog of reference genes in the human gut microbiome. *Nat. Biotechnol.* **32**, 834–841 (2014).

38. M. L. Pedulla, M. E. Ford, J. M. Houtz, T. Karthikeyan, C. Wadsworth, J. A. Lewis, D. Jacobs-Sera, J. Falbo, J. Gross, N. R. Pannunzio, W. Brucker, V. Kumar, J. Kandasamy, L. Keenan, S. Bardarov, J. Kriakov, J. G. Lawrence, W. R. Jacobs, R. W. Hendrix, G. F. Hatfull, Origins of highly mosaic mycobacteriophage genomes. *Cell*. **113**, 171–182 (2003).

39. K. E. Wommack, R. R. Colwell, Virioplankton: viruses in aquatic ecosystems. *Microbiol. Mol. Biol. Rev. MMBR.* **64**, 69–114 (2000).

Acknowledgments: We are thankful to the animal facility team of Gustave Roussy and all the technicians from Centre GF Leclerc. We are very endebted to Dr Oliver Kepp, Gustave Roussy for figure design, and to Prof. Hans Georg Rammensee from the Department of Immunology, Institute for Cell Biology, University of Tübingen, Tübingen, Germany for his careful guidance in peptide selection and reading of the paper. LZ and GK were supported by the Ligue contre le Cancer (équipe labelisée); Agence National de la Recherche (ANR) – Projets blancs; ANR under the frame of E-Rare-2, the ERA-Net for Research on Rare Diseases; Association pour la recherche sur le cancer (ARC); Cancéropôle Ile-de-France; Chancelerie des universités de Paris (Legs Poix), Fondation pour la Recherche Médicale (FRM); a donation by Elior; the European Commission (Horizon 2020: Oncobiome); the European Research Council (ERC); Fondation Carrefour; High-end Foreign Expert Program in China (GDW20171100085 and GDW20181100051), Institut National du Cancer (INCa); Inserm (HTE); Institut Universitaire de France; LeDucq Foundation; the LabEx Immuno-Oncology; the RHU Torino Lumière; the Seerave Foundation; the SIRIC Stratified Oncology Cell DNA Repair and Tumor Immune

Elimination (SOCRATE); ONCOBIOME H2020 network, CARE network (directed by Prof. Mariette, Kremlin Bicêtre AP-HP), and the SIRIC Cancer Research and Personalized Medicine (CARPEM); RHU Torino Lumière (ANR-16-RHUS-0008). The results shown here are based upon data generated by the TCGA Research Network: http://cancergenome.nih.gov/. National Research, Development andInnovation Fund of Hungary Project no. FIEK_16-1-2016-0005. Z.S was supported by the Research and Technology Innovation Fund NAP2-2017-1.2.1-NKP-0002, Breast Cancer Research Foundation (BCRF-17-156). Z.S and I.C were supported by the Novo Nordisk Foundation Interdisciplinary Synergy Programme Grant (NNF15OC0016584). PN was supported by the Italian Association for Cancer Research AIRC IG 19822. Mouse TCR sequencing was performed by the TRiPoD ERC-Advanced EU (322856) grants to Prof. David Klatzmann.

Competing interests statement: RD, DR, LZ and GK are cofounders of everImmune, a biotech company devoted to the use of commensal microbes for the treatment of cancers. RD is a full-time employee of everImmune. RD and LZ hold patents on immunogenic phage sequences.

Supplementary Materials:

Materials and Methods

Figures S1-S15

Tables S1-S10

Reference *(1-17)*

Statistical report

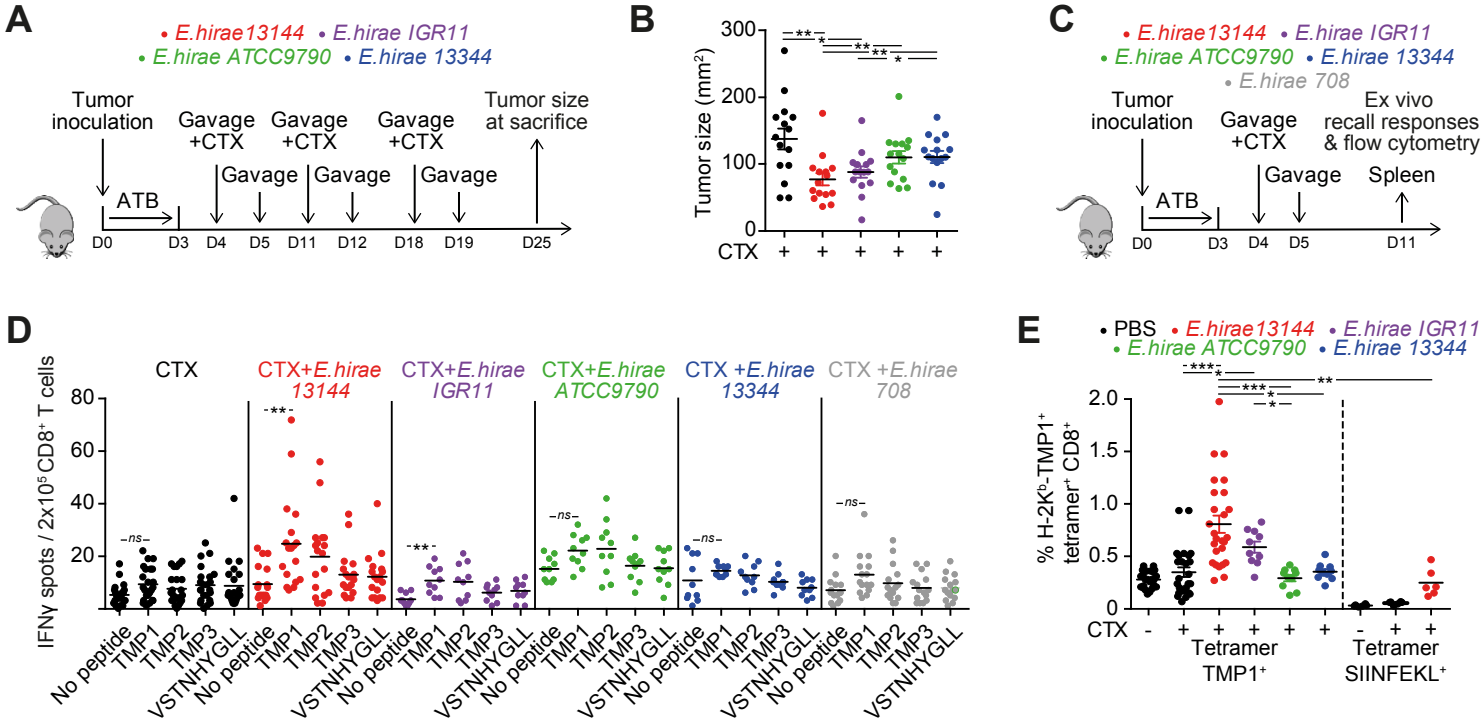
A
• E.hirae13144 • E.hirae IGR11
• E.hirae ATCC9790 • E.hirae 13344
Tumor inoculation
Gavage +CTX
Gavage +CTX
Gavage +CTX
Tumor size at sacrifice
Gavage
Gavage
Gavage
ATB
D0
D3
D4
D5
D11
D12
D18
D19
D25
B
Tumor size (mm²)
300
200
100
0
CTX + + + + +
C
• E.hirae13144 • E.hirae IGR11
• E.hirae ATCC9790 • E.hirae 13344
• E.hirae 708
Tumor inoculation
Gavage +CTX
Ex vivo recall responses & flow cytometry
Gavage
Spleen
ATB
D0
D3
D4
D5
D11
D
IFNγ spots / 2x10⁵ CD8⁺ T cells
CTX
CTX+E.hirae 13144
CTX+E.hirae IGR11
CTX+E.hirae ATCC9790
CTX +E.hirae 13344
CTX +E.hirae 708
No peptide
TMP1
TMP2
TMP3
VSTNHYGLL
E
• PBS • E.hirae13144 • E.hirae IGR11
• E.hirae ATCC9790 • E.hirae 13344
% H-2Kᵇ-TMP1⁺ tetramer⁺ CD8⁺
CTX - + + + + + - + +
Tetramer TMP1⁺
Tetramer SIINFEKL⁺

Figure 1

Legends to Figures

Figure 1. Phage Tail Length Tape Measure Protein as the unique antigenic sequence in *E. hirae* 13144.

A, B. C57BL/6 mice bearing MCA205 sarcomas were conditioned with broad spectrum antibiotics (streptomycin, colistin, ampicillin, vancomycin) for 3 days before performing oral gavages with *E. hirae* strain 13144 and i.p. injections of cyclophosphamide (CTX), as indicated (A), and tumor size was recorded for each mouse at sacrifice on day 25 (B). C-E. Naïve C57BL/6 mice were conditioned with antibiotics, gavaged with distinct *E. hirae* strains and treated with CTX (C). Day 11 purified $CD8^+$ T splenocytes were restimulated *ex vivo* in a recall assay with bone marrow-derived dendritic cells loaded with the indicated peptides (Table S2, group 7) to quantify IFNγ-secreting $CD8^+$T cells (D). H-$2K^b$/TMP1 (TSLARFANI) or H-$2K^b$/SIINFEKL tetramer binding $CD8^+$ splenocytes were detected by cytofluorometry at day 11 (E). Also refer to Figure S2. Each graph assembles results from 2-3 independent experiments containing groups of 5-6 mice. ANOVA statistical analyses (Kruskal-wallis test): *$*p<0.05$, **$p<0.01$, ***$p<0.001$*. Refer to the statistical report.

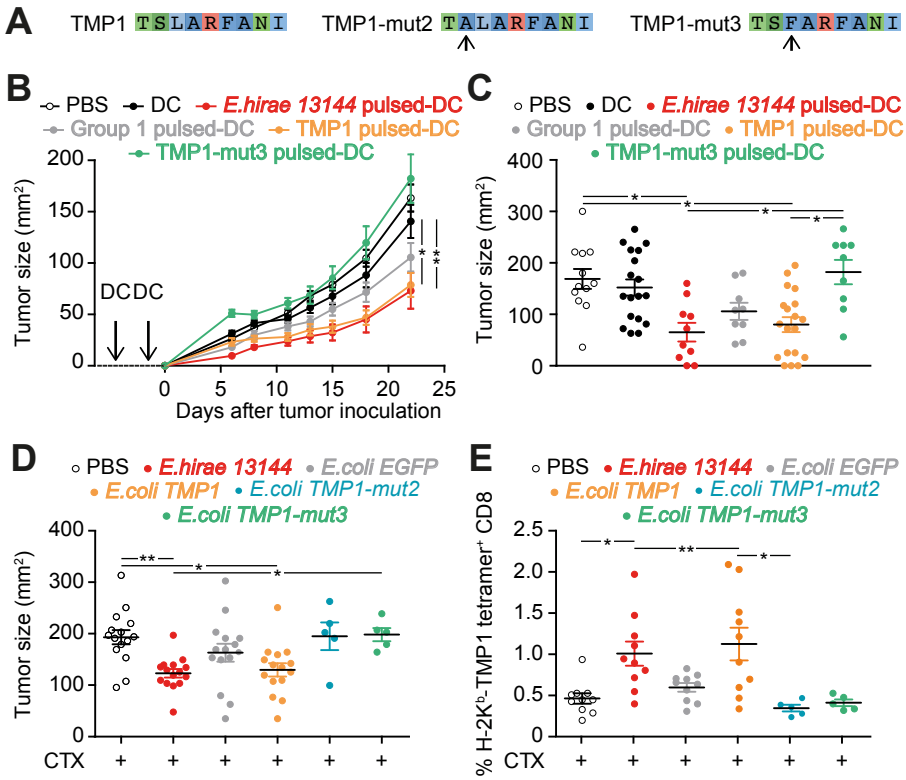
A
TMP1 TSLARFANI
TMP1-mut2 TALARFANI
TMP1-mut3 TSFARFANI
B
PBS
DC
E.hirae 13144 pulsed-DC
Group 1 pulsed-DC
TMP1 pulsed-DC
TMP1-mut3 pulsed-DC
Tumor size (mm²)
DC DC
Days after tumor inoculation
C
PBS
DC
E.hirae 13144 pulsed-DC
Group 1 pulsed-DC
TMP1 pulsed-DC
TMP1-mut3 pulsed-DC
Tumor size (mm²)
D
PBS
E.hirae 13144
E.coli EGFP
E.coli TMP1
E.coli TMP1-mut2
E.coli TMP1-mut3
Tumor size (mm²)
CTX
E
PBS
E.hirae 13144
E.coli EGFP
E.coli TMP1
E.coli TMP1-mut2
E.coli TMP1-mut3
% H-2Kᵇ-TMP1 tetramer⁺ CD8
CTX

Figure 2

Figure 2. Prophylactic and therapeutic immunization using Phage Tail Length Tape Measure Protein (TMP) against sarcomas.

A. Sequence of the immunogenic epitope TMP1 (TSLARFANI) with the artificial and naturally occuring mutations in positions 2 and 3, respectively. B-C. *Prophylactic vaccinations*. TLR3 ligand-exposed dendritic cell (DC) were pulsed with peptides or heat-inactivated bacteria and then s.c. inoculated twice into mice. One month later, MCA205 sarcomas were implanted in the opposite flank, followed by monitoring of tumor size (means±SEM in B, individual results in C). D-E. *Therapeutic settings.* MCA205 tumor bearing mice were treated with cyclophosphamide (CTX) and gavaged with *E. hirae* 13144 or *E. coli* (like in Fig. 1A) that were genetically modified to express the indicated peptides or enhanced green fluorescent protein (EGFP) as a negative control. Tumor growth at sacrifice (D) and the frequency of H-2K^{b}/TMP1 tetramer binding splenic CD8^{+} T cells (E) were monitored. Results are shown for 12-18 animals, gathered from 2-3 independent experiments. ANOVA statistical analyses (Kruskal-wallis test): *$p<0.05$, ** $p<0.01$, ***$p<0.001$. Refer to the statistical report.

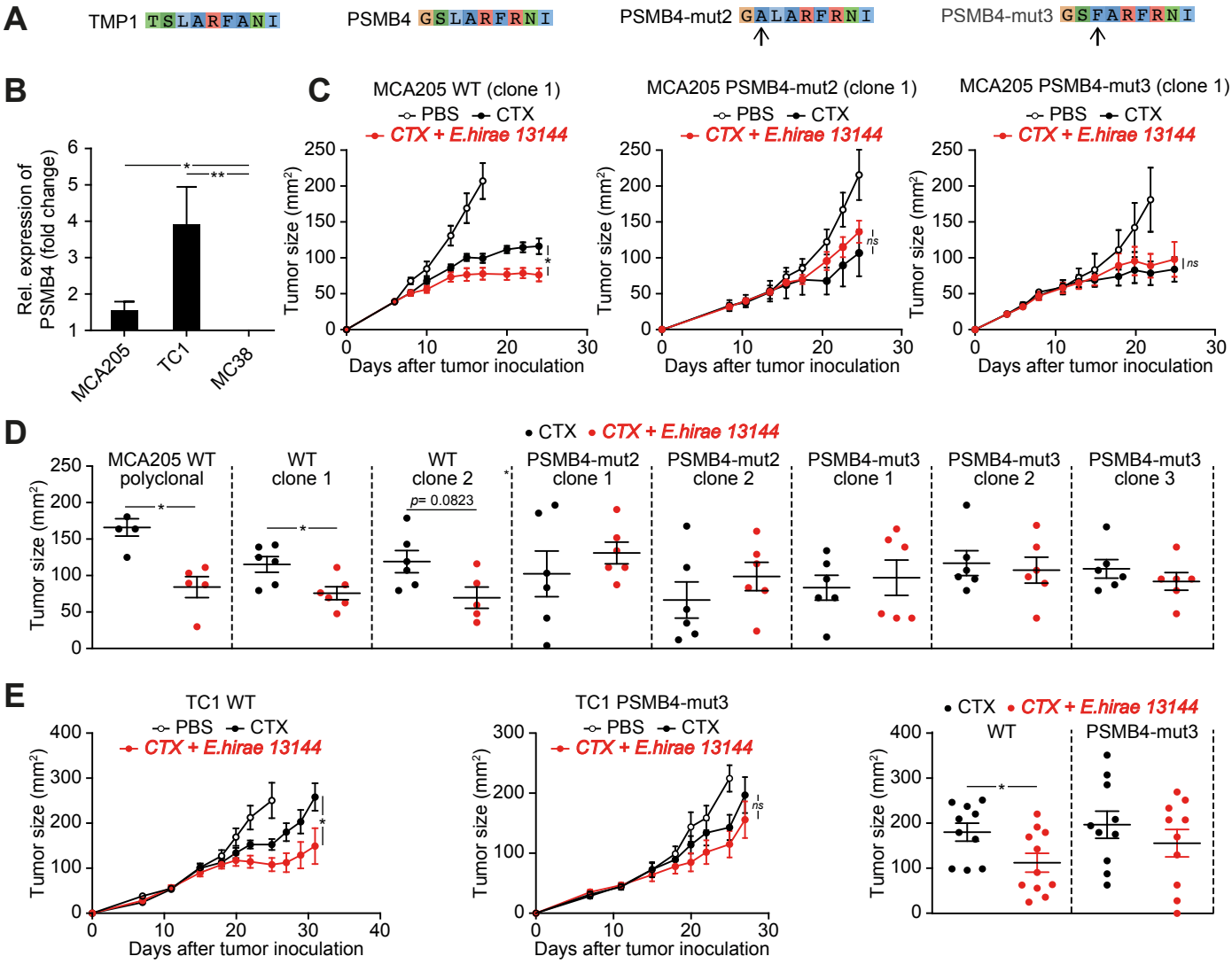
A
TMP1 TSLARFANI
PSMB4 GSLARFRNI
PSMB4-mut2 GALARFRNI
PSMB4-mut3 GSFARFRNI
B
Rel. expression of PSMB4 (fold change)
MCA205
TC1
MC38
C
MCA205 WT (clone 1)
MCA205 PSMB4-mut2 (clone 1)
MCA205 PSMB4-mut3 (clone 1)
PBS
CTX
CTX + E.hirae 13144
Tumor size (mm²)
Days after tumor inoculation
ns
D
CTX
CTX + E.hirae 13144
MCA205 WT polyclonal
WT clone 1
WT clone 2
p= 0.0823
PSMB4-mut2 clone 1
PSMB4-mut2 clone 2
PSMB4-mut3 clone 1
PSMB4-mut3 clone 2
PSMB4-mut3 clone 3
E
TC1 WT
TC1 PSMB4-mut3
WT
PSMB4-mut3

Figure 3

Figure 3. Molecular mimicry between enterophage TMP and the oncogenic driver PSMB4 in two mouse cancers.

A. Sequence alignment of the enterophage TMP1 peptide and a PSMB4 epitope with its two experimental mutants. B. Relative expression of PSMB4 mRNA in MCA205 sarcoma, TC1 lung cancer and MC38 colon carcinomas as compared to their healthy tissue of origin (mean ratio±SEM, n=3). C-D. Therapeutic response of wild type *versus* knock-in mutants of MCA205 to cyclophosphamide (CTX) alone or in combination with immunogenic *E. hirae* strain 13144 (setting as in Fig. 1A). Results are shown as tumor growth kinetics (means±SEM) for selected MCA205 clones (C) or as individual results (one dot corresponds to one mouse) on day 25 (D). E. Therapeutic response of wild type *versus* mutated TC1 lung cancers to CTX alone or in combination with *E. hirae* 13144 (setting as in Fig. 1A, but without antibiotic preconditioning) reflected by tumor growth kinetics and individual tumor sizes at sacrifice. Results are shown as means ±SEM. Mann Whitney test or ANOVA statistical analyses (Kruskal-wallis test): *$p<0.05$, ** $p<0.01$, ***$p<0.001$. Refer to the statistical report.

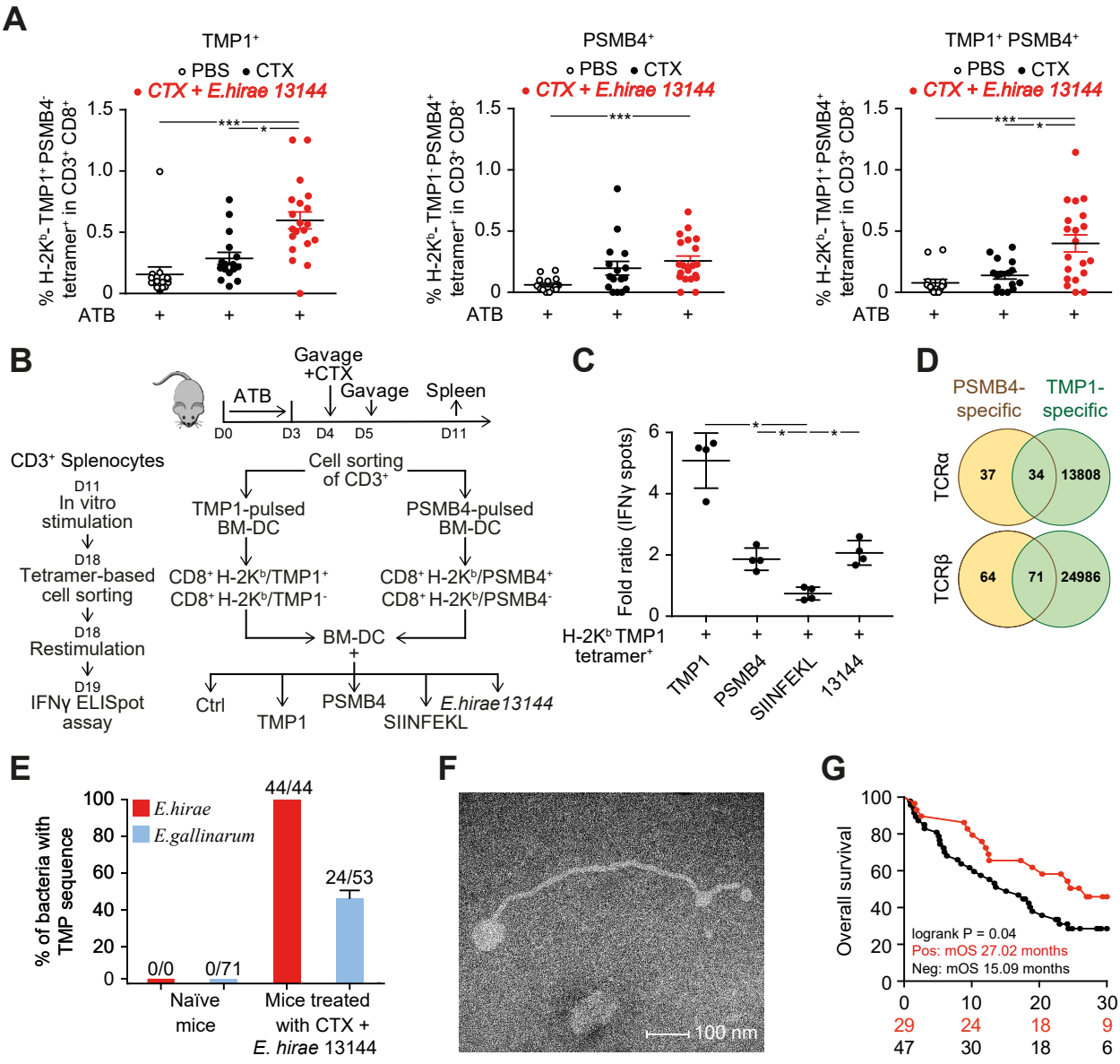
A
TMP1+
PSMB4+
TMP1+ PSMB4+
PBS CTX
CTX + E.hirae 13144
% H-2Kb- TMP1+ PSMB4- tetramer+ in CD3+ CD8+
% H-2Kb- TMP1- PSMB4+ tetramer+ in CD3+ CD8+
% H-2Kb- TMP1+ PSMB4+ tetramer+ in CD3+ CD8+
ATB
B
Gavage +CTX
Gavage
Spleen
D0 D3 D4 D5 D11
CD3+ Splenocytes
D11
In vitro stimulation
D18
Tetramer-based cell sorting
D18
Restimulation
D19
IFNγ ELISpot assay
Cell sorting of CD3+
TMP1-pulsed BM-DC
PSMB4-pulsed BM-DC
CD8+ H-2Kb/TMP1+
CD8+ H-2Kb/TMP1-
CD8+ H-2Kb/PSMB4+
CD8+ H-2Kb/PSMB4-
BM-DC
Ctrl
TMP1
PSMB4
SIINFEKL
E.hirae13144
C
Fold ratio (IFNγ spots)
H-2Kb TMP1 tetramer+
TMP1
PSMB4
SIINFEKL
13144
D
PSMB4- specific
TMP1- specific
TCRα
TCRβ
37
34
13808
64
71
24986
E
% of bacteria with TMP sequence
E.hirae
E.gallinarum
0/0
0/71
44/44
24/53
Naïve mice
Mice treated with CTX + E. hirae 13144
F
100 nm
G
Overall survival
logrank P = 0.04
Pos: mOS 27.02 months
Neg: mOS 15.09 months
0 10 20 30
29 24 18 9
47 30 18 6

Figure 4

Figure 4. TMP crossreacts with the PSMB4 cancer epitope and affects human anticancer immune responses.

A. Flow cytometry analysis of $CD8^+$ tumor-infiltrating lymphocytes (from tumors treated as in Fig. 1A) after co-staining with two different tetramers (H-$2K^b$/TMP1 and H-$2K^b$/PSMB4, sequences in Fig. 3A). Each dot depicts one tumor. The graphs assemble the results of 3 independent experiments with 5 mice/group. B,C. Purified $CD3^+$ T splenocytes from animals treated with CTX and *E. hirae 13144* were restimulated *ex vivo* with bone marrow-derived dendritic cells (DC) loaded with TMP1 or PSMB4 peptide. One week after *ex vivo* restimulation, peptide- specific $CD8^+$ T cells were purified after staining with the corresponding tetramer to measure IFNγ secretion in response to DC loaded with peptides (TMP1, PSMB4, SIINFEKL as negative control) or heat-inactivated *E. hirae* 13144. These results were performed in parallel on the tetramer-binding *versus* non-binding fraction and were normalized to the PBS controls (Ctrl). Each dot represents one culture. Mann Whitney test or ANOVA statistical analyses (Kruskal-wallis test): *$p<0.05$, ** $p<0.01$, ***$p<0.001$. D. Venn diagram of TCRα and β chains from tetramer positive $CD8^+$ T cells specific for PSMB4 (yellow) or TMP1 (green). E. Lysogenic conversion of *E. gallinarum* by the *E. hirae* siphoviridae phage *in vivo*. Ileal content was obtained from naïve mice or from mice receiving *E. hirae* together with cyclophosphamide (CTX), followed by cultivation and isolation of bacterial colonies, MALDI-TOF identification and PCR-based detection of TMP. Results are from 5 mice/group. F. Transmission electron microscopy of the phage produced by *E. hirae* 13144. G. Kaplan Meier survival plots of 76 patients with non-small cell lung cancer or renal cell cancer subjected to PD-1-targeting immunotherapy, stratified according to the presence or absence of TMP in at least 5 *E. faecalis* or *E. hirae* colonies/patient. Univariate Log-rank (Mantel-Cox) analysis. Refer to the statistical report.

Science
AAAS

Crossreactivity between MHC class I-restricted antigens from cancer cells and an enterococcal bacteriophage.

Authors: Aurélie Fluckiger, Romain Daillère, Mohamed Sassi, Barbara Susanne Sixt, Peng Liu, Friedemann Loos, Corentin Richard, Catherine Rabu, Maryam Tidjani Alou, Anne-Gaëlle Goubet, Fabien Lemaitre, Gladys Ferrere, Lisa Derosa, Connie PM Duong, Meriem Messaoudene, Andréanne Gagné, Luisa De Sordi, Laurent Debarbieux, Sylvain Simon, Clara-Maria Scarlata, Maha Ayyoub, Belinda Palermo, Francesco Facciolo, Romain Boidot, Richard Wheeler, Ivo Gomperts Boneca, Zsofia Sztupinszki, Krisztian Papp, Istvan Csabai, Edoardo Pasolli, Nicola Segata, Carlos Lopez-Otin, Zoltan Szallasi, Fabrice Andre, Valerio Iebba, Valentin Quiniou, David Klatzmann, Jacques Boukhalil, Saber Khelaifia, Didier Raoult, Laurence Albiges, Bernard Escudier, Alexander Eggermont, Fathia Mami-Chouaib, Paola Nistico, Nathalie Labarrière, François Ghiringhelli, Bertrand Routy, Vincent Cattoir, Guido Kroemer*, and Laurence Zitvogel*.

*Correspondence to: laurence.zitvogel@gustaveroussy.fr; kroemer@orange.fr

This PDF file includes:

Methods:

Cell culture, reagents and tumor cell lines. MC38, TC1, MCA205 (WT or PSMB4-mutated) tumor cell lines or clones were cultured at 37°C with 5% CO_2 in RPMI 1640 medium containing 10% fetal calf serum (FCS), 2 mM L-glutamine, 100 UI/mL penicillin/streptomycin, 1 mM sodium pyruvate and MEM non-essential amino acids (henceforth referred to as complete RPMI 1640). All these reagents were purchased from Gibco-Invitrogen (Carlsbad, CA, USA).

Mice. All animal experiments were carried out in compliance with French and European laws and guidelines and regulations. The local institutional board approved all mouse experiments (permission number: 2016-109-7450). All mouse experiments were performed at the animal facility in Gustave Roussy Cancer Campus where animals were housed in specific pathogen-free conditions. Female C57BL/6 were purchased from Harlan (Gannat, France). Mice were used at an age between 7 and 12 weeks of age.

Antibiotic treatments. Mice were treated during 3 days (biotinylated) an antibiotic (ATB) solution containing ampicillin (1 mg/mL), streptomycin (5 mg/mL), colistin (1 mg/mL) and vancomycin (0.25 mg/mL) (Sigma-Aldrich) added to the sterile drinking water of mice. Antibiotic activity was confirmed by cultivating fecal pellets resuspended in brain heart infusion (BHI) broth + 15% glycerol at 0.1 g/mL on COS (BD Columbia agar with 5% sheep blood, BioMérieux) plates for 48h at 37°C in aerobic and anaerobic conditions. In the context of bacterial or fecal transplantation, mice received 3 days of ATB before undergoing bacterial or fecal transplantation the next day by oral gavage using animal feeding needles. ATB were not used for Figure 3E and Figure S6E.

Tumor challenge and treatment. Syngeneic C57BL/6 mice were inoculated subcutaneously (s.c.) with 1×10^6 MC38 colon cancer cells, 0.8×10^6 MCA205 sarcoma cells or 0.8×10^6 TC1 lung cancer cells. When tumors reached 20 to 35 mm^2 in size, the mice were treated intraperitoneally (i.p.) with cyclophosphamide (CTX, 100mg/kg) (Endoxan Baxter, was provided by Institut de Cancérologie Gustave Roussy, Villejuif, France) or anti-PD-1 mAb (250µg/mouse; clone RMP1-14) or isotype control (clone 2A3) (BioXcell, NH, USA). Depending on the experimental setting, mice were injected with CTX once or 3 times at 1-week intervals. Mice

were injected 4 times at 3-day intervals with anti-PD-1 mAb. Tumor size was routinely monitored every 3 days by means of a caliper.

Gut colonization with dedicated commensal species. *Enterococcus hirae* 13144 were originally isolated from spleens of SPF mice treated with CTX in our laboratory. *E. hirae 708* was provided by INRA (P. Langella), while *E. hirae 13344, ATCC9790* were provided by Prof. Cattoir, CHU de Caen, France. *L. plantarum* was provided by Prof. Ivo Gomperts Boneca from the Institut Pasteur strain repository, France. All *E.hirae* IGR strains were isolated from the stools of NSCLC patients in our laboratory, according to patient informed consent and local IRB approval (ancillary study "Oncobiotics"). All bacteria were grown in COS plates for 24 to 48 hours at 37°C in aerobic conditions. Colonization of ATB pre-treated mice was performed by oral gavage with 100 µl of suspension containing 1×10^9 bacteria. For bacterial gavage, we used suspensions of 10^{10} CFU/mL, monitored using a fluorescence spectrophotometer (Eppendorf) at an optical density of 600 nm in PBS. Depending on the experimental setting, 2 or 6 bacterial gavages were performed for each mouse: the first, the same day as CTX injection, and then 24 hours after the injection of CTX. For anti-PD1 mAb, 5 bacterial oral gavages were performed for each mouse: the first, the same day and 24h before the first anti-PD1 injection, and the same day for the three other injections of anti-PD1 Abs. The efficacy of colonization was confirmed by culturing the feces 48 hours post-gavage. Fecal pellets were harvested and resuspended in BHI+15% glycerol at 0.1 g/mL. Serial dilutions of feces were plated onto COS plates and incubated for 48 hours at 37°C in aerobic and anaerobic conditions. After 48 hours, the identification of specific bacteria was accomplished using a Matrix-Assisted Laser Desorption/Ionisation Time of Flight (MALDI-TOF) mass spectrometer (Andromas, Beckman Coulter, France).

Culture and propagation of bone marrow-derived dendritic cells. Bone marrow-derived dendritic cells (BM-DCs) were generated by flushing bone marrow precursors from the femurs and tibia of female C57Bl/6 WT mice aged between 8 and 12 weeks. Bones were collected in sterile PBS, washed in alcohol and Iscove's medium (IMDM, Sigma-Aldrich) baths, extremities of bones were cut and flushed using a 26G needle. After red blood cell lysis, cells were cultured in IMDM supplemented with 10% of FCS + 2mM L-glutamine + 100 UI/mL penicillin/streptomycin + 50µM 2-mercaptoethanol (Sigma-Aldrich) (referred herein as complete

IMDM medium) at 0.5×10^6/mL and treated with 40ng/mL of GM-CSF (supernatant of GM-CSF transfected-cells J558) and 10 ng/mL of recombinant interleukin-4 (IL-4) for BM-DCs (from Peprotech). Cells were split at day 3 and used in experiments on day 7 or 8.

Test of memory TC1 immune response and H-2K^b restricted-peptides on splenic CD8$^+$ T cells. Interferon-γ (IFN-γ) ELISPOT assay were performed in 96-well PVDF bottomed sterile plates (Millipore MSIP S4510) by means of a commercial kit (Cell sciences, Newburyport, US) according to the manufacturer's instructions. After PVDF membrane activation with ethanol 35%, plates were coated overnight with capture antibody to IFN-γ and washed before incubation of blocking buffer during 2 hours. BM-DC (1×10^5/well) were exposed to heat-inactivated (2 hours at 65°C) bacterial strains (*E. hirae* 13144, *E.hirae* 708, *E.hirae* 13344 and *L.plantarum* at a multiplicity of infection [MOI] of 1:10) or pulsed with peptides (20μg/mL) and were added to CD8$^+$ T cells (2×10^5/well) for 20 hours at 37°C. Cells were then removed and plates were developed with a biotinylated antibody specific for IFN-γ during 1 hour and 30 minutes, followed by streptavidin-alkaline phosphatase during 1 hour. Finally, the substrate of streptavidin (BCIP/NBT buffer) was added for 5-20 min. Spots were counted by means of a CTL Immunospot Analyzer (Cellular Technology Limited, Cleveland, OH).

Vaccination of mice. BM-DCs were activated with poly I:C (10μg/mL, Invivogen) overnight before infection with heat-inactivated (2 hours at 65°C) bacterial strains (MOI 10) or pulsed with peptides (20μg/mL, peptide 2.0). After 6 hours of incubation with bacteria or 1 hour of incubation with peptides, BM-DCs were washed 3 times with PBS before subcutaneous injection in the right flank of mice (1.5×10^5 cells per mice). Mice were vaccinated twice at 10 days apart and challenged 4 weeks after the second vaccination with the minimal tumorigenic dose of MCA205 tumor cells in left flank.

Flow cytometry analyses. In experiments without tumor, spleens were harvested 7 days after the injection of CTX. In tumor growth experiments, spleens, tumors and tumor draining lymph node were harvested at different time points, 7, 14 and 21 days after the first injection of CTX into mice bearing MCA205 tumors. Excised tumors were cut into small pieces and digested in RPMI medium containing Liberase^{TM} at 25 μg/mL and DNase1 at 150 UI/mL (Roche) for 30 minutes at

37°C and then crushed and filtered twice using 100 and 40μm cell strainers (Becton & Dickinson, BD). Lymph nodes and spleen were crushed in RPMI medium and subsequently filtered through a 70 μm cell strainer. Two million splenocytes, tumor cells or lymph node cells were pre-incubated with purified antimouse CD16/CD32 (clone 93; eBioscience) for 15 minutes at 4°C, before membrane staining. Dead cells were excluded using the Live/Dead Fixable Yellow dead cell stain kit (Life Technologies). Anti-mouse antibodies for CD3 (145-2C11), CD4 (GK1.5), CD8 (eBioH35-17.2), CXCR3 (CXCR3-173), CCR9 (CW-1.2), and TMP specific tetramer (BD, BioLegend, eBioscience and Cliniscience). Stained samples were acquired on Canto II 7 colors cytometer (BD) and analyses were performed with FlowJo software (Tree Star, Ashland, OR, USA).

Human T cell responses to HLA-A*0201 restricted-TMP epitopes. Cytapheresis cones were collected from healthy volunteers (Etablissement français du sang, EFS) and peripheral blood mononuclear cells (PBMC) were separated using a Ficoll Hypaque (Sigma Aldrich) gradient. We selected only donors with the HLA-A02*01 haplotype determined by immunofluorescence and flow cytometry. PBMC were washed and resuspended in the separation medium (PBS, 1mM ethylenediaminetetraacetic acid, 2% human AB^+ serum) for magnetic bead separation. $CD14^+$ monocytic cells (human CD14 MicroBeads, Miltenyi) were enriched from 75×10^6 peripheral blood mononuclear cells (PBMC) and cultured at 0.5 x 10^6/mL in IMDM supplemented with 10% human AB^+ serum, 1% of 2 mmol/L glutamine (GIBCO Invitrogen), 1000 IU/mL GM-CSF and 1000 IU/mL IL-4 (Miltenyi). Cells were split at day 3 and used in experiments on day 6 or 7. Such (DC-like) cells were seeded in 96-well plates at 1×10^5 cells/well either alone or in the presence of peptides (20μg/mL) for 2 hours at 37°C, 5% CO2. The remaining autologous PBMC fractions were enriched for $CD8^+$ T cells ($CD8^+$ T Cell Isolation Kit, human, Miltenyi). The enriched $CD8^+$ T cells were washed, counted and resuspended at 1×10^5cells/well in RPMI-1640 supplemented with 10% human AB+ serum, 1% 2 mMol/L glutamine, 1% penicillin/streptomycin (GIBCO Invitrogen) and 50 U/mL IL-2 (Proleukin). DC-peptide/ T cell co-cultures were incubated for one week at 37°C, 5% CO_2 (medium was changed every 2 days). Then, the pools of cells were seeded in 96-well ELIspot plates at 2 x 10^5 cells/well and restimulated with or without peptides (20μg/mL) or anti-CD3/anti-CD28 coated beads (1μL/mL, Dynabeads T-Activator, Invitrogen) as a positive control for 20 hours at 37°C. IFN-γ ELISPOT

assays were performed in 96-well PVDF bottomed sterile plates (Millipore MSIP S4510) by using a IFN-γ ELISPOT kit (Cell sciences, Newburyport, Etats-Unis) according to the manufacturer's instructions.

In vitro stimulation of PBMCs from healthy volunteers and cancer patients with HLA-A2-restricted phage and cancer peptides. Cytapheresis cones were collected from healthy volunteers (EFS) and peripheral blood mononuclear cells (PBMC) were separated using a Ficoll Hypaque gradient. We selected only donors with HLA-A02*01 haplotype determined by flow cytometry with anti-HLA-A2 antibody (BB7-2 clone). 4 x 10^7 PBMC were seeded in 96 well/plates at 2 x 10^5 cells/well in RPMI 1640 medium supplemented with 8% human serum (HS), 50 IU/mL of IL-2 (Proleukin, Novartis) and stimulated with 5 µM of KLAKFASVV peptide. After 14 days, each microculture was evaluated for the percentage of specific $CD8^+$ T lymphocytes by double staining with a HLA-A2- KLAKFASVV peptide tetramer and anti-CD8 mAb (Clone RPA-T8, Biolegend) using a FACS Canto HTS. Cross-reactivity of positive microcultures was evaluated by double staining with a HLA-A2 KLQKFASTV peptide tetramer and anti-CD8. HLA-A2 /peptide monomers were produced by the recombinant platform facility P2R, from SFR Santé, as previously described (*1*). Microcultures that contained at least 0.5% of specific T cells were selected, pooled and sorted with the relevant tetramer-coated beads and amplified as previously described (*2*). After the amplification step, purity and cross-reactivity of sorted T cell lines were evaluated by tetramer/CD8 double labeling. CD107A mobilization and TNFα production were evaluated after stimulation of sorted T cells with 5 µM of each peptide (KLAKFASVV or KLQKFASTV). After a 5 hour-stimulation period in the presence of brefeldin A at 10 µg/mL (Sigma, B7651), T cells were labeled with phycoerythrin (PE)-conjugated anti-CD8 antibody (Clone RPA-T8, Biolegend) and fixed with PBS 4% paraformaldehyde (VWR, 100504-858). Lymphocytes were then stained for TNF production using APC conjugated anti-TNFα (clone Mab11, Biolegend). Concerning CD107A labeling, specific T cells were stimulated for 3 hours at 37°C in the presence of Alexa-F647-conjugated mAb specific for CD107A (clone H4A3, Biolegend). T cells were then stained with anti-CD8 antibody (Clone RPA-T8, Biolegend) and analyzed by flow cytometry.

Short-term Ag-specific T cell lines from HLA-A*0201 lung cancer patients. Peripheral blood was collected from non-small cell lung cancer (NSCLC) patients at the time of surgery, after informed consent and PBMC were isolated on a Ficoll Hypaque gradient. Only PBMC from patients bearing the HLA-A*02*01 haplotype were used for *in vitro* short-term Ag-specific stimulation. $CD8^+$ T cells were positively enriched using an anti-CD8-coated magnetic microbeads (Miltenyi Biotec) selection process resulting in more than 95% purity. $CD8^+$ T cells were seeded in 96-well plates at 2 x 10^5 cells/well in RPMI-1640 medium supplemented with 10% human serum. Autologous CD8-depleted PBMC were used as antigen presenting cells (APCs), irradiated, pulsed with TMP epitope 10 (KLAKFASVV) (5 µg/mL) for 2 hours at 37°C in 5% CO_2 and plated with $CD8^+$ T cells at a 1:3 ratio. After 24 hours, human recombinant IL-2 (Miltenyi Biotec) and IL-7 (PeproTech Inc.) (25 U/mL and 5 ng/mL, respectively) were added to the culture wells. After one week, cells were restimulated with the soluble TMP epitope 10 peptide (1 µg/mL) for an additional week before functional analysis.

HLA-A2/peptide tetramer staining. Phycoerythrin (PE)-labeled HLA-A*0201/peptide (KLAKFASVV) tetramers were used. FITC-CD8 monoclonal antibody was purchased from Miltenyi Biotec (BW135/80). Briefly, 2-3 x 10^5 short-term *in-vitro* expanded T cells were first incubated with tetramer (10 µg/mL, 30 minutes, room temperature). After washing, cells were incubated with FITC-CD8 mAb (20 minutes, 4°C). Dead cells were excluded using propidium iodide staining (MP Biomedicals). Cells were immediately acquired on BD FACS Celesta and analyzed using FACS Diva software (BD).

Interferon (IFN)-γ and granzyme B (GrB) production. 3-4 x 10^5 autologous CD8-depleted PBMC isolated from NSCLC patients were pulsed with the relevant TMP epitope 10 (KLAKFASVV) or the irrelevant TMP epitope 14 (KMAALAASA) (1 µg/mL) (Figure S13E). Alternatively, instead of autologous APC, T2 cell lines (purchased from the American Type Culture Collection and routinely checked for mycoplasma using Mycoplasma PCR Reagent, Euroclone, Italy) were used at 1 x 10^5 cells/well and pulsed (or not) with the relevant TMP epitope 10, the irrelevant TMP epitope 14, or with irrelevant MART-1 A27L (ELAGIGILTV) and gp100 209-217 (IMDQVPFSV) peptides (1 µg/mL) (Figure S13F). Whenever indicated, the HLA Class I-blocking antibody (W6/32 mAb) was added (*3*). After 1 hour incubation at 37°C in

5% CO2, autologous 2-3 x 10^5 $CD8^+$ T-cell lines were added to monitor antigen-specific activation markers, IFN-γ and GrB production. Cells were co-cultured for 5 hours at 37°C in 5% CO_2, in the presence of the protein transport inhibitor GolgiStop (BD). After 5 h, T cells were collected, washed in PBS and incubated for 30 minutes at 4°C with the following mAbs from BD Biosciences: PE-CD3 (SP34-2), APC-H7-CD8 (SK1), FITC-CD4 (SK3), BV786-CD137 (4B4-1). After washing, cells were fixed and permeabilized by means of the Cytofix/Cytoperm kit (BD Biosciences), following the manufacturer's instructions. Intracellular staining was performed for 30 minutes at room temperature by the use of following mAbs from BD Biosciences: PE-Cy7-IFN-γ (B27), and Alexa Fluor647-GrB (GB11). Cells were immediately acquired on a FACS Celesta and analyzed using FACS Diva software (BD).

MART-1 and MELOE-1-specific T cell clones and responses to bacterial peptides.

Principles.

We identified microbial analogs of non-mutated tumor-associated antigens relevant to human malignancies (such as the MART-1/Melan-A melanoma differentiation antigen or MELOE-1 abberrantly expressed antigen). In the public microbiome database (metaHIT), 5 and 11 microbial sequences shared more than 78% homology with EAAGIGILTV (from MART-1/Melan-A) (Figure S14A) and TLNDECWPA (from MELOE-1) (Figure S15A), respectively. The cross-reactivity of 11 MART-1/Melan-A -specific T-cell clones to each of the 5 bacterial peptides was measured. All the 11 T cell clones recognized 2 out of the 5 bacterial peptides with EC_{50} values similar to those found for the MART-1/Melan-A-AA27L peptide (Figure S14B). Another bacterial peptide was recognized by 2 of the 11 T cell clones, though with a low affinity (Fig S14B). The cross-reactivity of all the MART-1/Melan-A-specific T-cell clones tested might be linked to the frequent occurrence of TRAV12-2 segments (which are highly flexible) (*33*) within the alpha chains of their TCRs (Table S8). We also evaluated 11 microbial peptides for their capacity to stimulate 10 MELOE-1 specific T cell clones, which exhibited a bias towards another TRAV segment (TRAV19, Table S9). Four out of 10 MELOE-1 specific T cell clones responded to at least 1 bacterial peptide (Figure S15B). One of these peptides, differing from the cognate peptide at positions 6 (P6) and 8 (P8) (predicted as weak binder to the HLA-A2 molecule), was recognized by 3 MELOE-1-specific T-cell clones with EC_{50} values similar to the one observed for the WT MELOE-1 peptide (Figure S15B). The two other analogous peptides with different P6

and P8 residues were also recognized by two T cell clones, with an EC_{50} around 10^{-9} M (Figure S15B), suggesting that these two positions are not essential for TCR recognition.

Calculation of EC50 for bacterial epitopes.

EC50 of MART-1 and MELOE-1-specific T-cell clones were evaluated for each bacterial peptide, by measuring TNFα production after co-culture with TAP-deficient T2 cells loaded with a range of peptides, at an effector/target ratio of 1:2. After a 5h-stimulation period in the presence of brefeldin A at 10 µg/mL (Sigma, B7651), T cells were labeled with PE-conjugated specific anti-CD8 antibody (Clone RPA-T8, BioLegend) and fixed with PBS 4% paraformaldehyde (VWR, 100504-858). Lymphocytes were then stained for cytokine production using APC conjugated anti-TNFα (clone cA2, Miltenyi Biotec).

Stool detection of phage TMP sequence by PCR in human or mouse samples (Figure S10). We cultivated the stools (from cancer patients) or ileal material (mice) after several dilutions in aerobic conditions and permissive medium to allow for the isolation of enterococci colonies (according to a procedure described in (*4*). We performed a PCR of the TMP sequence in each single cultivatable *Enterococcus* colony. One colony was placed into 100µl of nuclease-free water to release the bacterial DNA and PCR was performed with 5µl of DNA, 12.5µl of PCR master mix (Thermofischer Scientific), 5µl nuclease-free water and 1.25µl of pairs of TMP primers (20 µM) (refer to Figure S10 for the position of the probe sets). PCR products were separated on 1.5% agarose gel containing ethidium bromide and revealed by UV exposure. The sequence of primers are: forward 5'-ACTGCAGCCGTAAAATGGGA-3' and reverse 5'-TCCGTATCGTTTGCCAGCTT-3' (amplicon 1026 bp).

Lysogenic conversion of *E. gallinarum* by the *E.hirae* 13144 phage.

In vivo. To investigate the capacity of the *E. hirae 13144* phage to lysogenize other bacterial species *in vivo*, we performed culturomic analyses of the ileal content from C57BL/6 mice subjected to oral gavage with *E. hirae* 13144 and systemic CTX therapy, followed by PCR analyses seeking TMP sequences (Figure S8A-B). We tested 7 to 18 bacterial colonies from each animal and a total of 76 colonies. We only found lysogenic conversion of *E. gallinarum* by the *E. hirae*-temperate phage *in vivo*, as confirmed by sequencing of the phage genome in the second

host (Figure 4F, Figure S8B-C). In contrast, none of the 90 colonies (mostly of *E. gallinarum)* isolated from naive mice harbored the TMP sequence (Figure S8A).

In vitro. One *E. gallinarum* strain (isolated from naïve mice) were incubated at a ratio of 1:1 (10^7 of each bacteria), in the presence of small intestinal organoids, during one hour before treatment with mafosfomide (25µg/mL). Six and twenty hours post-incubation, organoid supernatants were plated to allow for the isolation of *E.gallinarum* colonies followed by PCR-based detection of the TMP sequence on each *E.gallinarum* colony. For preparation of small intestine organoids, ileal intestinal crypts were isolated and enriched from 8-12 week old C57BL/6 mice as previously described (5) with the following modifications. Briefly, pieces of ileum washed in PBS were incubated in PBS containing 2mM EDTA for 30 minutes on ice. Fragments were then rinsed 3 times with PBS containing 10% FCS and filtered through a 70-µm cell strainer. Crypts were pelleted, washed with Advanced DMEM/F12 (ADF) (Invitrogen), resuspended in 1mL of Cultrex PathClear Reduced Growth Factor BME (Bio-Techne, Minnesota, United States) and 50µL drops were pipetted into a 24 well plate. Drops were overlayed with ADF containing the following: 100 U/mL penicillin G sodium, 100 µg/mL streptomycin sulfate, 2 mM L-glutamine, 10 mM HEPES, 1x N2 supplement, 1x B27 supplement, 50 ng/mL mEGF, 100 ng/mL mNoggin (Peprotech, Hamburg, Germany), N-acetylcysteine (Sigma) (reagents from Invitrogen unless otherwise indicated) and 10% conditioned medium of Cultrex® HA-R-Spondin1-Fc 293T Cells (Bio-Techne). Organoids were passaged once per week and utilized in experiments 7 days post splitting.

Transmission electron micrographs of the bacteriophage. The negative staining of particles was realized on supernatant of a co-culture of *E. hirae* 13144 and *E. gallinarum* admixed at a 1:10 ratio for 20 hours. Staining was performed using a 5% solution of ammonium molybdate. Images were acquired using a Tecnai G2, operating at 200 keV. Scale bars are shown on micrograph pictures.

Generation of TMP-expressing *E. coli.* A DNA fragment containing the P23 promoter sequence was generated by annealing two complementary primers (5'-CAATAAAAAATCAGACCTAAGACTGATGACAAAAAGAGCAAATTTTGATAAAATAG TATTAGAATTAAATTAAAAAGGGAGGCCAAATATAG-3' and 5'-

GATCCTATATTTGGCCTCCCTTTTTAATTTAATTCTAATACTATTTTATCAAAATTTGC TCTTTTTGTCATCAGTCTTAGGTCTGATTTTTTATTGCATG-3'). The sequence was then inserted into SphI/BamHI-digested vector pDL278 (Addgene 46882, gift from Gary Dunny) (*6*) to generate vector pDL278-P23. A part of the TMP gene (N-terminal 1185 nucleotides of TMP, including the epitope TSLARFANI, fused to a C-terminal FLAG-tag) was amplified from E. hirae 13144 genomic DNA (5'-TCCGGATCCATGGCACAAAGTAAAACAGTCAAAGCG-3', 5'-CAGGAATTCTTACTTGTCGTCATCGTCTTTGTAGTCACGTAGTAAACTATCACGTAAT CGAACTTC-3') and inserted into BamHI/EcoRI-digested vector pDL278-P23 to generate vector pDL278-P23-TMP-FLAG. Mutations in the epitope were introduced using the QuikChange Lightning Kit (Agilent). Primers 5'-AACGAGCTAAGGCAGTAGCAGCTGTATCTGCAGAC-3' and 5'-GTCTGCAGATACAGCTGCTACTGCCTTAGCTCGTT-3' were used to mutate position 2 (S to A, pDL278-P23-TMP-mut2-FLAG), primers 5'-ATTAGCAAAACGAGCGAAGGAAGTAGCAGCTGTATCTG-3' and 5'-CAGATACAGCTGCTACTTCCTTCGCTCGTTTTGCTAAT-3' were used to mutate position 3 (L to F, pDL278-P23-TMP-mut3-FLAG). To generate the control plasmid pDL278-P23-EGFP, EGFP was amplified from pCIB1(deltaNLS)-pmGFP (Addgene 28240, gift from Chandra Tucker (*7*)) using primers 5'-CTTGGATCCATGGTGAGCAAGGGCGAG-3' and 5'-CAGGAATTCCTACATAATTACACACTTTGTC-3' and inserted into BamHI/EcoRI-digested vector pDL278-P23. Plasmids were transformed into chemically competent E.coli DH5α (NEB) and the presence of plasmids with the correct insert was verified by sequence analysis (5'-CCCAGTCACGACGTTGTAAAACG-3' and 5'-GAGCGGATAACAATTTCACACAGG-3'). Expression of EGFP and TMP-FLAG in E. coli was verified by western blot analysis using antibodies targeting GFP (Cell Signaling, 2956) or FLAG (Sigma-Aldrich, F7425), respectively.

CRISPR/Cas9-mediated mutations of mouse *Psmb4* in MCA205 and TC1 lung cancer cells. Wild type MCA205 cell line was purchased from the American Type Culture Collection (ATCC, Manassas, VA, USA) and was maintained in RPMI-1640 medium (Thermo Fisher Scientifc, Inc., Waltham, MA, USA) supplemented with 10% FBS (Thermo Fisher Scientific, Inc), 100 U/mL penicillin and 100µg/mL streptomycin (Thermo Fisher Scientific, Inc.) at 37˚C. For the CRISPR knock in mutations, we designed the gRNA (sequence AGATATTGCGGAAACGAGCC) by using the CRISPR design tool developed by the Zhang lab (http://crispr.mit.edu/).

Oligonucleotides containing the designed sequence were synthesized (Sigma) and ligated into the pX458 backbone (Addgene #48138, (*8*)) containing the Cas9 gene (human codon-optimised and fused with 2A-GFP allowing for selection) under a CBh promoter and the cloned sgRNA under a U6 promoter. Homology templates (sequence attached) containing the mutation sites were synthesized by Invitrogen GeneArt Gene Synthesis (Thermo Fisher Scientifc, Inc.). The cloned pX458 plasmid and synthesized homology arms were cotransfected into MCA205 cells by means of lipofectamine 3000 (Thermo Fisher Scientific, Inc.) following the manufacturer's protocol. Forty-eight hours after transfection, GFP-positive cells were sorted to 96-well plates as single cells before surviving clones were expanded in duplicated conditions, one for frozen storage at -80 and the other for genomic DNA extraction. The targeted region in genomic DNA from clones was further amplified by PCR using the Phusion® High-Fidelity PCR Master Mix (New England BioLabs; pswich, MA, USA) and primers 5'CTCAGGGACCCTTTTCACGA 3' and 5'CCCACTCCCTGTTCTACACA 3', and purified with the Monarch® DNA Gel Extraction Kit (New England BioLabs) before being sent to Eurofins Genomics GmbH (BERSBERG GERMANY) for sequencing with the primer 5'GGACCCTTTTCACGATTCAGG 3'. Positive clones were expanded and subjected to DNA extraction for further validating the mutations.

Genome sequencing and analysis. The whole genome sequence of 5 *E. hirae* (13144, 708, 13152, 13344 and EH-17) strains was determined with PacBio technology (GATC Biotech, Konstanz, Germany). Genomic DNA was isolated from 15 other *E. hirae* isolates using the using the Quick-DNA fungal/bacterial miniprep kit (Zymo Research, Irvine, CA) according to the manufacturer's recommendations. After DNA shearing, the DNA libraries were prepared using the NEBNext Ultra DNA library prep kit for Illumina (New England Biolabs, Ipswich, MA) and sequenced as paired-end reads (2 x 300 bp) using an Illumina MiSeq platform and the MiSeq reagent kit version 3. The Illumina reads were trimmed using Trimmomatic (*9*), quality filtered with the Fastx-toolkit (http://hannonlab.cshl.edu/fastx_toolkit/) and assembled using SPAdes (*10*). Protein sequences were predicted using prokka v1.11 software (*11*). Prophage regions were detected using PHAST software. Predicted proteins were annotated using BLASTp against the National Center for Biotechnology Information (NCBI) non- redundant (NR) database.

Phylogenomic and comparative genomics. Single nucleotide polymorphisms in 20 *E. hirae* genomes was investigated using the parsnp program (*12*) and using the genome of strain 13144

genome as a reference. Phylogenetic analysis was performed by considering the 47,303 polymorphic sites retained in the core genome of the 20 genomes. Maximum likelihood phylogeny was constructed using Fastree (*13*). Phylogenetic tree was visualized using figtree (http://tree.bio.ed.ac.uk/ software/figtree/). Complete proteome sequences of 20 *E. hirae* strains were compared using by BlastP and pairwise alignments using ClustalW. We clustered the *E. hirae* homologous genes using orthoMCL (*14*) on the translated protein sequences of all predicted genes with a conservative parameter value of 70% amino acid sequence identity and 50% sequence coverage. The determination of the different unique core genomes was based on the homology clusters found by orthoMCL.

TCR sequencing of TMP1- and PSMB4-specific CD8$^+$ T cells. H-2K^b-TMP1 tetramer binding CD8$^+$T cells were isolated from spleen, tumor draining lymph nodes and MCA205 tumor beds after animal exposure to CTX+*E.hirae* 13144, using Facs cell sorting and were pooled into two fractions (positive or negative for the H-2K^b-TMP1 staining, regardless of tissue location). H-2K^b-PSMB4 tetramer binding CD8$^+$T cells from tumor draining lymph nodes and MCA205 tumor beds were cell sorted by Facs after exposure of the animal to CTX+*E. hirae* 13144 and were pooled into 2 fractions (positive or negative for the H-2K^b-PSMB4 staining, regardless of tissue location). Moreover, H-2K^b-PSMB4 tetramer binding CD8$^+$T cells were harvested (cell sorted by FACS) from vaccine draining lymph nodes after immunization of naive mice with PSMB4 peptides admixed with TLR3 ligands. RNA from those T cell pools (positive and negative fractions) were isolated by means of lysis buffer with the RNAqueous-Kit (Invitrogen®) extraction kit, according to the manufacturer's protocol. The RNA concentration and sample integrity were determined on Nanodrop (ThermoFisher). T cell receptor (TCR) libraries were prepared with the RNA from each sample with SMARTer Human TCR α/β Profiling Kit (Takarabio) following the provider's protocol. Briefly, the reverse transcription was performed using TRBC reverse primers and further extended with a template-switching oligonucleotide (SMART-Seq v4). cDNAs were then amplified following two semi-nested PCR: a first PCR with TRBC and TRAC reverse primers as well as a forward primer hybridizing to the SMART-Seqv4 sequence added by template-switching and a second PCR targeting the PCR1 amplicons with reverse and forward primer including Illumina Indexes allowing for sample barcoding. PCR2 are then purified using AMPure beads (Beckman-Coulter). The quantification and integrity of cDNA

samples was carried out using DNA electrophoresis performed on Agilent 2100 Bioanalyser System in combination with the Agilent DNA 1000 kit, according to the manufacturer's protocol. Sequencing has been performed with Miseq (Illumina) SR-300 protocols at Institut du Cerveau et de la Moelle (Paris, France). FASTQ raw data files were processed for TRAs and TRBs sequences annotation using MiXCR (*15*) software (v2.1.10) with RNA-Seq parameter. MiXCR extracts TRA and TRB providing corrections of PCR and sequencing errors. Generation of datasets was done by concatenating the FASTQ raw data files based on the specificity of the different sorted cell population samples from the different organs. We obtained 4 datasets representing $CD8^+TMP^+$ (meaning CD8 binding to H-$2K^b$-TMP1 tetramer) $CD8^+TMP^-$, $CD8^+PSMB4^+$ and $CD8^+PSMB4^-$ TCR repertoires. These repertoires were respectively composed of 40.734, 416.541, 208 and 532.360 unique clonotypes. Venn diagrams and samples comparisons were performed using R software version 3.5.0 (www.r-project.org) and Prism (GraphPad Software, LaJolla, CA). To compare the TCR sharing of $PSMB4^+$ with TMP^+ vs TMP^- TCRs, a random sampling of 13842 αTCRs and 25057 βTCRs was performed 10 times within the TMP^- repertoire (Fig. 4H).

Statistical analyses. A statistical report has been written for each panel (online material). Data analyses and representations were performed with Prism 6 software (GraphPad, San Diego, CA, USA). Tumor size differences were calculated either using Anova or a dedicated software (https://kroemerlab.shinyapps.io/TumGrowth/). Briefly, tumor growth was subjected to a linear mixed effect modeling applied to log pre-processed tumor surfaces. P-values were calculated by testing jointly whether both tumor growth slopes and intercepts (on a log scale) were different between treatment groups of interests. Survival probabilities were estimated using the Kaplan-Meier method. Cutoffs for continuous variables were chosen using the median value or an optimal cutoff approach. Survival curves were evaluated using the log-rank test. All reported tests are two-tailed and were considered significant at P-values <0.05.

References:

1. M. Bodinier, M. A. Peyrat, C. Tournay, F. Davodeau, F. Romagne, M. Bonneville, F. Lang, Efficient detection and immunomagnetic sorting of specific T cells using multimers of MHC class I and peptide with reduced CD8 binding. *Nat. Med.* **6**, 707–710 (2000).

2. N. Labarriere, A. Fortun, A. Bellec, A. Khammari, B. Dreno, S. Saïagh, F. Lang, A full GMP process to select and amplify epitope-specific T lymphocytes for adoptive immunotherapy of metastatic melanoma. *Clin. Dev. Immunol.* **2013**, 932318 (2013).

3. C. J. Barnstable, W. F. Bodmer, G. Brown, G. Galfre, C. Milstein, A. F. Williams, A. Ziegler, Production of monoclonal antibodies to group A erythrocytes, HLA and other human cell surface antigens-new tools for genetic analysis. *Cell*. **14**, 9–20 (1978).

4. B. Samb-Ba, C. Mazenot, A. Gassama-Sow, G. Dubourg, H. Richet, P. Hugon, J.-C. Lagier, D. Raoult, F. Fenollar, MALDI-TOF identification of the human Gut microbiome in people with and without diarrhea in Senegal. *PloS One*. **9**, e87419 (2014).

5. T. Sato, R. G. Vries, H. J. Snippert, M. van de Wetering, N. Barker, D. E. Stange, J. H. van Es, A. Abo, P. Kujala, P. J. Peters, H. Clevers, Single Lgr5 stem cells build crypt-villus structures in vitro without a mesenchymal niche. *Nature*. **459**, 262–265 (2009).

6. D. J. LeBlanc, L. N. Lee, A. Abu-Al-Jaibat, Molecular, genetic, and functional analysis of the basic replicon of pVA380-1, a plasmid of oral streptococcal origin. *Plasmid*. **28**, 130–145 (1992).

7. M. J. Kennedy, R. M. Hughes, L. A. Peteya, J. W. Schwartz, M. D. Ehlers, C. L. Tucker, Rapid blue-light-mediated induction of protein interactions in living cells. *Nat. Methods*. **7**, 973–975 (2010).

8. F. A. Ran, P. D. Hsu, J. Wright, V. Agarwala, D. A. Scott, F. Zhang, Genome engineering using the CRISPR-Cas9 system. *Nat. Protoc.* **8**, 2281–2308 (2013).

9. A. M. Bolger, M. Lohse, B. Usadel, Trimmomatic: a flexible trimmer for Illumina sequence data. *Bioinforma. Oxf. Engl.* **30**, 2114–2120 (2014).

10. A. Bankevich, S. Nurk, D. Antipov, A. A. Gurevich, M. Dvorkin, A. S. Kulikov, V. M. Lesin, S. I. Nikolenko, S. Pham, A. D. Prjibelski, A. V. Pyshkin, A. V. Sirotkin, N. Vyahhi, G. Tesler, M. A. Alekseyev, P. A. Pevzner, SPAdes: a new genome assembly algorithm and its applications to single-cell sequencing. *J. Comput. Biol. J. Comput. Mol. Cell Biol.* **19**, 455–477 (2012).

11. T. Seemann, Prokka: rapid prokaryotic genome annotation. *Bioinforma. Oxf. Engl.* **30**, 2068–2069 (2014).

12. T. J. Treangen, B. D. Ondov, S. Koren, A. M. Phillippy, The Harvest suite for rapid core-genome alignment and visualization of thousands of intraspecific microbial genomes. *Genome Biol.* **15**, 524 (2014).

13. S. Guindon, J.-F. Dufayard, V. Lefort, M. Anisimova, W. Hordijk, O. Gascuel, New algorithms and methods to estimate maximum-likelihood phylogenies: assessing the performance of PhyML 3.0. *Syst. Biol.* **59**, 307–321 (2010).

14. L. Li, C. J. Stoeckert, D. S. Roos, OrthoMCL: identification of ortholog groups for eukaryotic genomes. *Genome Res.* **13**, 2178–2189 (2003).

15. D. A. Bolotin, S. Poslavsky, I. Mitrophanov, M. Shugay, I. Z. Mamedov, E. V. Putintseva, D. M. Chudakov, MiXCR: software for comprehensive adaptive immunity profiling. *Nat. Methods*. **12**, 380–381 (2015).

16. B. Routy, E. Le Chatelier, L. Derosa, C. P. M. Duong, M. T. Alou, R. Daillère, A. Fluckiger, M. Messaoudene, C. Rauber, M. P. Roberti, M. Fidelle, C. Flament, V. Poirier-Colame, P. Opolon, C. Klein, K. Iribarren, L. Mondragón, N. Jacquelot, B. Qu, G. Ferrere, C. Clémenson, L. Mezquita, J. R. Masip, C. Naltet, S. Brosseau, C. Kaderbhai, C. Richard, H. Rizvi, F. Levenez, N. Galleron, B. Quinquis, N. Pons, B. Ryffel, V. Minard-Colin, P. Gonin, J.-C. Soria, E. Deutsch, Y. Loriot, F. Ghiringhelli, G. Zalcman, F. Goldwasser, B. Escudier, M. D. Hellmann, A. Eggermont, D. Raoult, L. Albiges, G. Kroemer, L. Zitvogel, Gut microbiome influences efficacy of PD-1-based immunotherapy against epithelial tumors. *Science*. **359**, 91–97 (2018).

17. S. Simon, Z. Wu, J. Cruard, V. Vignard, A. Fortun, A. Khammari, B. Dreno, F. Lang, S. J. Rulli, N. Labarriere, TCR Analyses of Two Vast and Shared Melanoma Antigen-Specific T Cell Repertoires: Common and Specific Features. *Front. Immunol.* **9**, 1962 (2018).

Figure S1

A

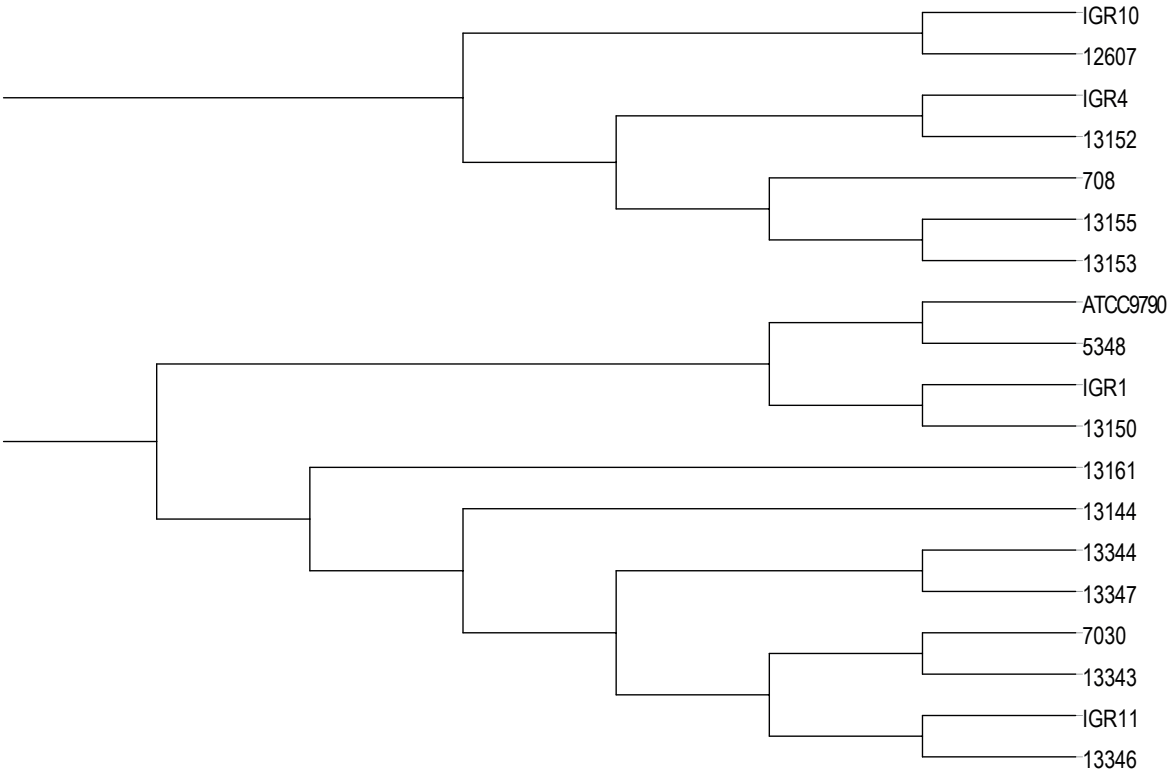
IGR10
12607
IGR4
13152
708
13155
13153
ATCC9790
5348
IGR1
13150
13161
13144
13344
13347
7030
13343
IGR11
13346

B

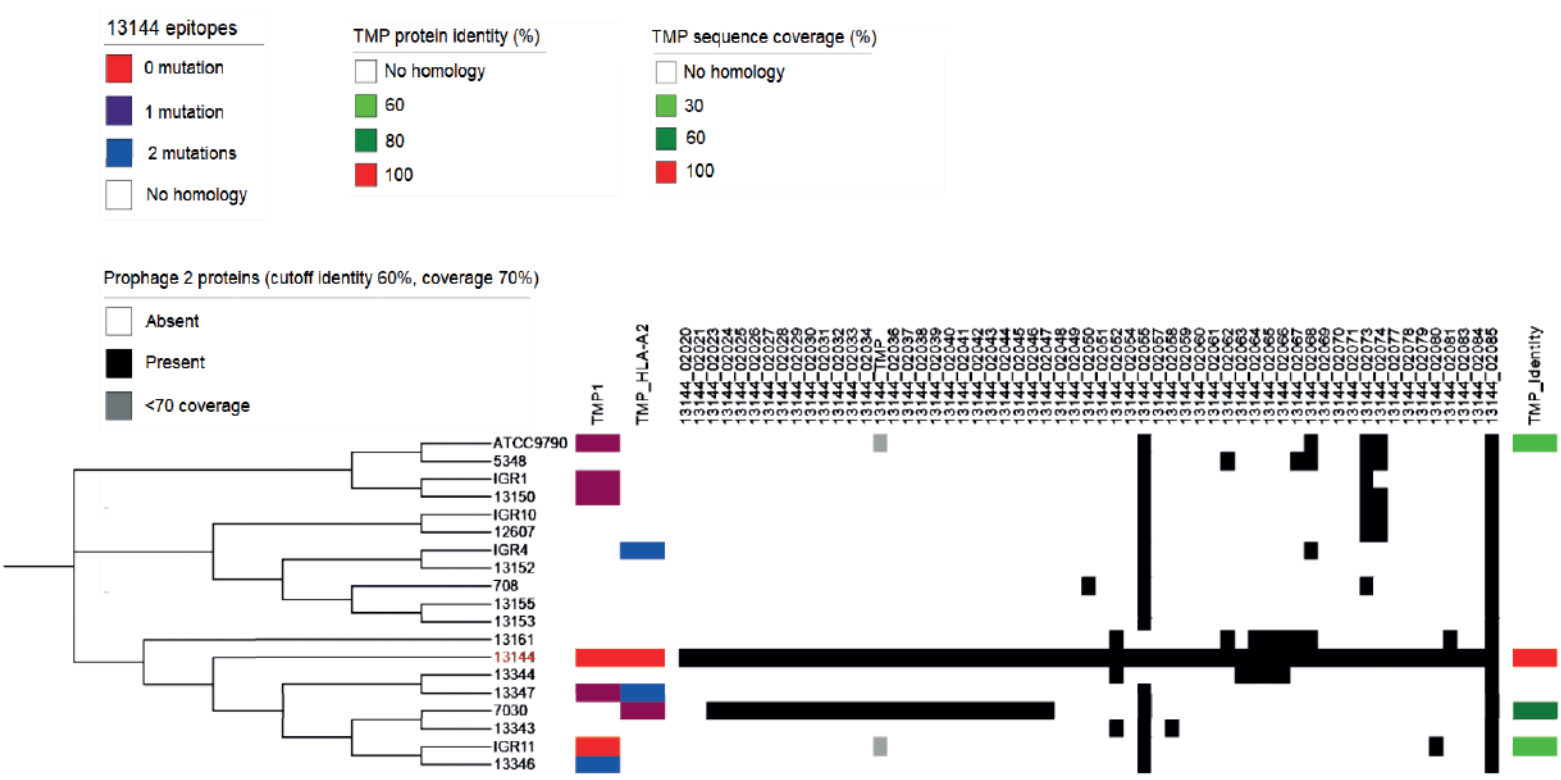
13144 epitopes
0 mutation
1 mutation
2 mutations
No homology
TMP protein identity (%)
No homology
60
80
100
TMP sequence coverage (%)
No homology
30
60
100
Prophage 2 proteins (cutoff identity 60%, coverage 70%)
Absent
Present
<70 coverage
TMP1
TMP_HLA-A2
TMP
TMP_Identity
ATCC9790
5348
IGR1
13150
IGR10
12607
IGR4
13152
708
13155
13153
13161
13144
13344
13347
7030
13343
IGR11
13346

Figure S1. Clading and comparative analysis of *E. hirae* 13144 39.2kb-prophage protein sequence with other *E. hirae* strains.

A. Phylogenetic tree of 19 *E.hirae* genomes based on SNP alignments.

B. A particular genomic trait of *E. hirae* 13144 is that it encodes two intact prophage regions (of 40.6 kb and 39.2 kb) showing weak sequence identities with the most common *Enterococcus* phage phiEf11 *vB_EfaS_IME197* (14% and 11% of shared genes, respectively) (Table S3). Comparative analysis of the 39.2kb prophage of *E. hirae* 13144 with 18 other sequenced *E. hirae* genomes showed that this phage was strain-specific, although portions of its genome were detectable in other *E.hirae* strains. Comparative analysis through a "heatmap" clustering based on a matrix of presence (black) and absence (white) of the *E.hirae* 13144 39.2kb-prophage protein sequence or the TMP1 epitope and HLA-A2 TMP epitope 10 without mutation (red), with 1 mutation (violet) or 2 mutations (blue).

Figure S2

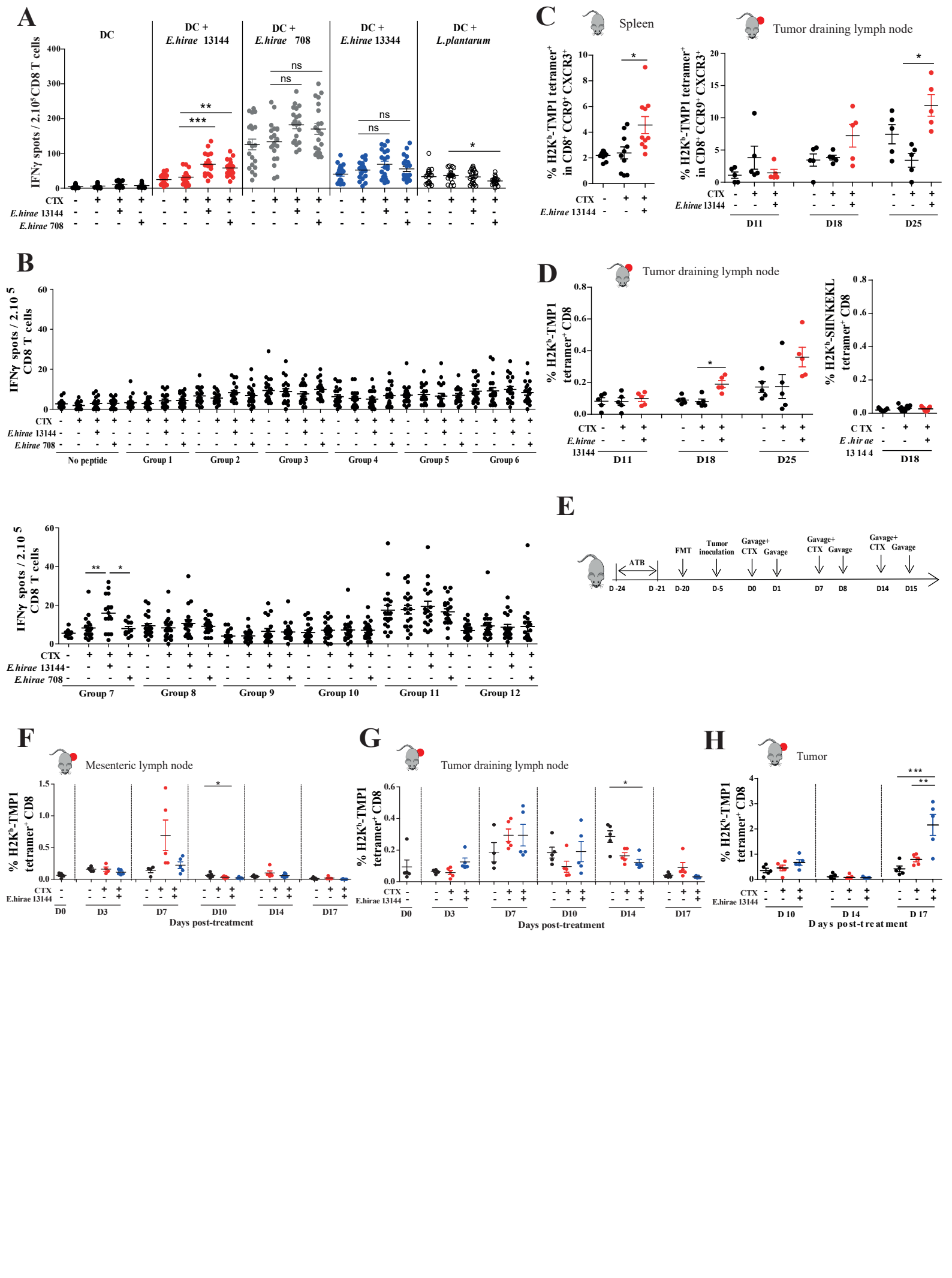
A
DC
DC + E.hirae 13144
DC + E.hirae 708
DC + E.hirae 13344
DC + L.plantarum
IFNγ spots / 2.10^5 CD8 T cells
CTX
E.hirae 13144
E.hirae 708
B
IFNγ spots / 2.10^5 CD8 T cells
No peptide
Group 1
Group 2
Group 3
Group 4
Group 5
Group 6
Group 7
Group 8
Group 9
Group 10
Group 11
Group 12
C
Spleen
Tumor draining lymph node
% H2K^b-TMP1 tetramer+ in CD8+ CCR9+ CXCR3+
D11
D18
D25
D
Tumor draining lymph node
% H2K^b-TMP1 tetramer+ CD8
% H2K^b-SHNKEKL tetramer+ CD8
E
ATB
FMT
Tumor inoculation
Gavage+ CTX
Gavage
D -24
D -21
D-20
D-5
D0
D1
D7
D8
D14
D15
F
Mesenteric lymph node
% H2K^b-TMP1 tetramer+ CD8
Days post-treatment
G
Tumor draining lymph node
% H2K^b-TMP1 tetramer+ CD8
Days post-treatment
H
Tumor
% H2K^b-TMP1 tetramer+ CD8
Days post-treatment

Figure S2. Identification of group 7 as the only group of peptides containing an immunogenic one.

A-B. Naive mice were treated with broad spectrum antibiotics (streptomycin, colistin, ampicillin, vancomycin) for 3 days before oral gavage with *E. hirae* strain 13144 or 708 ($1x10^9$ bacteria) was performed prior to and after systemic administration of cyclophosphamide (ip CTX - 100 mg/kg) or saline solution (NaCl) at day 4 once (like in Fig. 1C). One week later, purified $CD8^+$ T splenocytes were restimulated *ex vivo* in a recall assay with bone marrow-derived DC loaded with saline or distinct heat killed (65°C during 2 hours) bacterial strains (A) or groups of peptides (Table S2) (B). IFNγ-secreting $CD8^+$T cells (spots) were determined after 24h of coculture. Each dot represents one mouse. The experiment (with 5 mice/group) was performed three times. Statistical analyses revealed that only group 7 of peptides induced a significant response (B). C. Flow cytometric determination of H-$2K^b$/TSLARFANI tetramer-binding $CD8^+$ T cells in the spleen of naive mice (left panel) and tumor draining lymph node (right panel) of tumor bearers in the gate of $CXCR3^+CCR9^+$ double positive cells. D. Flow cytometry analyses of H-$2K^b$/TSLARFANI (left panel) or H-$2K^b$/SIINFEKL (right panel) tetramer binding CTL in tumor draining lymph nodes at various time points in tumor bearing mice treated with CTX and *E. hirae* 13144 (like in Fig. 1A). One representative experiment out of two yielding similar conclusions is shown. Each dot represents one animal, each experiment containing 5-6 mice/group. Data from two independent experiments are depicted. E-H. Avatar mice are SPF C57BL/6 animals treated with 3 days of ATB to allow establishment of a fecal microbial transplant (FMT from a breast cancer patient) 21 days prior to *CTX+E. hirae* 13144 therapy (E). Kinetic study of H-$2K^b$/TSLARFANI tetramer-binding $CD8^+$ T cells by flow cytometry analyses in various organs (mesenteric lymph nodes (mLN) (F), tumor draining lymph nodes (tdLN) (G) and tumor beds (MCA205) (H) during a therapy of established MCA205 with the combination of CTX+*E. hirae* 13144 in human fecal material (FMT) subjected avatar mice according to the experimental setting detailed in E. Each dot represents one animal, each experiment containing 5-6 mice/group. Data from one representative experiment are depicted. ANOVA statistical analyses (Kruskal-wallis test): $*p<0.05$, $**p<0.01$, $***p<0.001$. Refer to the statistical report.

Figure S3

TMP 39.2-kb prophage (1506 aa)

Figure S3. *E. hirae* 13144 39.2kb-prophage sequence alignment with location of the TMP protein and TMP epitopes. The position of the H-2K^{b}-restricted TMP1 epitope and HLA-A2*0201 TMP epitope 10 are indicated in red and green, respectively.

Figure S4

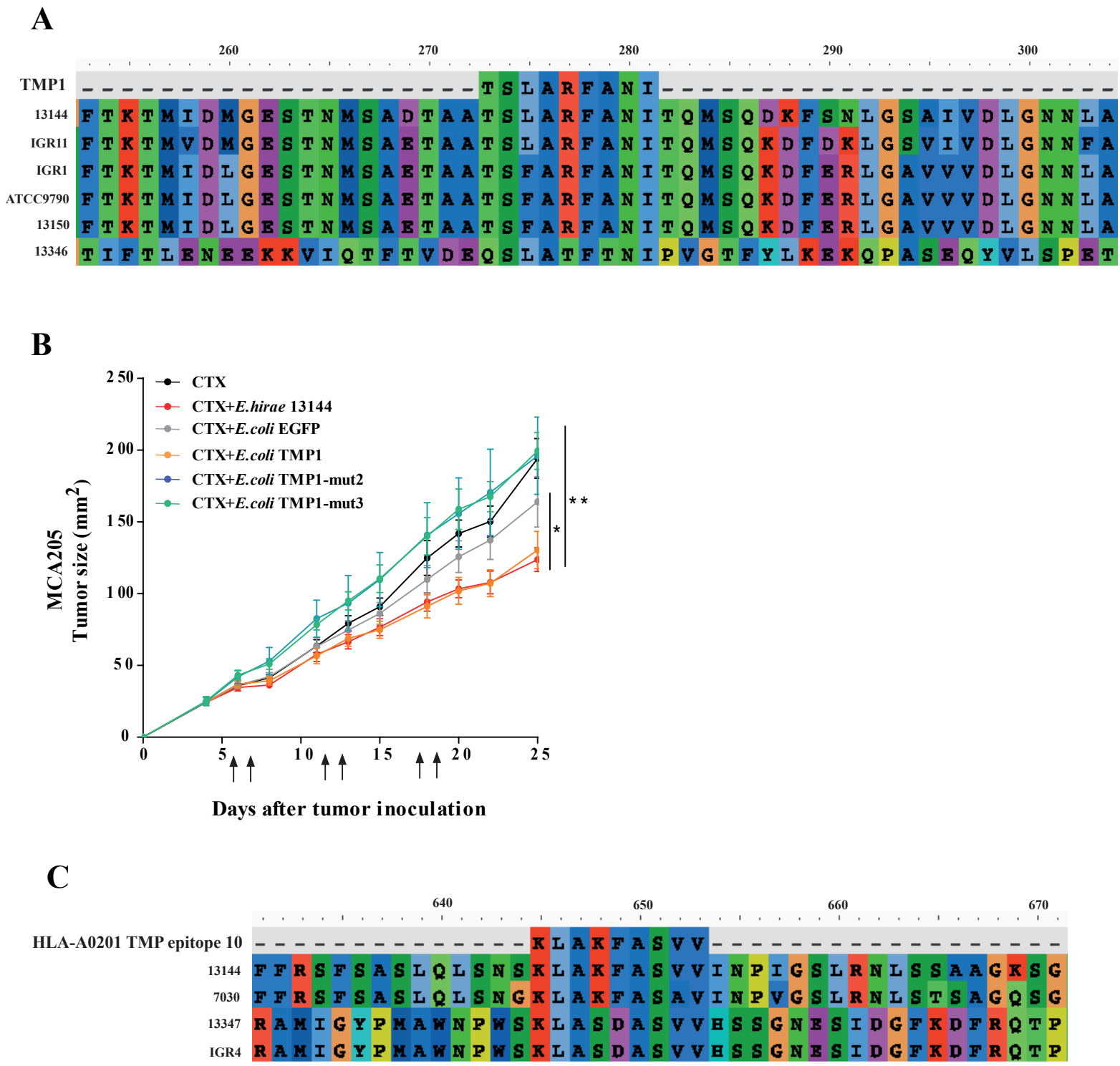
A
260
270
280
290
300
TMP1
13144
IGR11
IGR1
ATCC9790
13150
13346
B
CTX
CTX+E.hirae 13144
CTX+E.coli EGFP
CTX+E.coli TMP1
CTX+E.coli TMP1-mut2
CTX+E.coli TMP1-mut3
MCA205 Tumor size (mm2)
Days after tumor inoculation
*
**
C
640
650
660
670
HLA-A0201 TMP epitope 10
13144
7030
13347
IGR4

Figure S4. Sequence alignment of the immunogenic epitope region within 39.2kb-prophage of *E. hirae* 13144. A. The immunogenic peptide TMP1 (TSLARFANI, A) from *E. hirae* 13144 identified in Figure 1 and Figure S2 is aligned to sequences from other *E.hirae* strains tested in this study. B. Complete tumor growth curves of the experiment shown in Fig. 2D. C57BL/6 mice bearing MCA205 sarcomas were treated with CTX and gavaged with *E. hirae* 13144 or *E.coli* genetically modified to express TMP1 (TSLARFANI), TMP1 mut2 (TALARFANI), TMP1 mut3 (TSFARFANI) or EGFP sequence (as control). The means±SEM of tumor sizes at different time points for 12-18 animals, gathered from 2-3 independent experiments are shown. C. The immunogenic peptide HLA-A*0201 TMP epitope 10 (KLAKFASVV) from *E. hirae* 13144 identified is aligned to the sequences from other *E.hirae* strains.

Figure S5

A

TMP-FLAG = TSLARFANI

MAQSKTVKAVLTAIDKGFTQTMGSATSSLKKLSSNASDIPSNLNTVSGAMKSFGDKTASIGQSIEKVGGSMTKGITLPIAGAVGAVTTAA
VKWESAFTGVKKTNDEMVDSNGKVIYSYDDLEKGLRDLAKELPTSHEEIAKVAEAAGQLGIKTDKVVGFTKTMIDMGESTNMSADTAA
TSLARFANITQMSQDKFSNLGSAIVDLGNNLATTESEITEMGLRLAGAGKQIGMTEGDIVGFAAALSSVGIEAEAGGSAFSRLMVQMQ
LATETGVKAFEPLKQAVAIQGVSWEKFVHAVNWGGKELTAVSKQMGVPASELKKLYKEASKASGSLEDFANVTGRTGEEFAELFKSNP
SQAMIEFIQGLKDSEKHGISAIKVLDMGITEVRLRDSLLRDYKDDDDK

TMP-mut2-FLAG (mutation in position 2) = TSLARFANI to TALARFANI

MAQSKTVKAVLTAIDKGFTQTMGSATSSLKKLSSNASDIPSNLNTVSGAMKSFGDKTASIGQSIEKVGGSMTKGITLPIAGAVGAVTTAA
VKWESAFTGVKKTNDEMVDSNGKVIYSYDDLEKGLRDLAKELPTSHEEIAKVAEAAGQLGIKTDKVVGFTKTMIDMGESTNMSADTAA
TALARFANITQMSQDKFSNLGSAIVDLGNNLATTESEITEMGLRLAGAGKQIGMTEGDIVGFAAALSSVGIEAEAGGSAFSRLMVQMQ
LATETGVKAFEPLKQAVAIQGVSWEKFVHAVNWGGKELTAVSKQMGVPASELKKLYKEASKASGSLEDFANVTGRTGEEFAELFKSNP
SQAMIEFIQGLKDSEKHGISAIKVLDMGITEVRLRDSLLRDYKDDDDK

TMP-mut3-FLAG (mutation in position 3) = TSLARFANI to TSFARFANI

MAQSKTVKAVLTAIDKGFTQTMGSATSSLKKLSSNASDIPSNLNTVSGAMKSFGDKTASIGQSIEKVGGSMTKGITLPIAGAVGAVTTAA
VKWESAFTGVKKTNDEMVDSNGKVIYSYDDLEKGLRDLAKELPTSHEEIAKVAEAAGQLGIKTDKVVGFTKTMIDMGESTNMSADTAA
TSFARFANITQMSQDKFSNLGSAIVDLGNNLATTESEITEMGLRLAGAGKQIGMTEGDIVGFAAALSSVGIEAEAGGSAFSRLMVQMQ
LATETGVKAFEPLKQAVAIQGVSWEKFVHAVNWGGKELTAVSKQMGVPASELKKLYKEASKASGSLEDFANVTGRTGEEFAELFKSNP
SQAMIEFIQGLKDSEKHGISAIKVLDMGITEVRLRDSLLRDYKDDDDK

B

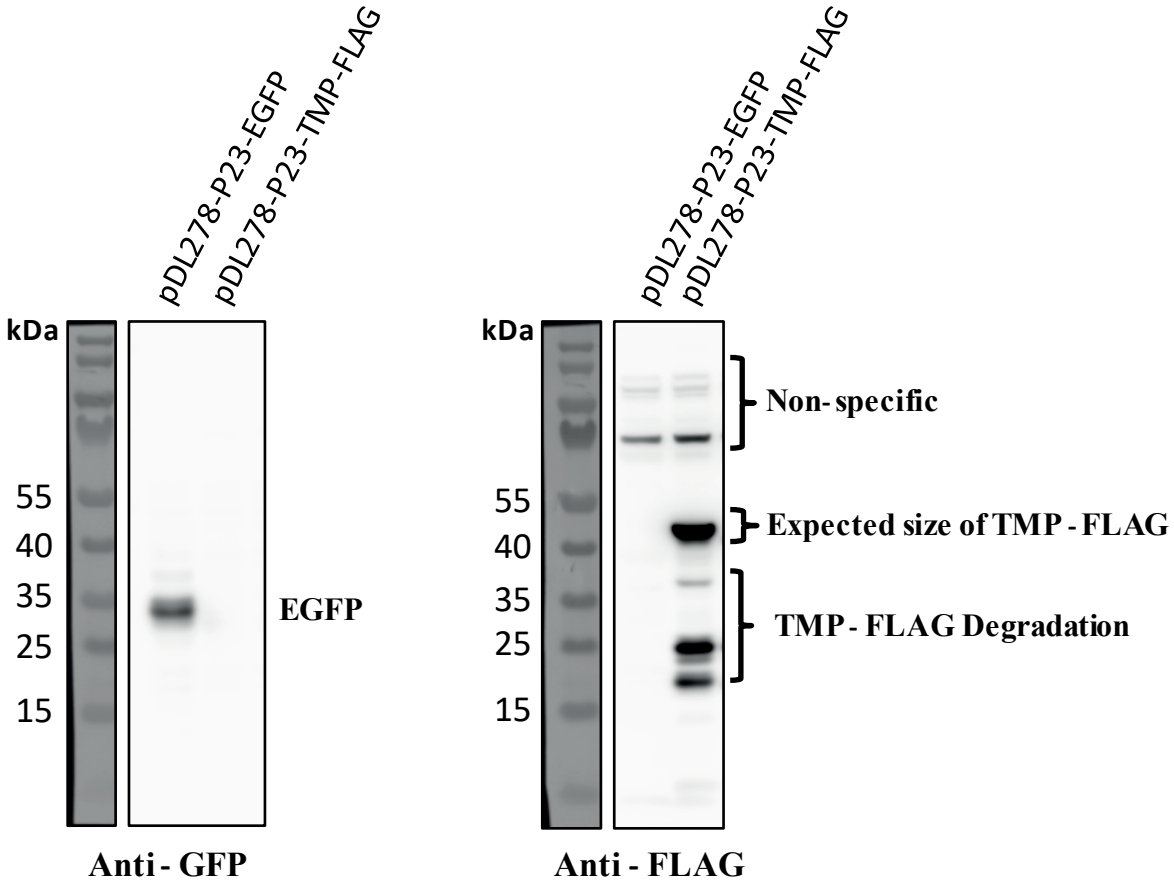

Figure S5. Sub-cloning expression of part of the TMP gene in *E.coli.*

A. Amino acid sequences of TMP-FLAG, TMP-mut2-FLAG and TMP-mut3-FLAG expressed in *E. coli* DH5α. Note that only the N-terminal part of the TMP protein, including the indicated variants of the epitope (green), was expressed as fusion protein with a C-terminal FLAG tag (blue). B. Western blot analysis demonstrating expression of EGFP and TMP-FLAG in *E. coli* strains transformed with pDL28-P23-EGFP or pDL28-P23-TMP-FLAG, respectively.

Figure S6

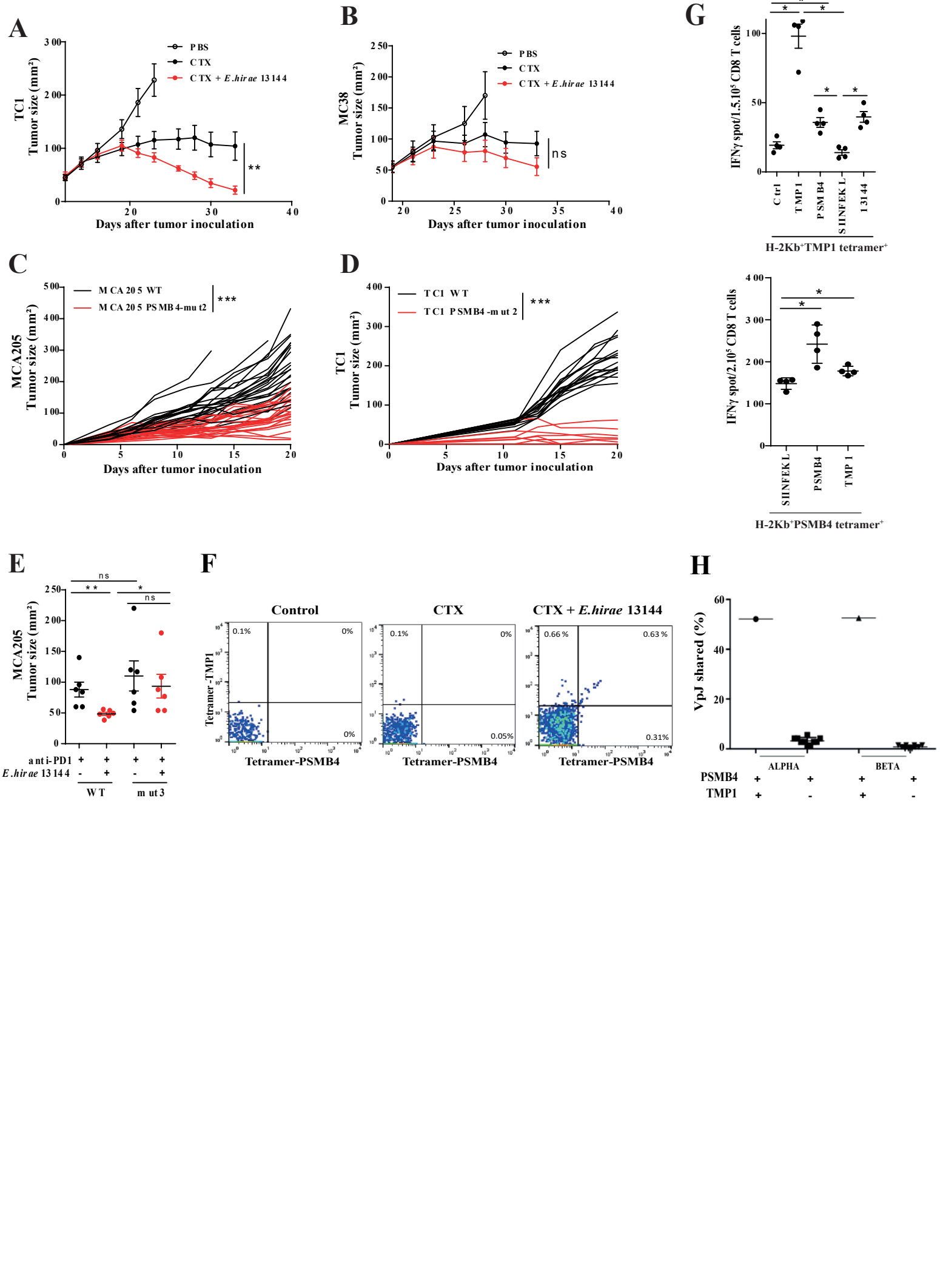
A
TC1
Tumor size (mm²)
PBS
CTX
CTX + E.hirae 13144
**
Days after tumor inoculation
B
MC38
Tumor size (mm²)
PBS
CTX
CTX + E.hirae 13144
ns
Days after tumor inoculation
G
IFNγ spot/1.5.10⁵ CD8 T cells
Ctrl
TMP1
PSMB4
SIINFEKL
13144
H-2Kb⁺TMP1 tetramer⁺
C
MCA205
Tumor size (mm²)
MCA205 WT
MCA205 PSMB4-mut2
***
Days after tumor inoculation
D
TC1
Tumor size (mm²)
TC1 WT
TC1 PSMB4-mut2
***
Days after tumor inoculation
IFNγ spot/2.10⁵ CD8 T cells
SIINFEKL
PSMB4
TMP1
H-2Kb⁺PSMB4 tetramer⁺
E
MCA205
Tumor size (mm²)
ns
**
*
ns
anti-PD1
E.hirae 13144
WT
mut3
F
Control
CTX
CTX + E.hirae 13144
Tetramer-TMP1
Tetramer-PSMB4
0.1%
0%
0%
0.1%
0%
0.05%
0.66%
0.63%
0.31%
H
VpJ shared (%)
ALPHA
BETA
PSMB4
TMP1

Figure S6. Molecular mimicry between the TMP1 phage and the PSMB4 oncogenic driver.
A-B. Tumor growth of TC1 (A) and MC38 (B) cancers with or without therapy combining CTX ± *E. hirae* 13144 (or saline) following the experimental setting described in Fig1A. C-D. Tumor growth of WT clones or clone harboring a knock-in mutation in position 2 (mut2) of GSLARFRNI for MCA205 (C) and TC1 (D). Each line represents one animal. Two concatenated experiments comprising each 6 mice/group are depicted. E. Tumor sizes at day 9 of SPF mice implanted with WT or mut3 MCA205 clones treated every 3 days three times with anti-PD1 ± *E. hirae* 13144. F. Flow cytometric determination of splenic T cells co-staining with two different tetramers (TMP1 related H-2K^{b}/TSLARFANI or PSMB4-related GSLARFRNI/H-2K^{b} complexes). Representative dot plot of CD3^{+}CD8^{+} splenic T lymphocytes staining with either or both tetramers in one representative tumor bearing animal treated with PBS, or CTX or CTX+*E.hirae 13144*. G. Cells were prepared following a protocol of *in vitro* expansion (detailed in Figure 4B) in which BM-DC were pulsed with TMP1 or PSMB4 peptide. The number of IFNγ secreting CD8^{+} GSLARFRNI/H-2K^{b+} (reexpanded after *in vitro* stimulation with PSMB4 peptides, and apostrophed "CD8^{+}PSMB4^{+}" on the graph) after stimulation with BM-DC pulsed with the three different peptides, and the number of IFNγ secreting CD8^{+} H-2K^{b}/TSLARFANI^{+} (reexpanded after *in vitro* stimulation with TMP1 peptides and apostrophed "CD8^{+}TMP1^{+}" on the graph) after stimulation with BM-DC pulsed with the three different peptides are both depicted in two representative experiments (lower and upper graph respectively). Of note, the binding affinity for H2-K^{b} of GSLARFRNI peptide is lower than that of TSLARFANI (EC50 :216.85 versus 7.81 nM respectively). We did not observe any IFNγ secretion by the negative fraction CD8^{+} H-2K^{b}/TSLARFANI^{-} cells. H. TCRα/β sequences shared between PSMB4-specific TCRs and TCRs from CD8^{+} T cells that bind H-2K^{b}TMP1-tetramers or fail to do so. Each point represents the result of a random sampling of the same number of clonotypes as for the comparison with TMP1-specific TCRs. Mann Whitney test or ANOVA statistical analyses (Kruskal-wallis test): *$p<0.05$, ** $p<0.01$, ***$p<0.001$. Refer to the statistical report.

Figure S7

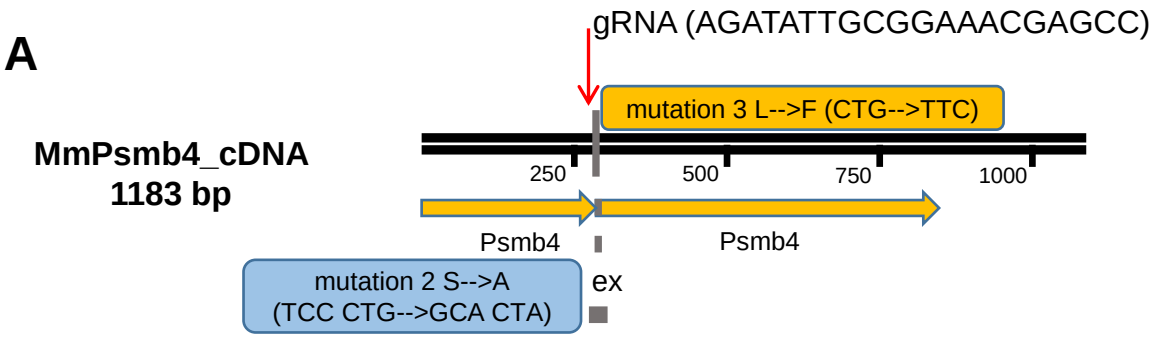
A
gRNA (AGATATTGCGGAAACGAGCC)
mutation 3 L-->F (CTG-->TTC)
MmPsmb4_cDNA
1183 bp
250
500
750
1000
Psmb4
Psmb4
mutation 2 S-->A
(TCC CTG-->GCA CTA)
ex

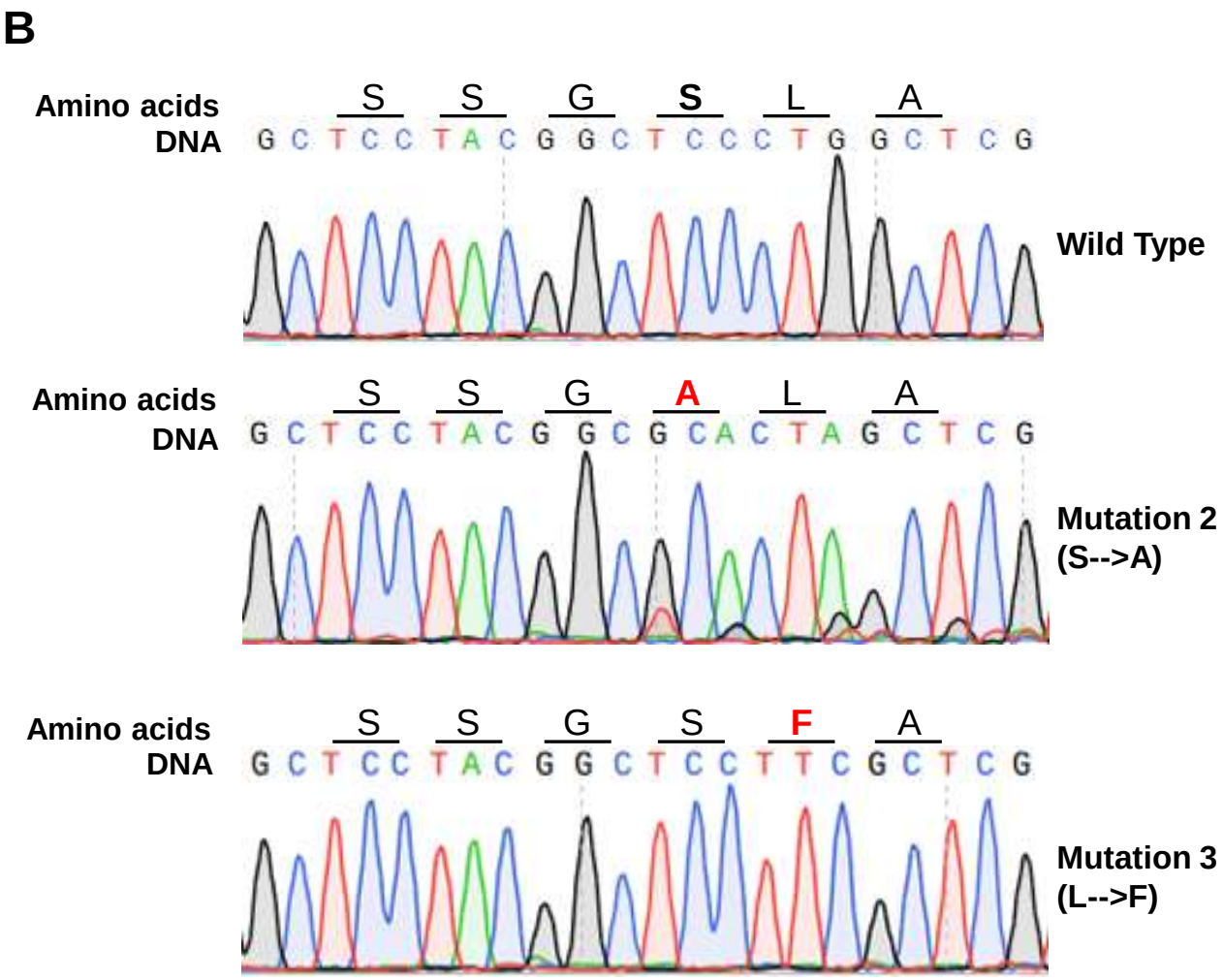
B
Amino acids
DNA
S S G S L A
G C T C C T A C G G C T C C C T G G C T C G
Wild Type
Amino acids
DNA
S S G A L A
G C T C C T A C G G C G C A C T A G C T C G
Mutation 2
(S-->A)
Amino acids
DNA
S S G S F A
G C T C C T A C G G C T C C T T C G C T C G
Mutation 3
(L-->F)

Figure S7. Generation of *pmsb4*-mutated MCA205 cell lines by means of the CRISPR/Cas9 technology. A. Schematic diagrams of *Psmb4* cDNA, and the designed mutation sites. The target site of sgRNA and point mutations are indicated. B. Representative sequence electropherograms for the validation of Pmsb4 mutation 2 and mutation 3 introduced by CRISPR/Cas9. Mutated amino acids are highlighted in red. Similar methods were used for engineering TC1 cells.

Figure S8

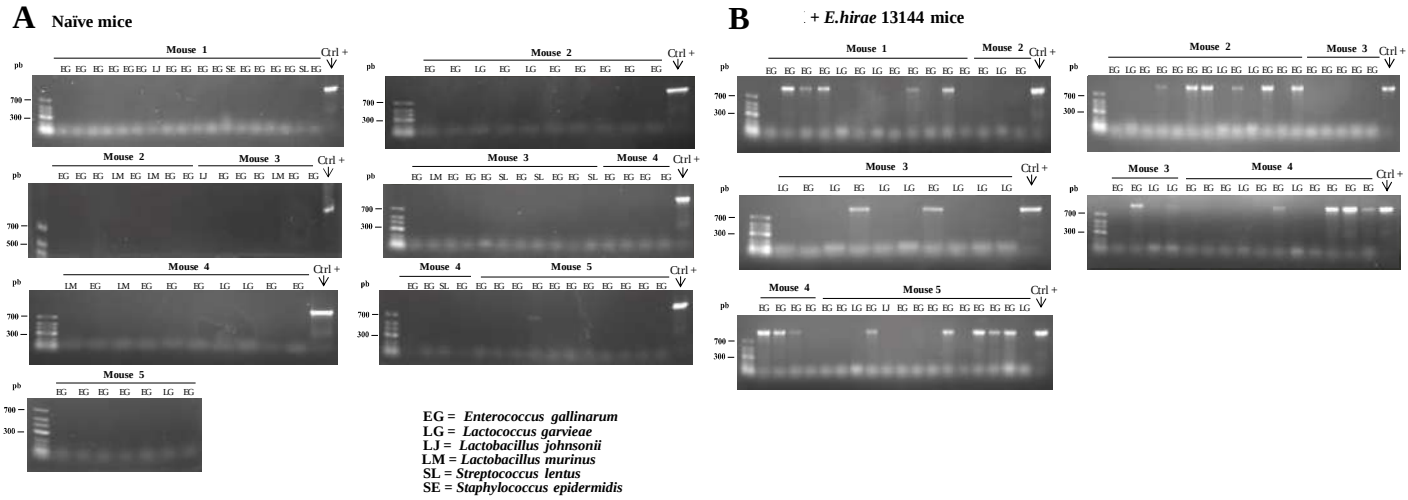
A
Naïve mice
B
+ E.hirae 13144 mice
Mouse 1
Mouse 2
Mouse 3
Mouse 4
Mouse 5
Ctrl +
pb
700
500
300
EG = Enterococcus gallinarum
LG = Lactococcus garvieae
LJ = Lactobacillus johnsonii
LM = Lactobacillus murinus
SL = Streptococcus lentus
SE = Staphylococcus epidermidis

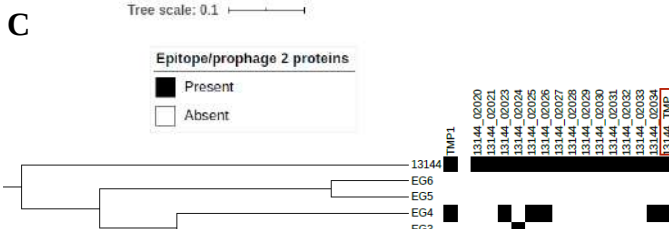
C
Tree scale: 0.1
Epitope/prophage 2 proteins
Present
Absent
TMP1
TMP
13144
EG6
EG5
EG4
EG3
EG2
EG1

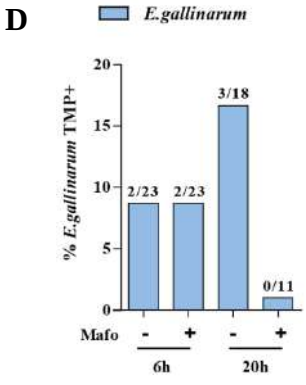
D
E.gallinarum
% E.gallinarum TMP+
20
15
10
5
0
2/23
2/23
3/18
0/11
Mafo
-
+
-
+
6h
20h

Figure S8. Identification of ileal bacterial colonies after treatment with CTX+oral gavage with *E. hirae* 13144.

A-B. PCR amplification of the TMP sequence in each colony growing after seeding of ileal content in aerobic conditions to isolate $Gram^+$ bacteria. A photograph of each agarose electrophoresis gel is shown for each animal. A depicts the results in 5 naive mice (A) and B depicts the findings after CTX+oral gavage with the phage encoding bacterium *E. hirae* 13144 (10^9 cfu) (B). Each vertical lane corresponds to the bacterium identified in MALDI-TOF. Initials are detailed in the lower part of panel A. The positive control (Ctl+) represents the DNA of *E. hirae 13144*. C. Sequence alignment of the prophage harbored by *E.hirae 13144* in 6 strains of *E. gallinarum* (EG1 to EG6) harvested from ileal material after oral gavage of naive mice with *E.hirae 13144* and therapy with CTX. Comparative analysis through a "heatmap" clustering based on a matrix of presence (black) and absence (white) of the *E.hirae* 13144 39.2kb-prophage protein sequence or the TMP1 epitope and TMP protein. D. Small intestine stem cell crypt derived-organoids were incubated with *E. hirae* 13144 and *E. gallinarum* at a 1:1 ratio for 6 or 20 hrs ± the CTX derivative mafosfamide. Then, live colonies of *E. gallinarum* were harvested and analyzed by PCR. The percentages of *E. gallinarum* which turned positive for TMP detection are indicated in a representative experiment out of two yielding similar results.

Figure S9

A

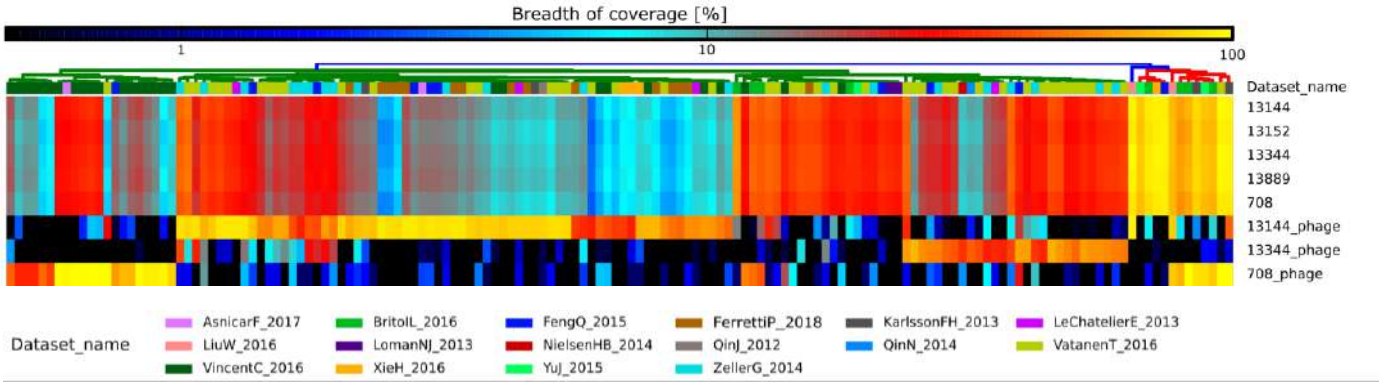
Breadth of coverage [%]
1
10
100
Dataset_name
13144
13152
13344
13889
708
13144_phage
13344_phage
708_phage
Dataset_name
AsnicarF_2017
BritoIL_2016
FengQ_2015
FerrettiP_2018
KarlssonFH_2013
LeChatelierE_2013
LiuW_2016
LomanNJ_2013
NielsenHB_2014
QinJ_2012
QinN_2014
VatanenT_2016
VincentC_2016
XieH_2016
YuJ_2015
ZellerG_2014

B

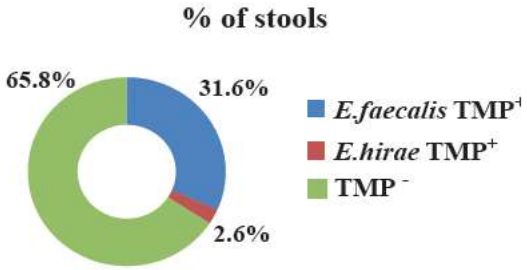
% of stools
65.8%
31.6%
2.6%
E.faecalis TMP+
E.hirae TMP+
TMP -

Figure S9. Breadth of coverage of the *E. hirae* genome and its phage in the MG reference catalog and culturomics analyses of patients stools. A. Breadth of coverage (BOC) of different *E.hirae* sequences *(E.hirae* 13144, 708, ATCC9790) and its phage in 3,027 adult and mother-infant metagenomes (mostly from human stools but also from various mucosae) by reference-based mapping of metagenomic reads from 17 publicly available datasets annotated in curatedMetagenomicData. The BOC measures the fraction of the genome that is covered by the reads in the metagenomes. The color code is indicated with highest BOC towards yellow/red colors and no BOC in black. We first screened a total of 3,027 adult and mother-infant metagenomes (mostly from human stools but also from other mucosae) by reference-based mapping of metagenomic reads from 17 publicly available datasets annotated in curatedMetagenomicData to assess the breadth of coverage (BOC) of the *E. hira*e genome and its phages. *E. hirae* was present with 100% confidence (i.e. BOC > 80%) in 13 samples from disparate geography, age and datasets. In another ~40 cases, the presence of *E. hirae* was very likely but could not be confirmed with high confidence because of insufficient sequencing depth. In 70% of the samples in which *E. hirae* was confidently found, one of the three phage sequences (from *E. hira*e 13144, 708 or 13344) were also detected, though in a partially mutually exclusive fashion (Figure S9A). Of note, the *E. hirae* 13144 phage was detectable in many samples lacking the presence of the *E. hirae* core genome, suggesting that other bacteria than *E. hirae* can host this phage. Analysis of the global prevalence of these phages (irrespective of the presence of *E. hira*e) further confirmed their mutually co-exclusion in the microbiome. We could detect the presence of phage 13144 at 0.66 BOC in three mother-infant paired stool specimens and in the infants at 1, 3, and 7 days after birth suggesting that this phage (and its host) can be vertically transmitted from mothers to infants and then colonize the neonate. We complemented this analysis by a metagenomic-assembly based screening of 9,428 metagenomes, confirming the presence of phage 13144 in humans across the world at a low prevalence (272 positive samples), though possibly with a overrepresentation among a non-Westernized population from Madagascar (19 positive samples). Importantly, this analysis highlighted an increased prevalence of the phage (57%) in fecal microbiomes from children (representing 16% of all metagenomes, Fisher's test p-value <0.00001). We confirmed the integration of the phage into the genome of distinct bacterial species for 128 positive samples (47%), when re-evaluating 154,723 microbial genomes reconstructed from the same 9,428 samples. All host genomes belonged to the

Enterococcus genus (except two assigned to *Coprobacillus*), in particular *E. faecalis* (80 genomes), *E. faecium* (23 genomes), and *E. hirae* (15 genomes), suggesting that phage 13144 (and its homologues from *E. hirae* 708, and 13344) are genus-specific but not species-specific. B. Percentages of stools with detectable TMP sequences in *E. hirae* and/or *E. faecalis* colonies assessed by culturomics followed by PCR in 76 NSCLC and RCC bearing patients (cohort described in (*16*)), the corresponding Kaplan Meier curves indicating overall survival featuring in Figure S11E-F. Up to 5 colonies per species and individual (either colonies from *E. avium, E. casseliflavus, E. durans, E. faecium*, *E. faecalis, E. gallinarum, E. hirae*) from 76 cancer patients led to the detection of the TMP sequence encompassing the TMP1 peptide (aligned in Figure S10) in 34% of the patients. PCR detected TMP sequences only in *E. faecalis, with* 29 colonies positive out of 118 colonies that were tested (not in *E. faecium* nor *E. durans*).

Figure S10

TCAACTACGATACCTCCCATCTTGCTTTTGTTGTTCTGCTAAATTAAGATTCATCGGGCTACCTAGTGCTCCCACTACTTGGCCAGTATCC
ATCACAACAGTTAAATGACGTATTTCTTCTAAGATTTCTACCATTTTCCCCATCGGCGTATTATCTATAGAATGTTTTACCTCAATTGCATT
TGATCGTTTTATCAAACGACTGCCTGTAATAGACTGGTGAATGCTTGAAATCATATCTTTTGCACTTTGTACGGCAACTGACGTATCTTC
TCGAATACCTGCTGCCACACCCTGTGCAAGGAAAACACCAACGTCATATTTCAATAGGCGTGATGGAGATTTAATCTTTGCTTTTTTCTG
TGCTTCTGCATTAACTGCAGCTACTAAATTTTGCATAGCAGATACTGCTTCTCCTTGGCTAGCTCTAATACCAGAAGCAACACCTTTAGC
CATATTAGATCCAACGGATGTCATATTGACTGAACCAGCACCACTTTTTACTGCGTTTCCTAATTCTCTACCAGCGTTATTAGCTGAACCA
ACCTGTGATGCCAATCCTTGAACGAAACTACGCCCAAGCTGTTCTCCTACGCTTCGCATAGCAGAAGCTTTCGTTTTTACTCCTTCAACA
GGCGCTGATCCTAATTCTGCACCTTTTTGTTTTGCGTTGCTTTTCTGTTTCGCTAGCCCTGTGTTATACTCTCCAGCATTAGAATTACCGCC
GCTATTGTATTCTTTACCTTTACTTTTTGCGCCCTTTGCACCAGATGAAGCTACATCACCAGAAGTTTTTTCCGCTTCTGCTTTCTTATTTTT
TACGCCTGAGTTCATCTGATTCATTAACTCTTGACCGACATTATTGATTTCAACTTTTCCTGAGTTCAACCCGTCGATTAATTTGTTTTTAC
CATCTTGACCGTTTTTAAACAAATCAGGCGGTAATGATTGCAAGGTATTCACAATGTCAGCTTTTGACATATTCGCCCATAATTTAGGAT
CGTTGCTTTGCAATCCTTGAACTAGTCCGTTAGAACCATCAATTCCTCGTTGACGTAACATTCCAGCTAATAAAGCCATTTGTTGGTCAA
TGCTAGCACCGTTGTTTACATACGATTGATAAATTCCTAATAACTGTTGGTCTGTCACTCCTTTTAATTGAGCTAAATTATCAGCCGTCAC
CGCAATTTTATTTGCACCATTTTGTGAAATAATCGCTAGAAGCTGCGCTCCTTGTTCTAATTCACTTTGACGTATCTGATCGTTCTGTGTT
TGTAATTGCGTAATTTGGTTTTGGAAAGCCGCCTTTTCTGATTCAGTTTTCGCTTGGTTCTTTTGTGTTTCCAATTGCTGAATTTGTGCATT
ATTCTCCTGCACTTGCTGTGCTTGAATTTCTCCAAAAGTTTTTAAACTTGATAAAGTTTGTTCTTTTTCTTGTTCACTTAACGCTTGGTTGT
TATTCAGCTTATTCACACCAGCTTCGACAAACTGTTTCTGTTGATCCAACAATTGATCACGAATAATATTCGTTTGATTTTGCAAAGTTGC
TCTTTGCTGATCGGTTAACTCTTGACCTTCTACCGTTTTATTATTCTTCAACTGATTAGAGTAATCTGTGTATACTTTCAACAGATCGCTAT
TGTTTGATTGAACAGCCTTCATATACTCAGTTGAAGCATTGGCAAAAATCTTTTGTTTTTCAGCTTCCGATTTACCTTCTGCCGCTTCAAT
CTGCTTATTATAGGTTTCAACAGCCTTTTTCTGTTGTTCTTTTAGATTTGTCACTAAATCAAGTGTATGATTGAAATAAGCTTCTACGCCA
GCCGTGCTACCGTTTTGCTGTGAGAAAAGTTCAGTCATTGCCTGTTTAGCTTCATCAAGTTTTGATGAGTAATTTTCAACACTATTTGATA
CCTCTTCCATATTCATGGACATGGCTTTCGTAGTGTCTTTCGATTTCTTCCCTAATTCTTCTGTGCTTTTAGCTGCTTTTTTTAGAGCAGAA
TCAGAAAACATGGTATCCCAGTCTTTTCCGATATCAGCTAAACTTTTCTTCACATCTTTAAATGATTTATCGGCTCCTTTTGAATCGCCTTT
TAATCTTTGCCAAAGTCCTTTTACTCCGTTAGCAATGGCCATTATTGCATTTACTGCTGTCTTTCCTACAGTAATAATGGCTCGCAATCCA
TCTACAAAACCTGCAATAGCAAAAGTAACTCCGACAAGAGTTCCTGTTCCTAACCATTTAAAAATATTTCCTAATCCTTTTATTGTTTTAG
TAACACTCGCGGAGCTAGGAAGTACACTTTTAAACGATTTTACTATTCCGCTAAAAGCGGTTTTCACGTAGCCTTGAATGTTCATAAAAT
TGGATTTCCAAGCTTGCACTACACCAACTATTGTAGTGGTTATTGCTACTAAAATTGCAGTTATAGGATTGCTCAACATAGCTCCTGTTA
AACTAGCTATAGATCGTATACCCGTTGCTGCAAATGTTCTAAAACCTCCACCTGCTTTTGAGGCGGCTACACCAAGTCCTGATAAAACC
GTCCCTGATTTACCAGCTGCAGAAGATAAATTCCTTAGCGACCCAATAGGATTAATAACAACGGAGGCGAATTTCGCTAATTTGCTATT
AGATAATTGTAAAGAAGCAGAAAAAGAACGGAAAAAGTTAGTAACTTTATTCCCTTCCCCTAGCATATTTAGCTGTCTTTGGCTTGCTC
GAAGATTTGCTCCAAAAGTGTCCAATGTGGGAAAGAGACCTACAATGGTATCTTTTAGCGTAGTAAAACGGGTAAGCAGATTTACATTT
ATCCCCGCACTTTCAAGCCCTGCAAGATTTGATTTATATTTAGAAACAAACCCTTTTACAGCTTGTAATGCGCTACTAGAACCGTTTTTGA
TAGGAGTAACGATAAATTGTTTCCACTTGCTATCTATGTTTCCAGCTTTCTCAAACATTGTTGAAATTGTTTTGCCAAAAACACTAGTCAT
TTTCCCAAACACTTTTAATACAGGACCAGCAGAAGCAGCTAATGCAGCCATTTTTAAAATAAATTCTTGAGTTTTTGGATCAGCTGATGC
AAAAGCCTCGGCCATATTTGCTAAAGCTTCAATCATAGGCTTAGCAGCACTTATTGCGCTATTTAATGCGGCTACTAATGGACCGCCAA
ACGTAATTGCTACATCGTTTAATTGACCACGTAAAATCTTTAACTGTGATTCTGTAGT**TCCGTATCGTTTGCCAGCTT**CTTCTGCTAGAGC
TGTATTTTCGTTAAACGCTTCGTTACCTCGTTTTACAGCACCTTCAAAGACATCACTCGCATTAGCCGCACGTAGTAAACTATCACGTAAT
CGAACTTCGGTAATCCCCATATCATCAAGTACTTTAATAGCTGAGATTCCATGCTTTTCTGAGTCTTTCAAACCTTGAATAAACTCAATCA
TAGCTTGAGAAGGATTACTCTTGAATAATTCCGCGAACTCTTCGCCAGTTCGACCAGTAACATTTGCAAAATCTTCCAAACTTCCAGACG
CCTTGCTTGCTTCTTTATATAATTTTTTCAATTCTGAAGCTGGTACTCCCATTTGTTTAGAAACAGCTGTTAATTCTTTACCACCCCAATTA
ACAGCATGAACAAATTTTTCCCAAGACACTCCTTGTATAGCTACAGCTTGTTTTAAAGGTTCAAAAGCTTTAACCCCTGTTTCGGTGGCT
AATTGCATTTGTACCATCAACCTAGAAAAAGCTGAACCACCCGCTTCGGCCTCTATACCAACAGATGATAACGCCGCTGCAAAACCGAC
AATGTCTCCTTCAGTCATACCAATTTGTTTTCCTGCACCAGCCAAACGGAGTCCCATTTCTGTGATTTCTGATTCAGTAGTTGCTAAGTTA
TTCCCTAAGTCAACAATAGCTGAGCCAAGATTGCTAAATTTATCTTGAGACATTTGAGT**AATATTAGCAAAACGAGCTAAGGAAGT**AG
CAGCTGTATCTGCAGACATATTTGTTGATTCGCCCATATCGATCATTGTTTTAGTAAATCCGACAACTTTATCAGTTTTTATTCCTAACTG
TCCAGCTGCTTCTGCTACTTTTGCAATTTCTTCATGACTAGTAGGTAATTCTTTTGCTAAATCTCTAAGGCCTTTTTCTAAATCATCATAAG
AATAAATGACTTTACCGTTAGAATCGACCATCTCATCGTTGGTCTTTTTAACACCAGTAAATGCACTT**TCCCATTTTACGGCTGCAGT**TGT
GACTGCTCCAACAGCACCCGCAATTGGGAGTGTGATACCTTTAGTCATCGAACCGCCGACTTTTTCAATGCTTTGGCCGATACTTGCAG
TTTTATCACCAAAACTTTTCATCGCACCACTAACTGTGTTCAAATTACTGGGAATATCAGAAGCATTCGAACTAAGTTTTTTTAGCGAAG
AGGTAGCACTCCCCATTGTCTGAGTAAACCCTTTATCTATTGCTGTAAGTACCGCTTTGACTGTTTTACTTTGTGCCAC

Primers

Sequence of TMP1

Figure S10. Sequence of the Phage Tail Length Tape Measure Protein in *E. hirae*. Nucleotide sequence of the whole TMP protein as well as binding area for PCR primers indicated in green and TMP1 epitope sequence indicated in red.

Figure S11

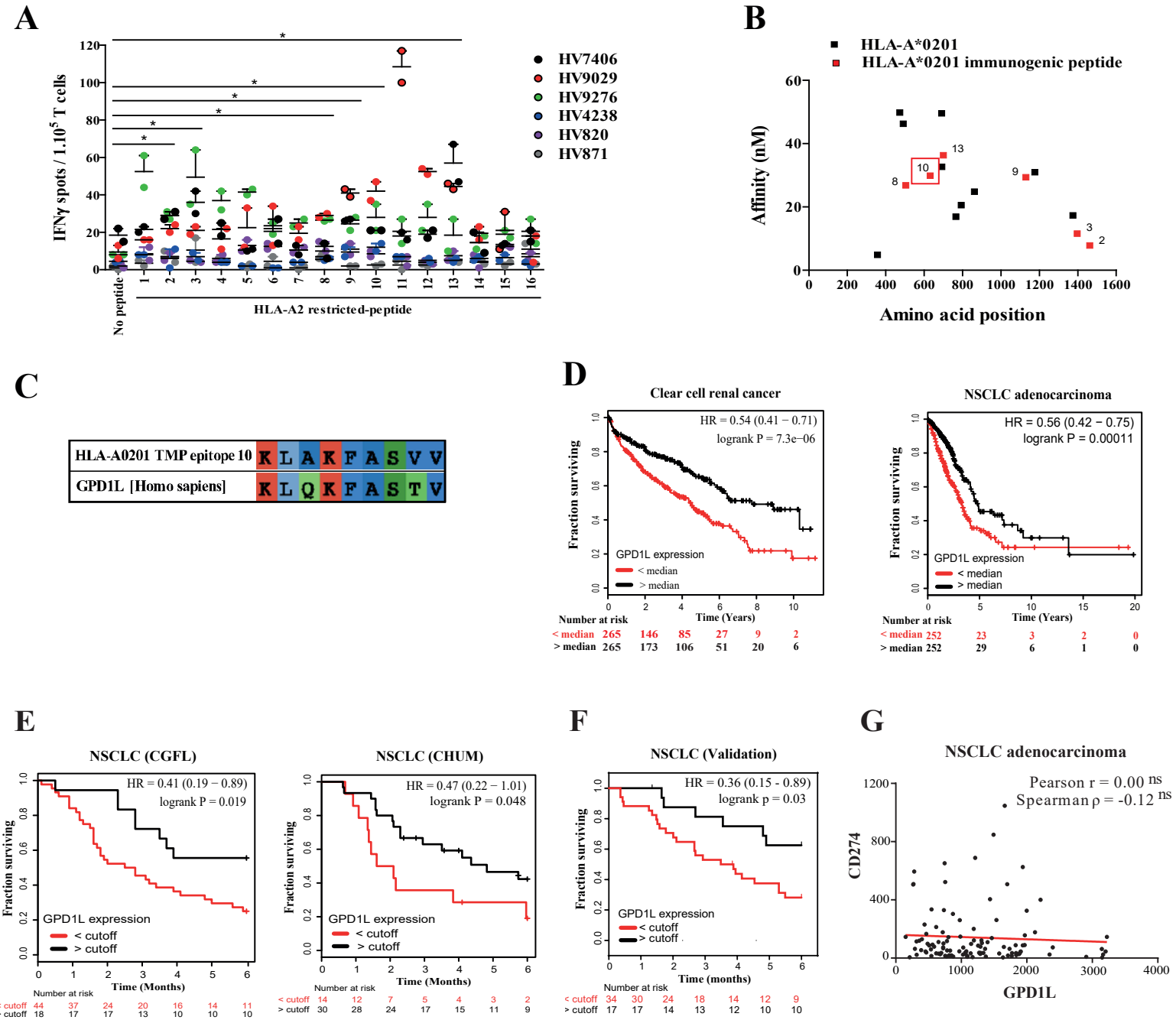
A
IFNγ spots / 1.10^5 T cells
HV7406
HV9029
HV9276
HV4238
HV820
HV871
No peptide
HLA-A2 restricted-peptide
B
HLA-A*0201
HLA-A*0201 immunogenic peptide
Affinity (nM)
Amino acid position
C
HLA-A0201 TMP epitope 10 K L A K F A S V V
GPD1L [Homo sapiens] K L Q K F A S T V
D
Clear cell renal cancer
HR = 0.54 (0.41 − 0.71)
logrank P = 7.3e−06
GPD1L expression
< median
> median
Fraction surviving
Time (Years)
Number at risk
< median 265 146 85 27 9 2
> median 265 173 106 51 20 6
NSCLC adenocarcinoma
HR = 0.56 (0.42 − 0.75)
logrank P = 0.00011
GPD1L expression
< median
> median
Fraction surviving
Time (Years)
Number at risk
< median 252 23 3 2 0
> median 252 29 6 1 0
E
NSCLC (CGFL)
HR = 0.41 (0.19 − 0.89)
logrank P = 0.019
GPD1L expression
< cutoff
> cutoff
Fraction surviving
Time (Months)
Number at risk
< cutoff 44 37 24 20 16 14 11
> cutoff 18 17 17 13 10 10 10
NSCLC (CHUM)
HR = 0.47 (0.22 − 1.01)
logrank P = 0.048
GPD1L expression
< cutoff
> cutoff
Fraction surviving
Time (Months)
Number at risk
< cutoff 14 12 7 5 4 3 2
> cutoff 30 28 24 17 15 11 9
F
NSCLC (Validation)
HR = 0.36 (0.15 - 0.89)
logrank p = 0.03
GPD1L expression
< cutoff
> cutoff
Fraction surviving
Time (months)
Number at risk
< cutoff 34 30 24 18 14 12 9
> cutoff 17 17 14 13 12 10 10
G
NSCLC adenocarcinoma
Pearson r = 0.00 ns
Spearman ρ = -0.12 ns
CD274
GPD1L

Figure S11. Identification and functional impact of TMP-crossreactive epitopes in the GPD1-L protein .

A. Priming of naive $CD8^+$ T cells from six HLA-A*0201 healthy volunteers with autologous monocyte-derived DC pulsed (or not) with 16 HLA-A*0201 binding TMP epitopes (Table S6). Restimulation at day 7 with each of the 16 TMP peptides for IFNγ ELIspot assays and enumeration of positive spots. ANOVA statistical analyses: *$p<0.05$. B. The HLA-A*0201 binding and immunogenic epitopes (Table S6) are located in defined domains of the TMP protein, as indicated by the color code (red: 6 peptides with significant reactivity in A) and the amino acid sequence position, as a function of their binding affinity to the MHC class I allele (calculated *in silico*). C. Blast sequence alignment of the immunogenic HLA-A*0201-restricted TMP epitope 10 (KLAKFASVV) with a sequence belonging to the GPD1-L protein (KLQKFASTV). D. Impact of GPD1-L mRNA expression on survival in 530 clear renal cell cancers (left panel) and lung adenocarcinoma (right panel) from the TCGA. Patients were segregated according to the median value of GPD1-L expression, and Kaplan Meier curves of overall survival were compared by Cox regression univariate analysis. E-F. Kaplan Meier curves for time to progression following PD-1 blockade in second line therapy in 44 stage IIIC/IV NSCLC patients (CHUM test cohort, E) corroborated with a second cohort of 62 stage IIIC/IV NSCLC patients (CGFL cohort, E) and then a validation cohort of stage IIIC/IV NSCLC patients (F, n=51) using an optimal cut-off value for GPD1-L tumor expression obtained in RNA sequencing for each cohort (Table S7 for patients description). G. Absence of correlations between GPD1-L and CD274/PD-L1 mRNA expression in lung cancers (TCGA, CHUM and CGFL cohorts together), as determined by Spearman and Pearson calculations.

Figure S12

A GPD1L

>sp|Q8N335|GPD1L_HUMAN Glycerol-3-phosphate dehydrogenase 1-like protein

MAAAPLKVCIVGSGNWGSAVAKIIGNNVKKLQKFASTVKMW VFEETVNGRKLTDIINNDHENVKYLPGHKL

PENVVAMSNLSEAVQDADLLVFVIPHQFIHRICDEITGRVPKKALGITLIKGIDEGPEGLKLISDIIREKMGIDISVL

MGANIANEVAAEKFCETTIGSKVMENGLLFKELLQTPNFRITVVDDADTVELCGALKNIVAVGAGFCDGLRCG

DNTKAAVIRLGLMEMIAFARIFCKGQVSTATFLESCGVADLITTCYGGRNRRVAEAFARTGKTIEELEKEMLNGQ

KLQGPQTSAEVYRILKQKGLLDKFPLFTAVYQICYESRPVQEMLSCLQSHPEHT

^{30}KLQKFASTV^{38}

B

Gene Name	Sample Name	AA Mutation	Primary Tissue
GPD1L	TCGA-DZ-6132-01	K30T	Kidney
GPD1L	TCGA-17-Z053-01	L31F	Lung
GPD1L	U343	K33N	Central nervous system

C

Gene Name	Sample Name	AA Mutation	Primary Tissue
GPD1L	TCGA-AA-3667-01	K29N	Large intestine
GPD1L	TCGA-KN-8431-01	K39_W41del	Kidney
GPD1L	TCGA-KN-8431-01	K39_V42delinsI	Kidney
GPD1L	T593	M40V	Large intestine
GPD1L	EGC3	W41R	Stomach

D

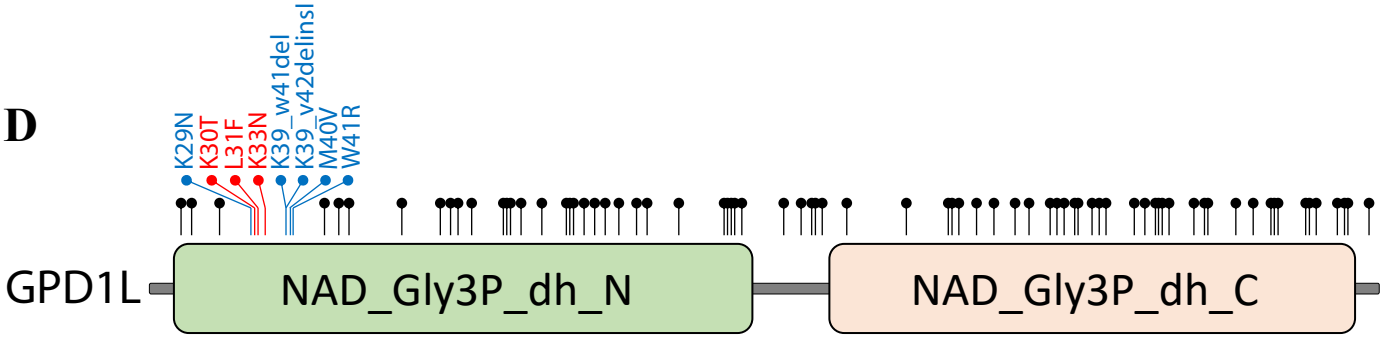

Figure S12. Cancer-associated mutations in GPD1-L from cBIOPORTAL and COSMIC. A. Protein sequence of GPD1-L. B. Mutations annotated in the conserved sequence KLQKFASTV (highlighted in red). C. Mutations annotated in positions adjacent to the conserved sequence KLQKFASTV (highlighted in blue). Gray background indicates two mutations found in the same sample. D. Distribution of all cancer-associated GPD1-L mutations. Mutations in the conserved sequence KLQKFASTV are highlighted in red and adjacent mutations are highlighted in blue.

Figure S13

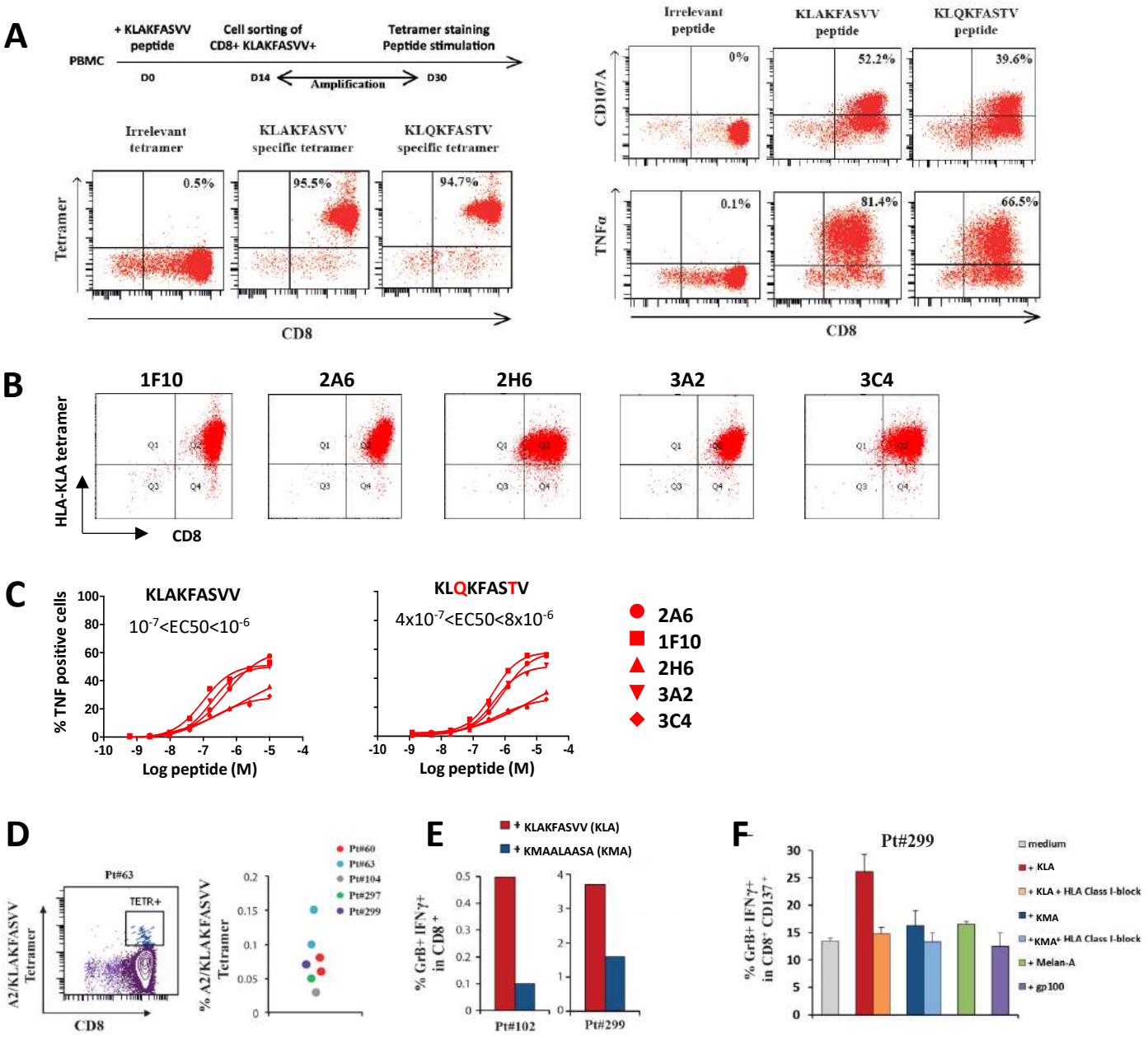
A
+ KLAKFASVV peptide
Cell sorting of CD8+ KLAKFASVV+
Tetramer staining Peptide stimulation
PBMC
D0
D14
Amplification
D30
Irrelevant tetramer
KLAKFASVV specific tetramer
KLQKFASTV specific tetramer
0.5%
95.5%
94.7%
Tetramer
CD8
Irrelevant peptide
KLAKFASVV peptide
KLQKFASTV peptide
0%
52.2%
39.6%
CD107A
0.1%
81.4%
66.5%
TNFα
CD8
B
1F10
2A6
2H6
3A2
3C4
HLA-KLA tetramer
CD8
C
KLAKFASVV
10-7<EC50<10-6
KLQKFASTV
4x10-7<EC50<8x10-6
% TNF positive cells
Log peptide (M)
2A6
1F10
2H6
3A2
3C4
D
Pt#63
TETR+
A2/KLAKFASVV Tetramer
CD8
% A2/KLAKFASVV Tetramer
Pt#60
Pt#63
Pt#104
Pt#297
Pt#299
E
+ KLAKFASVV (KLA)
+ KMAALAASA (KMA)
% GrB+ IFNγ+ in CD8+
Pt#102
Pt#299
F
Pt#299
% GrB+ IFNγ+ in CD8+ CD137+
medium
+ KLA
+ KLA + HLA Class I-block
+ KMA
+KMA+ HLA Class I-block
+ Melan-A
+ gp100

Figure S13. Crossreactive T cells recognizing HLA-A*0201-restricted peptides from TMP and GPD1-L proteins.

A-C. In vitro stimulation of T cells from normal volunteers. A. Experimental setting (upper left panel). HLA-A*0201^{+} PBMC extracted from a healthy volunteer were stimulated in microculture assays for 14 days, *ex vivo*, with KLAKFASVV peptide. Each well was screened for costaining with both tetramers (HLA-A*0201/KLAKFASVV from TMP and HLA-A*0201 /KLQKFASTV from GPD1-L). One well out of 192 tested was positive and subjected to cell sorting using HLA-A*0201/KLAKFASVV multimer-coated beads and re-expanded for 15 days. The resulting T cell line was further characterized by flow cytometric analyses for binding to each and both tetramers (A, lower panels) and for its functional cross-reactivity with both epitopes (KLAKFASVV from TMP and KLQKFASTV from GPD1-L), as measured by degranulation (CD107A surface expression) and TNFα release assays. One representative dot plot is depicted for each experimental condition of stimulation (A, upper right panels). B. After cloning of the T cell line by limiting dilution assays, we studied the five KLAKFASVV-specific CD8^{+} CTL clones (1F10, 2A6, 2H6, 3A2 and 3C4) for their capacity to bind the HLA-A*0201/KLAKFASVV tetramer (B) and to secrete TNFα after exposure to increasing concentrations of the two peptides. Three clones exhibited lower or similar affinity for KLQKFASTV (KLQ) compared with KLAKFASVV (KLA) peptides (C). D-F. *In vitro* stimulation of T cells from NSCLC patients. Representative flow cytometry dot plot analyses of PBMC from one of the five HLA-A*0201 NSCLC patients tested, after short term *ex vivo* restimulation with KLAKFASVV peptide followed by tetramer staining using HLA-A*0201/KLAKFASVV tetramers (D, left). Results from 5 different NSCLC patients (D, right panel), each dot representing the percentages of tetramer^{+}CD8^{+} T cells for each patient evaluated. Dots with a similar color represent values from two independent experiments performed using the same patient's PBMC. E-F. Percentages of co-production of GrB and IFN-γ, as measured by multicolor intracellular staining, in CD8^{+} T-cell lines obtained from three HLA-A*0201 NSCLC patients (out of 6 tested) after priming with TMP epitope 10 (KLAKFASVV) and final exposure to the same TMP epitope p10 or irrelevant TMP epitope p14 (KMAALAASA) (E) or irrelevant MART-1/MelanA or pg100 peptides with or without neutralizing antibodies blocking MHC class I molecules (W6/32) (F). The percentages of effector cells in CD8^{+} T cells (Pt#102, Pt#299, panel E) or in CD8^{+} CD137^{+} T cells (means± SEM of Pt#297 and Pt#299, panel F) are shown.

Figure S14

A

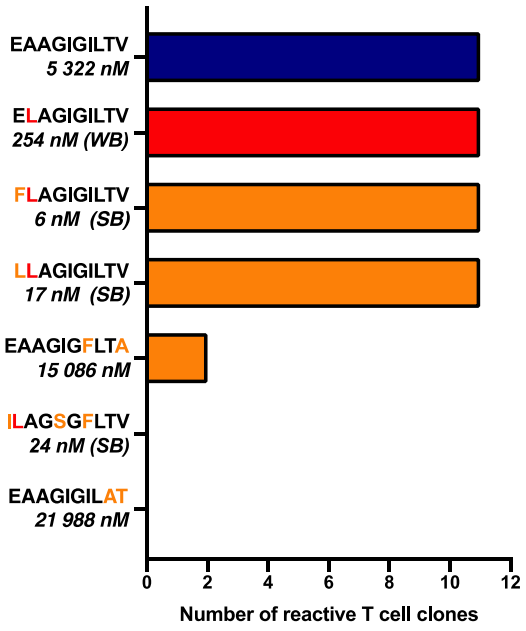

B

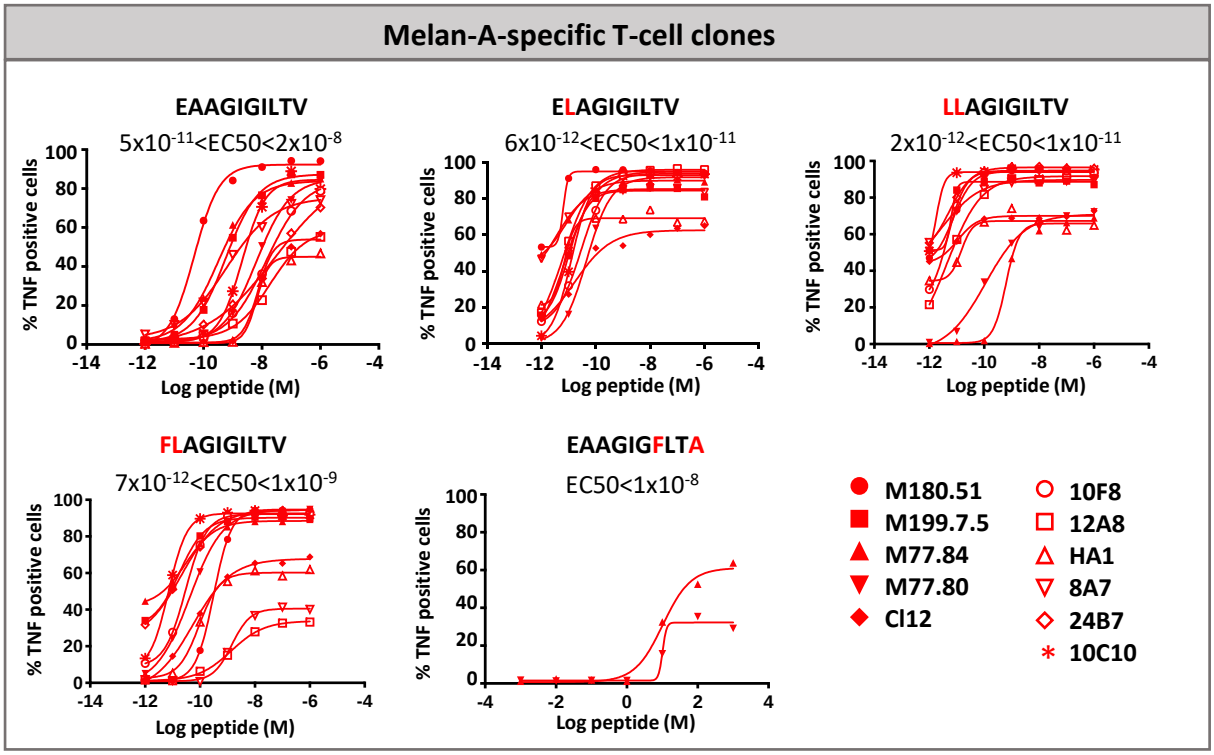

Figure S14. Crossreactivity of T cell clones specific for the MART-1 melanoma peptide with microbial antigens.

A. Numbers of Melan-A specific $CD8^+$T cell clones reactive against bacterial peptides. The blue histogram represents the number of clones reactive against their cognate/naturally processed epitope (11/11 T cell clones). The red histogram represents the number of Melan-A-specific T cell clones reactive against the high affinity analog peptide Melan-A A27L. Orange histograms represent the number of crossreactive T-cell clones against each bacterial peptide (as selected by an *in silico* approach, Table S8), the differences in the decapeptide amino-acid sequence being highlighted with orange letters. HLA-A*0201-predicted binding affinities (NetMHCprediction) are indicated for each peptide (strong (SB) *versus* weak (WB) binding affinity). B. Functional avidities of MART-1/Melan-A specific $CD8^+$T cell clones in response to naturally processed versus synthetic versus bacterial analogs. Red curves represent T cell clones crossreactive against at least one bacterial peptide. Functional avidities were evaluated by measuring TNFα production in response to T2 cells loaded with a dose range of each indicated peptide, at an E:T ratio of 1:2, by intracellular staining in flow cytometry. Ranges of EC_{50} for each peptide were calculated using PRISM software.

Figure S15

A

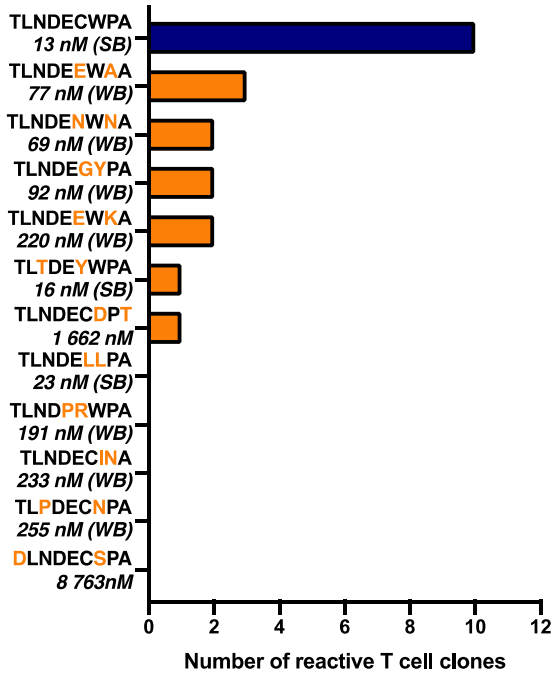

B

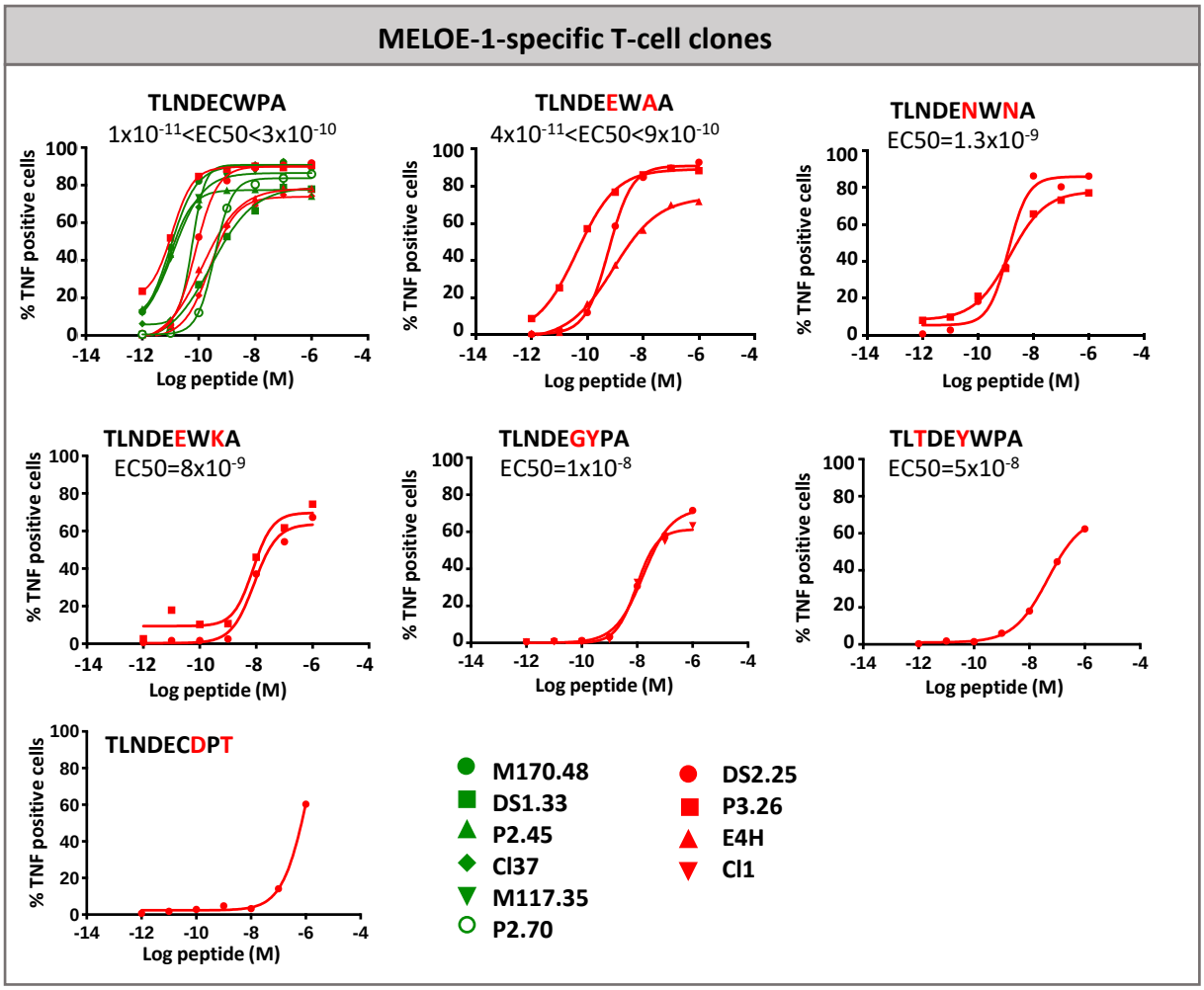

Figure S15. Cross-reactivity of T cell clones specific for the MELOE-1 melanoma peptide with microbial antigens.

A. Numbers of MELOE-1 specific $CD8^+$T cell clones reactive against bacterial peptides. The blue histogram represents the number of clones reactive against their cognate/naturally processed epitope (10 T cell clones). Orange histograms represent the number of crossreactive T-cell clones against each bacterial peptide (designed upon *in silico* selection, Table S8), the differences in the decapeptide amino-acid sequence being highlighted with orange letters. HLA-A*0201-predicted binding affinities (NetMHCprediction) are indicated for each peptide (strong (SB) versus weak (WB) binding affinity). B. Functional avidities of MELOE-1 specific $CD8^+$T cell clones in response to naturally processed versus bacterial analogs. Red curves represent T cell clones cross-reactive against at least one bacterial peptide and green curves represent MELOE-1-specific T-cell clones reactive only to the cognate peptide TLNDECWPA. Functional avidities were evaluated by measuring TNFα production in response to T2 cells loaded with a dose range of each indicated peptide, at an E:T ratio of 1:2, by flow cytometry. Ranges of EC_{50} for each peptide were calculated using PRISM software.

Supplemental Tables:

Table S1. Description of *E. hirae* strains.

Table S2. H-2K^b restricted-*E. hirae* epitopes (<50nM).

We performed sequence alignments of bacterial genes encoding putative cell wall and secreted proteins for immunogenic (13144) *versus* non-immunogenic (708 and 13344) *E. hirae* strains (using the PSORT software), followed by a selection of high affinity epitopes for the MHC class I H-2K^b protein (<50 nM binding affinity) using the NetMHC software.

Table S3. Seeking prophage sequences in *E. hirae* 13144 genomes.

Table S4. List of TRA sequences shared between TMP1 and PSMB4-specific TCRs.

Table S5. List of TRB sequences shared between TMP1 and PSMB4-specific TCRs.

Table S6. List of TMP epitopes selected *in silico* to bind with high affinity (<50nM) HLA-A*0201 molecules.

Table S7. Description of cancer patients treated with anti-PD1 Abs in three independent cohorts (corresponding to Figure S11E-F).

Table S8. Sequence of peptides tested in MART-1 and MELOE-1-specific T cell clones.

Table S9. TCR sequence of MART-1-specific T cell clones. Recurrent motifs already described in the CDR3β of MART-1-specific T-cell clones (*17*) are indicated in bold.

Table S10. TCR sequence of MELOE-1-specific T cell clones. Recurrent motifs already described in the CDR3α of MELOE-1 specific –T-cell clones (*17*) are indicated in bold.

Table S1. Description of *E.hirae* strains

Species	Origin	Cancer	Patient outcome
Enterococcus hirae 13144	Murine – CTX-treated		
Enterococcus hirae 708	Human - Unknown		
Enterococcus hirae 13344	Human - Blood		
Enterococcus hirae ATCC9790	Type strain CIP 53.48T		
Enterococcus hirae 5348	Human - Unknown		
Enterococcus hirae 7030	Human – Liver abscess		
Enterococcus hirae 12607	Environmental – RiskManche project		
Enterococcus hirae 13150	Environmental - Water		
Enterococcus hirae 13152	Environmental - Water		
Enterococcus hirae 13153	Environmental - Water		
Enterococcus hirae 13155	Environmental – RiskManche project		
Enterococcus hirae 13161	Environmental - Cockle		
Enterococcus hirae 13343	Conservation liquid of kidney		
Enterococcus hirae 13346	Human - Urine		
Enterococcus hirae 13347	Blood culture		
Enterococcus hirae IGR1	Human (stool)	Lung	Responder
Enterococcus hirae IGR4	Human (stool)	Lung	Complete Responder
Enterococcus hirae IGR10	Human (stool)	Lung	Responder
Enterococcus hirae IGR11	Human (stool)	Lung	Responder

Table S2. H-2K^b restricted-*E.hirae* epitopes (<50nM binding affinity)

Group	Hirae	sequence	names of the proteins	
Group 1	708	INAKFSSQL	Membrane proteins related to metalloendopeptidases	
	708	YIYNHYKDM	Membrane proteins related to metalloendopeptidases	
	708	YVYGKSRTM	Membrane proteins related to metalloendopeptidases	
	708	IAFLSYKLF	cell surface protein precursor	
Group 2	708	IMYEYMYPV	hypothetical protein	
	708	SSMEYFLKV	Phage tail length tape-measure protein	
	708	ISFFQENQL	Collagen adhesin	
	708	TNLLFMTSL	extracellular protein	
Group 3	708	KIFSIFMLL	Phosphatidylinositol-specific phospholipase C	
	708	LNIFKFNRF	Chitinase	
	708	MTYDYRGGF	Chitinase	
	708	PSYMFRTSF	Chitinase	
Group 4	708	QSYTYYMTA	cell wall surface anchor family protein	
	708	ITFSHYEPT	cell wall surface anchor family protein	
	13144	SAFPYEQEL	C3 family ADP-ribosyltransferase	
	13144	YNYSKSYPV	hypothetical protein	
Group 5	13144	VSFSHYRPG	hypothetical protein	
	13144	VTFLGYNAF	cell surface protein	
	13144	TVYTFHVNI	cell surface protein	
	13144	TSYSPLFLL	cell surface protein (putative)	
Group 6	13144	TNYIYPNIL	2',3'-cyclic-nucleotide 2'-phosphodiesterase	
	13144	VVPILFLGL	FmtB protein	
	13144	KNYKAYVEL	hypothetical protein	
	13144	SAMKYGIPL	hypothetical protein	
Group 7	13144	TSLARFANI	Phage tail length tape-measure protein	→ TMP1
	13144	AMIEFIQGL	Phage tail length tape-measure protein	→ TMP2
	13144	VAITFGGPL	Phage tail length tape-measure protein	→ TMP3
	13144	VSTNHYGLL	hypothetical protein	
Group 8	13144	VMFGLFITI	cell surface protein precursor	
	13144	TVFSLVSLL	Chitinase	
	13144	SIYNLEKPL	IgA1 protease	
	13144	YTIIRYGNL	IgA1 protease	
Group 9	13144	SNGLLYTPM	IgA1 protease	
	13144	NNYHYVGGL	IgA1 protease	
	13144	SMFLNCNNL	hypothetical protein	
	13144	IAFQGYSSL	hypothetical protein	
Group 10	13144	QVTNFFNMF	hypothetical protein	
	13144	IMLGLFMTM	cell surface protein precursor	
	EH17	MSFTFFSST	hypothetical protein	
	EH17	IAFQNFVNL	Chitinase	
Group 11	EH17	SMFIAFQNF	Chitinase	
	EH17	LNYDYGNRI	Chitinase	
	EH17	AGICFFTGV	Peptidoglycan N-acetylglucosamine deacetylase	
	EH17	VEYTYFPTL	Membrane proteins related to metalloendopeptidases	
Group 12	EH17	AAYVFEMNF	Membrane proteins related to metalloendopeptidases	
	EH17	EMYRKLSTL	Membrane proteins related to metalloendopeptidases	
	EH17	YNYGYKSVL	enhancin family protein	
	EH17	VIHELYNSL	bacteriocin immunity protein	

Table S3. Seeking prophage sequence in *E.hirae* 13144 genome

Region	Region Length	Completeness	Score	# Total Proteins	Region Position	Most Common Phage	GC%
1	40.6Kb	intact	150	58	481066-521729	PHAGE_Entero_phiEf11_NC_013696(9)	33.79%
2	39.2Kb	intact	140	59	2123983-2163272	PHAGE_Entero_vB_IME197_NC_028671(6)	34.95%

Table S4. List of TRA sequences shared between TMP1 and PSMB4-specific TCRs

V	J	aaSeqCDR3	CDR3dna	VpJ	VJ	cloneCount
TRAV14D-2	TRAJ22	CAASASSGSWQLIF	TGTGCAGCAAGCGCATCTTCTGGCAGCTGGCAACTCATCTTT	TRAV14D-2 CAASASSGSWQLIF TRAJ22	TRAV14D-2 TRAJ22	57
TRAV14-1	TRAJ26	CAASDNYAQGLTF	TGTGCAGCAAGTGATAACTATGCCCAGGGATTAACCTTC	TRAV14-1 CAASDNYAQGLTF TRAJ26	TRAV14-1 TRAJ26	405
TRAV16D-DV11	TRAJ17	CAMRDLNSAGNKLTF	TGTGCTATGAGAGACCTTAACAGTGCAGGGAACAAGCTAACTTTT	TRAV16D-DV11 CAMRDLNSAGNKLTF TRAJ17	TRAV16D-DV11 TRAJ17	19
TRAV16D-DV11	TRAJ27	CAMREDTNTGKLTF	TGTGCTATGAGAGAGGACACCAATACAGGCAAATTAACCTTT	TRAV16D-DV11 CAMREDTNTGKLTF TRAJ27	TRAV16D-DV11 TRAJ27	123
TRAV3D-3	TRAJ30	CAVSDTNAYKVIF	TGCGCAGTCAGTGACACAAATGCTTACAAAGTCATCTTT	TRAV3D-3 CAVSDTNAYKVIF TRAJ30	TRAV3D-3 TRAJ30	297
TRAV7-3	TRAJ9	CAVSNMGYKLTF	TGTGCAGTGAGCAACATGGGCTACAAACTTACCTTC	TRAV7-3 CAVSNMGYKLTF TRAJ9	TRAV7-3 TRAJ9	208
TRAV8-1	TRAJ18	CATGDRGSALGRLHF	TGTGCTACTGGAGATAGAGGTTCAGCCTTAGGGAGGCTGCATTTT	TRAV8-1 CATGDRGSALGRLHF TRAJ18	TRAV8-1 TRAJ18	19
TRAV6D-7	TRAJ31	CALGGNSNNRIFF	TGTGCTCTGGGGGGGAATAGCAATAACAGAATCTTCTTT	TRAV6D-7 CALGGNSNNRIFF TRAJ31	TRAV6D-7 TRAJ31	17
TRAV14D-2	TRAJ22	CAASASSGSWQLIF	TGTGCAGCCTCTGCATCTTCTGGCAGCTGGCAACTCATCTTT	TRAV14D-2 CAASASSGSWQLIF TRAJ22	TRAV14D-2 TRAJ22	14
TRAV16N	TRAJ52	CAMRENTGANTGKLTF	TGTGCTATGAGAGAGAACACTGGAGCTAACACTGGAAAGCTCACGTTT	TRAV16N CAMRENTGANTGKLTF TRAJ52	TRAV16N TRAJ52	14
TRAV3D-3	TRAJ21	CAVRDLSNYNVLYF	TGCGCAGTCAGGGATTTGTCTAATTACAACGTGCTTTACTTC	TRAV3D-3 CAVRDLSNYNVLYF TRAJ21	TRAV3D-3 TRAJ21	10
TRAV14D-1	TRAJ26	CAARNNYAQGLTF	TGTGCAGCAAGAAATAACTATGCCCAGGGATTAACCTTC	TRAV14D-1 CAARNNYAQGLTF TRAJ26	TRAV14D-1 TRAJ26	156
TRAV12D-3	TRAJ33	CALSNYQLIW	TGTGCTCTGAGCAACTATCAGTTGATCTGG	TRAV12D-3 CALSNYQLIW TRAJ33	TRAV12D-3 TRAJ33	8
TRAV12D-3	TRAJ31	CALSDRDSNNRIFF	TGTGCTCTGAGTGATCGAGATAGCAATAACAGAATCTTCTTT	TRAV12D-3 CALSDRDSNNRIFF TRAJ31	TRAV12D-3 TRAJ31	5
TRAV6D-7	TRAJ31	CALGGNSNNRIFF	TGTGCTCTGGGTGGGAATAGCAATAACAGAATCTTCTTT	TRAV6D-7 CALGGNSNNRIFF TRAJ31	TRAV6D-7 TRAJ31	4
TRAV12D-3	TRAJ31	CALSDRDSNNRIFF	TGTGCTCTGAGTGATCGGGATAGCAATAACAGAATCTTCTTT	TRAV12D-3 CALSDRDSNNRIFF TRAJ31	TRAV12D-3 TRAJ31	255
TRAV14D-3-DV8	TRAJ22	CAASASSGSWQLIF	TGTGCAGCAAGTGCAAGTTCTGGCAGCTGGCAACTCATCTTT	TRAV14D-3-DV8 CAASASSGSWQLIF TRAJ22	TRAV14D-3-DV8 TRAJ22	2
TRAV12D-3	TRAJ31	CALSDRHSNNRIFF	TGTGCTCTGAGTGATCGACATAGCAATAACAGAATCTTCTTT	TRAV12D-3 CALSDRHSNNRIFF TRAJ31	TRAV12D-3 TRAJ31	1
TRAV8-1	TRAJ50	CATDPLASSSFSKLVF	TGTGCTACTGACCCCCTAGCATCCTCCTCCTTCAGCAAGCTGGTGTTT	TRAV8-1 CATDPLASSSFSKLVF TRAJ50	TRAV8-1 TRAJ50	49
TRAV10	TRAJ27	CAASRGTNTGKLTF	TGTGCAGCAAGCAGAGGCACCAATACAGGCAAATTAACCTTT	TRAV10 CAASRGTNTGKLTF TRAJ27	TRAV10 TRAJ27	446
TRAV7-2	TRAJ12	CAAPGTGGYKVVF	TGTGCAGCCCCCGGGACTGGAGGCTATAAAGTGGTCTTT	TRAV7-2 CAAPGTGGYKVVF TRAJ12	TRAV7-2 TRAJ12	360
TRAV6N-6	TRAJ22	CALRAASSGSWQLIF	TGCGCTCTGAGGGCAGCATCTTCTGGCAGCTGGCAACTCATCTTT	TRAV6N-6 CALRAASSGSWQLIF TRAJ22	TRAV6N-6 TRAJ22	332
TRAV13-2	TRAJ26	CAIDQYAQGLTF	TGTGCTATAGACCAATATGCCCAGGGATTAACCTTC	TRAV13-2 CAIDQYAQGLTF TRAJ26	TRAV13-2 TRAJ26	296
TRAV14-2	TRAJ44	CAGTGSGGKLTL	TGTGCAGGGACTGGCAGTGGTGGAAAACTCACTTTG	TRAV14-2 CAGTGSGGKLTL TRAJ44	TRAV14-2 TRAJ44	276
TRAV12D-3	TRAJ23	CALSGENYNQGKLIF	TGTGCTCTGAGTGGGGAGAATTATAACCAGGGGAAGCTTATCTTT	TRAV12D-3 CALSGENYNQGKLIF TRAJ23	TRAV12D-3 TRAJ23	256
TRAV19	TRAJ50	CAAGGVASSSFSKLVF	TGCGCAGCAGGGGGGGTAGCATCCTCCTCCTTCAGCAAGCTGGTGTTT	TRAV19 CAAGGVASSSFSKLVF TRAJ50	TRAV19 TRAJ50	236
TRAV13-1	TRAJ6	CALVLTSGGNYKPTF	TGTGCTTTGGTCCTAACCTCAGGAGGAAACTACAAACCTACGTTT	TRAV13-1 CALVLTSGGNYKPTF TRAJ6	TRAV13-1 TRAJ6	228
TRAV6N-6	TRAJ22	CALSVASSGSWQLIF	TGCGCTCTGAGTGTCGCATCTTCTGGCAGCTGGCAACTCATCTTT	TRAV6N-6 CALSVASSGSWQLIF TRAJ22	TRAV6N-6 TRAJ22	230
TRAV12-2	TRAJ58	CALSDPGTGSKLSF	TGTGCTTTGAGTGATCCAGGCACTGGGTCTAAGCTGTCATTT	TRAV12-2 CALSDPGTGSKLSF TRAJ58	TRAV12-2 TRAJ58	182
TRAV5D-4	TRAJ22	CAASTSSGSWQLIF	TGTGCTGCAAGTACATCTTCTGGCAGCTGGCAACTCATCTTT	TRAV5D-4 CAASTSSGSWQLIF TRAJ22	TRAV5D-4 TRAJ22	128
TRAV14D-2	TRAJ23	CAASEDYNQGKLIF	TGTGCAGCAAGTGAGGATTATAACCAGGGGAAGCTTATCTTT	TRAV14D-2 CAASEDYNQGKLIF TRAJ23	TRAV14D-2 TRAJ23	100
TRAV13N-1	TRAJ27	CAMEPGTNTGKLTF	TGTGCTATGGAACCGGGCACCAATACAGGCAAATTAACCTTT	TRAV13N-1 CAMEPGTNTGKLTF TRAJ27	TRAV13N-1 TRAJ27	80
TRAV12D-3	TRAJ31	CALSDRHSNNRIFF	TGTGCTCTGAGTGATCGACACAGCAATAACAGAATCTTCTTT	TRAV12D-3 CALSDRHSNNRIFF TRAJ31	TRAV12D-3 TRAJ31	58
TRAV13N-4	TRAJ28	CVLSLLPGTGSNRLTF	TGTGTTCTGAGTCTGCTACCAGGCACTGGGAGTAACAGGCTCACTTTT	TRAV13N-4 CVLSLLPGTGSNRLTF TRAJ28	TRAV13N-4 TRAJ28	2
TRAV8-1	TRAJ50	CATDPLASSSFSKLVF	TGTGCTACTGACCCCCTAGCATCCTCCTCCTTCAGCAAGCTGGTGTTT	TRAV8-1 CATDPLASSSFSKLVF TRAJ50	TRAV8-1 TRAJ50	2
TRAV12-2	TRAJ43	CVRNNNNAPRF	TGTGTTCGCAATAACAACAATGCCCCACGATTT	TRAV12-2 CVRNNNNAPRF TRAJ43	TRAV12-2 TRAJ43	346
TRAV16N	TRAJ40	CAMRENTGNYKYVF	TGTGCTATGAGAGAGAATACAGGAAACTACAAATACGTCTTT	TRAV16N CAMRENTGNYKYVF TRAJ40	TRAV16N TRAJ40	234
TRAV8D-2	TRAJ9	CATDVGYKLTF	TGTGCTACAGATGTGGGCTACAAACTTACCTTC	TRAV8D-2 CATDVGYKLTF TRAJ9	TRAV8D-2 TRAJ9	108
TRAV12-2	TRAJ43	CVRNNNNAPRF	TGTGTTCGCAATAACAACAATGCCCCAAGATTT	TRAV12-2 CVRNNNNAPRF TRAJ43	TRAV12-2 TRAJ43	30
TRAV16D-DV11	TRAJ17	CAMRDLNSAGNKLTF	TGTGCTATGAGAGACCTTAACAGTGCAGGGAACAAGCTAACTTTT	TRAV16D-DV11 CAMRDLNSAGNKLTF TRAJ17	TRAV16D-DV11 TRAJ17	2
TRAV3D-3	TRAJ21	CAVRDLSNYNVLYF	TGCGCAGTCAGGGATTTGTCTAATTACAACGTGCTTTACTTC	TRAV3D-3 CAVRDLSNYNVLYF TRAJ21	TRAV3D-3 TRAJ21	2
TRAV4D-3	TRAJ15	CAADQGGRALIF	TGTGCTGCTGACCAGGGAGGCAGAGCTCTGATATTT	TRAV4D-3 CAADQGGRALIF TRAJ15	TRAV4D-3 TRAJ15	2
TRAV14D-2	TRAJ22	CAASASSGSWQLIF	TGTGCAGCAAGTGCCTCTTCTGGCAGCTGGCAACTCATCTTT	TRAV14D-2 CAASASSGSWQLIF TRAJ22	TRAV14D-2 TRAJ22	180
TRAV14D-3-DV8	TRAJ22	CAASASSGSWQLIF	TGTGCAGCAAGTGCATCTTCTGGCAGCTGGCAACTCATCTTT	TRAV14D-3-DV8 CAASASSGSWQLIF TRAJ22	TRAV14D-3-DV8 TRAJ22	180
TRAV12D-3	TRAJ33	CALSNYQLIW	TGTGCTCTCAGCAACTATCAGTTGATCTGG	TRAV12D-3 CALSNYQLIW TRAJ33	TRAV12D-3 TRAJ33	135
TRAV6D-7	TRAJ31	CALGGNSNNRIFF	TGTGCTCTGGGTGGAAATAGCAATAACAGAATCTTCTTT	TRAV6D-7 CALGGNSNNRIFF TRAJ31	TRAV6D-7 TRAJ31	37

Table S5. List of TRB sequences shared between TMP1 and PSMB4-specific TCRs

V	J	aaSeqCDR3	CDR3dna	VpJ	VJ	count
TRBV13-3	TRBJ2-3	CARDGAETLYF	TGTGCCAGGGACGGTGCAGAAACGCTGTATTTT	TRBV13-3 CARDGAETLYF TRBJ2-3	TRBV13-3 TRBJ2-3	318
TRBV12-2	TRBJ2-5	CASAFNQDTQYF	TGTGCCAGCGCTTTTAACCAAGACACCCAGTACTTT	TRBV12-2 CASAFNQDTQYF TRBJ2-5	TRBV12-2 TRBJ2-5	696
TRBV13-2	TRBJ2-7	CASGDFYEQYF	TGTGCCAGCGGGGACTTTTATGAACAGTACTTC	TRBV13-2 CASGDFYEQYF TRBJ2-7	TRBV13-2 TRBJ2-7	16
TRBV13-2	TRBJ2-7	CASGDFYEQYF	TGTGCCAGCGGTGATTTCTATGAACAGTACTTC	TRBV13-2 CASGDFYEQYF TRBJ2-7	TRBV13-2 TRBJ2-7	138
TRBV13-2	TRBJ1-2	CASGDNANSDYPF	TGTGCCAGCGGGGACAATGCAAACTCCGACTACCCCTTC	TRBV13-2 CASGDNANSDYPF TRBJ1-2	TRBV13-2 TRBJ1-2	42
TRBV13-2	TRBJ1-2	CASGDNANSDYTF	TGTGCCAGCGGGGACAATGCAAACTCCGACTACACCTTC	TRBV13-2 CASGDNANSDYTF TRBJ1-2	TRBV13-2 TRBJ1-2	372
TRBV13-2	TRBJ2-4	CASGDRGSQNTLYF	TGTGCCAGCGGTGACAGGGGTAGTCAAAACACCTTGTACTTT	TRBV13-2 CASGDRGSQNTLYF TRBJ2-4	TRBV13-2 TRBJ2-4	1
TRBV13-2	TRBJ2-4	CASGDRGSQNTLYF	TGTGCCAGCGGTGATCGGGGTAGTCAAAACACCTTGTACTTT	TRBV13-2 CASGDRGSQNTLYF TRBJ2-4	TRBV13-2 TRBJ2-4	166
TRBV13-2	TRBJ1-4	CASGDSNERLFF	TGTGCCAGCGGGGATTCCAACGAAAGATTATTTTTC	TRBV13-2 CASGDSNERLFF TRBJ1-4	TRBV13-2 TRBJ1-4	6
TRBV13-2	TRBJ1-4	CASGDSNERLFF	TGTGCCAGCGGTGATTCCAACGAAAGATTATTTTTC	TRBV13-2 CASGDSNERLFF TRBJ1-4	TRBV13-2 TRBJ1-4	1
TRBV13-2	TRBJ1-4	CASGDSNERLFF	TGTGCCAGCGGTGACAGCAACGAAAGATTATTTTTC	TRBV13-2 CASGDSNERLFF TRBJ1-4	TRBV13-2 TRBJ1-4	45
TRBV13-2	TRBJ2-5	CASGGDRGQDTQYF	TGTGCCAGCGGTGGGGACAGGGGGCAAGACACCCAGTACTTT	TRBV13-2 CASGGDRGQDTQYF TRBJ2-5	TRBV13-2 TRBJ2-5	14
TRBV13-2	TRBJ2-1	CASGGTAPIYAEQFF	TGTGCCAGCGGTGGGACAGCTCCTATCTATGCTGAGCAGTTCTTC	TRBV13-2 CASGGTAPIYAEQFF TRBJ2-1	TRBV13-2 TRBJ2-1	18
TRBV17	TRBJ2-5	CASGTGTQDTQYF	TGTGCTAGCGGGACTGGGACCCAAGACACCCAGTACTTT	TRBV17 CASGTGTQDTQYF TRBJ2-5	TRBV17 TRBJ2-5	300
TRBV19	TRBJ1-3	CASRNRGSGNTLYF	TGTGCCAGCAGAAACAGGGGTTCTGGAAATACGCTCTATTTT	TRBV19 CASRNRGSGNTLYF TRBJ1-3	TRBV19 TRBJ1-3	584
TRBV13-1	TRBJ2-7	CASSDAAGQYF	TGTGCCAGCAGTGATGCGGCTGGGCAGTACTTC	TRBV13-1 CASSDAAGQYF TRBJ2-7	TRBV13-1 TRBJ2-7	268
TRBV13-3	TRBJ1-2	CASSDARGQDSDYTF	TGTGCCAGCAGTGATGCCAGGGGGCAGGACTCCGACTACACCTTC	TRBV13-3 CASSDARGQDSDYTF TRBJ1-2	TRBV13-3 TRBJ1-2	618
TRBV13-3	TRBJ2-1	CASSDGAEQFF	TGTGCCAGCAGTGATGGTGCTGAGCAGTTCTTC	TRBV13-3 CASSDGAEQFF TRBJ2-1	TRBV13-3 TRBJ2-1	5
TRBV13-3	TRBJ2-1	CASSDGAEQFF	TGTGCCAGCAGTGATGGAGCTGAGCAGTTCTTC	TRBV13-3 CASSDGAEQFF TRBJ2-1	TRBV13-3 TRBJ2-1	254
TRBV13-1	TRBJ1-4	CASSDGGSNERLFF	TGTGCCAGCAGTGATGGGGGGTCCAACGAAAGATTATTTTTC	TRBV13-1 CASSDGGSNERLFF TRBJ1-4	TRBV13-1 TRBJ1-4	1
TRBV13-1	TRBJ1-4	CASSDGGSNERLFF	TGTGCCAGCAGTGATGGGGGGTCCAACGAAAGATTATTTTTC	TRBV13-1 CASSDGGSNERLFF TRBJ1-4	TRBV13-1 TRBJ1-4	228
TRBV13-3	TRBJ1-2	CASSDHANSDYTF	TGTGCCAGCAGTGACCATGCAAACTCCGACTACACCTTC	TRBV13-3 CASSDHANSDYTF TRBJ1-2	TRBV13-3 TRBJ1-2	37
TRBV13-1	TRBJ2-7	CASSDRDWVYEQYF	TGTGCCAGCAGTGACCGGGACTGGGTCTATGAACAGTACTTC	TRBV13-1 CASSDRDWVYEQYF TRBJ2-7	TRBV13-1 TRBJ2-7	186
TRBV13-1	TRBJ2-4	CASSDRTGGFSQNTLYF	TGTGCCAGCAGTGATCGTACAGGGGGCTTCAGTCAAAACACCTTGTACTTT	TRBV13-1 CASSDRTGGFSQNTLYF TRBJ2-4	TRBV13-1 TRBJ2-4	1474
TRBV13-1	TRBJ2-1	CASSDWGNYAEQFF	TGTGCCAGCAGCGACTGGGGGAACTATGCTGAGCAGTTCTTC	TRBV13-1 CASSDWGNYAEQFF TRBJ2-1	TRBV13-1 TRBJ2-1	8
TRBV13-1	TRBJ2-1	CASSDWGNYAEQFF	TGTGCCAGCAGTGACTGGGGGAACTATGCTGAGCAGTTCTTC	TRBV13-1 CASSDWGNYAEQFF TRBJ2-1	TRBV13-1 TRBJ2-1	128
TRBV13-1	TRBJ2-5	CASSELWGGQDTQYF	TGTGCCAGCAGTGAACTCTGGGGGGGCCAAGACACCCAGTACTTT	TRBV13-1 CASSELWGGQDTQYF TRBJ2-5	TRBV13-1 TRBJ2-5	346
TRBV13-1	TRBJ2-7	CASSEPEYEQYF	TGTGCCAGCAGTGAACCAGAATATGAACAGTACTTC	TRBV13-1 CASSEPEYEQYF TRBJ2-7	TRBV13-1 TRBJ2-7	130
TRBV12-1	TRBJ2-7	CASSFRDISYEQYF	TGTGCCAGCTCTTTCCGGGACATCTCCTATGAACAGTACTTC	TRBV12-1 CASSFRDISYEQYF TRBJ2-7	TRBV12-1 TRBJ2-7	124
TRBV12-1	TRBJ2-7	CASSFRDSSYEQYF	TGTGCCAGCTCTTTCCGGGACAGCTCCTATGAACAGTACTTC	TRBV12-1 CASSFRDSSYEQYF TRBJ2-7	TRBV12-1 TRBJ2-7	38
TRBV14	TRBJ2-7	CASSFRGPYEQYF	TGTGCCAGCAGTTTCAGGGGTCCCTATGAACAGTACTTC	TRBV14 CASSFRGPYEQYF TRBJ2-7	TRBV14 TRBJ2-7	62
TRBV14	TRBJ2-7	CASSFRVPYEQYF	TGTGCCAGCAGTTTCAGGGTTCCCTATGAACAGTACTTC	TRBV14 CASSFRVPYEQYF TRBJ2-7	TRBV14 TRBJ2-7	288
TRBV12-1	TRBJ2-4	CASSGDRDKNTLYC	TGTGCCAGCTCTGGCGACAGGGACAAAAACACCTTGTACTGT	TRBV12-1 CASSGDRDKNTLYC TRBJ2-4	TRBV12-1 TRBJ2-4	2
TRBV12-1	TRBJ2-4	CASSGDRDQNTLYF	TGTGCCAGCTCTGGCGACAGGGACCAAAACACCTTGTACTTT	TRBV12-1 CASSGDRDQNTLYF TRBJ2-4	TRBV12-1 TRBJ2-4	326
TRBV13-3	TRBJ1-2	CASSGTRNSDYPF	TGTGCCAGCAGTGGAACCAGAAACTCCGACTACCCCTTC	TRBV13-3 CASSGTRNSDYPF TRBJ1-2	TRBV13-3 TRBJ1-2	12
TRBV13-3	TRBJ1-2	CASSGTRNSDYTF	TGTGCCAGCAGTGGAACCAGAAACTCCGACTACACCTTC	TRBV13-3 CASSGTRNSDYTF TRBJ1-2	TRBV13-3 TRBJ1-2	288
TRBV12-1	TRBJ2-3	CASSGTTSAETLYF	TGTGCCAGCTCCGGGACAACTAGTGCAGAAACGCTGTATTTT	TRBV12-1 CASSGTTSAETLYF TRBJ2-3	TRBV12-1 TRBJ2-3	2
TRBV19	TRBJ2-3	CASSIGGTSSAETLYF	TGTGCCAGCAGTATAGGGGGGACCTCTAGTGCAGAAACGCTGTATTTT	TRBV19 CASSIGGTSSAETLYF TRBJ2-3	TRBV19 TRBJ2-3	532
TRBV19	TRBJ2-3	CASSIGGTSSAETLYF	TGTGCCAGCAGTATAGGGGGGGACCTCTAGTGCAGAAACGCTGTATTTT	TRBV19 CASSIGGTSSAETLYF TRBJ2-3	TRBV19 TRBJ2-3	1
TRBV17	TRBJ2-7	CASSIGTGAYEQYF	TGTGCTAGCAGTATAGGGACAGGGGCCTATGAACAGTACTTC	TRBV17 CASSIGTGAYEQYF TRBJ2-7	TRBV17 TRBJ2-7	228
TRBV12-2	TRBJ2-5	CASSLDKDTQYF	TGTGCCAGCTCTCTCGACAAAGACACCCAGTACTTT	TRBV12-2 CASSLDKDTQYF TRBJ2-5	TRBV12-2 TRBJ2-5	14
TRBV12-2	TRBJ2-5	CASSLDKDTQYF	TGTGCCAGCTCTCTCGACAAAGACACCCAGTACTTT	TRBV12-2 CASSLDKDTQYF TRBJ2-5	TRBV12-2 TRBJ2-5	2
TRBV12-2	TRBJ2-3	CASSLDSSAETLYF	TGTGCCAGCTCTCTCGACTCTAGTGCAGAAACGCTGTATTTT	TRBV12-2 CASSLDSSAETLYF TRBJ2-3	TRBV12-2 TRBJ2-3	386
TRBV16	TRBJ2-4	CASSLERGASQNTLYF	TGTGCAAGCAGCTTAGAAAGGGGAGCTAGTCAAAACACCTTGTACTTT	TRBV16 CASSLERGASQNTLYF TRBJ2-4	TRBV16 TRBJ2-4	454
TRBV16	TRBJ2-4	CASSLETGGARQNTLYF	TGTGCAAGCAGCTTAGAAACTGGGGGGGCGCGTCAAAACACCTTGTACTTT	TRBV16 CASSLETGGARQNTLYF TRBJ2-4	TRBV16 TRBJ2-4	114
TRBV16	TRBJ2-5	CASSLGGQDTQYF	TGTGCAAGCAGCTTGGGGGGCCAAGACACCCAGTACTTT	TRBV16 CASSLGGQDTQYF TRBJ2-5	TRBV16 TRBJ2-5	33
TRBV16	TRBJ2-5	CASSLGGQDTQYF	TGTGCAAGCAGCTTGGGGGGACAAGACACCCAGTACTTT	TRBV16 CASSLGGQDTQYF TRBJ2-5	TRBV16 TRBJ2-5	7
TRBV16	TRBJ2-5	CASSLGGQDTQYF	TGTGCAAGCAGCTTAGGGGGACAAGACACCCAGTACTTT	TRBV16 CASSLGGQDTQYF TRBJ2-5	TRBV16 TRBJ2-5	260
TRBV26	TRBJ1-1	CASSLGQINTEVFF	TGTGCCAGCAGTCTGGGACAAATCAACACAGAAGTCTTCTTT	TRBV26 CASSLGQINTEVFF TRBJ1-1	TRBV26 TRBJ1-1	434
TRBV26	TRBJ1-1	CASSLGQSNTEVFF	TGTGCCAGCAGTCTGGGACAATCAAACACAGAAGTCTTCTTT	TRBV26 CASSLGQSNTEVFF TRBJ1-1	TRBV26 TRBJ1-1	4
TRBV26	TRBJ1-1	CASSLGQSNTEVFF	TGTGCCAGCAGTCTGGGACAAAGCAACACAGAAGTCTTCTTT	TRBV26 CASSLGQSNTEVFF TRBJ1-1	TRBV26 TRBJ1-1	28
TRBV12-2	TRBJ2-5	CASSLMGNQDTQYF	TGTGCCAGCTCTCTCATGGGGAACCAAGACACCCAGTACTTT	TRBV12-2 CASSLMGNQDTQYF TRBJ2-5	TRBV12-2 TRBJ2-5	9
TRBV12-2	TRBJ2-5	CASSLMGNQDTQYF	TGTGCCAGCTCTCTCATGGGGAACCAAGACACCCAGTACTTT	TRBV12-2 CASSLMGNQDTQYF TRBJ2-5	TRBV12-2 TRBJ2-5	2
TRBV29	TRBJ1-4	CASSLSSSNERLFF	TGTGCTAGCAGTTTAAGTAGTTCCAACGAAAGATTATTTTTC	TRBV29 CASSLSSSNERLFF TRBJ1-4	TRBV29 TRBJ1-4	370
TRBV19	TRBJ1-3	CASSMEETSSGNTLYF	TGTGCCAGCAGTATGGAGGAGACATCTTCTGGAAATACGCTCTATTTT	TRBV19 CASSMEETSSGNTLYF TRBJ1-3	TRBV19 TRBJ1-3	2
TRBV19	TRBJ1-1	CASSNRENTEVFF	TGTGCCAGCAGCAACAGGGAAAACACAGAAGTCTTCTTT	TRBV19 CASSNRENTEVFF TRBJ1-1	TRBV19 TRBJ1-1	25
TRBV19	TRBJ1-1	CASSNRENTEVFF	TGTGCCAGCAGCAACAGGGAAAACACAGAAGTCTTCTTT	TRBV19 CASSNRENTEVFF TRBJ1-1	TRBV19 TRBJ1-1	2
TRBV14	TRBJ2-1	CASSPDRGYAEQFF	TGTGCCAGCAGCCCAGACAGGGGGTATGCTGAGCAGTTCTTC	TRBV14 CASSPDRGYAEQFF TRBJ2-1	TRBV14 TRBJ2-1	18
TRBV14	TRBJ2-1	CASSPDRGYAEQFF	TGTGCCAGCAGCCCAGACAGGGGGTATGCTGAGCAGTTCTTC	TRBV14 CASSPDRGYAEQFF TRBJ2-1	TRBV14 TRBJ2-1	2
TRBV21	TRBJ2-4	CASSPGQGASQNTLYF	TGTGCTAGCAGTCCGGGACAGGGGGCCAGTCAAAACACCTTGTACTTT	TRBV21 CASSPGQGASQNTLYF TRBJ2-4	TRBV21 TRBJ2-4	165
TRBV29	TRBJ2-7	CASSPGTGGYEQYF	TGTGCTAGCAGTCCCGGGACAGGGGGCTATGAACAGTACTTC	TRBV29 CASSPGTGGYEQYF TRBJ2-7	TRBV29 TRBJ2-7	566
TRBV29	TRBJ2-5	CASSPGTGNQDTQYF	TGTGCTAGCAGCCCCGGGACAGGGAACCAAGACACCCAGTACTTT	TRBV29 CASSPGTGNQDTQYF TRBJ2-5	TRBV29 TRBJ2-5	47
TRBV29	TRBJ2-5	CASSPGTGNQDTQYF	TGTGCTAGCAGCCCCGGGACAGGGAACCAAGACACCCAGTACTTT	TRBV29 CASSPGTGNQDTQYF TRBJ2-5	TRBV29 TRBJ2-5	2
TRBV29	TRBJ2-3	CASSPGTNSAETLYF	TGTGCTAGCAGCCCCGGGACAAATAGTGCAGAAACGCTGTATTTT	TRBV29 CASSPGTNSAETLYF TRBJ2-3	TRBV29 TRBJ2-3	262
TRBV4	TRBJ1-1	CASSPQDTEVFF	TGTGCCAGCAGCCCCCAGGACACAGAAGTCTTCTTT	TRBV4 CASSPQDTEVFF TRBJ1-1	TRBV4 TRBJ1-1	28
TRBV4	TRBJ1-1	CASSPQDTEVFF	TGTGCCAGCAGCCCCCAGGACACAGAAGTCTTCTTT	TRBV4 CASSPQDTEVFF TRBJ1-1	TRBV4 TRBJ1-1	2
TRBV2	TRBJ2-7	CASSQDLGGRWEQYF	TGTGCCAGCAGCCAAGACCTGGGGGGGCGCTGGGAACAGTACTTC	TRBV2 CASSQDLGGRWEQYF TRBJ2-7	TRBV2 TRBJ2-7	658
TRBV5	TRBJ2-4	CASSQENGGSQNTLYF	TGTGCCAGCAGCCAAGAGAATGGGGGTAGTCAAAACACCTTGTACTTT	TRBV5 CASSQENGGSQNTLYF TRBJ2-4	TRBV5 TRBJ2-4	762
TRBV5	TRBJ1-3	CASSQRDRGSGNTLYF	TGTGCCAGCAGCCAACGGGACAGGGGATCTGGAAATACGCTCTATTTT	TRBV5 CASSQRDRGSGNTLYF TRBJ1-3	TRBV5 TRBJ1-3	59
TRBV5	TRBJ1-3	CASSQRDRGSGNTLYF	TGTGCCAGCAGCCAACGGGACAGGGGATCTGGAAATACGCTCTATTTT	TRBV5 CASSQRDRGSGNTLYF TRBJ1-3	TRBV5 TRBJ1-3	2
TRBV5	TRBJ2-4	CASSQVLGSQNTLYF	TGTGCCAGCAGCCAAGTGCTGGGGAGTCAAAACACCTTGTACTTT	TRBV5 CASSQVLGSQNTLYF TRBJ2-4	TRBV5 TRBJ2-4	282
TRBV17	TRBJ2-7	CASSRDRSYEQYF	TGTGCTAGCAGTAGGGACAGATCCTATGAACAGTACTTC	TRBV17 CASSRDRSYEQYF TRBJ2-7	TRBV17 TRBJ2-7	4
TRBV17	TRBJ2-7	CASSRDRSYEQYF	TGTGCTAGCAGTAGGGACAGGTCCTATGAACAGTACTTC	TRBV17 CASSRDRSYEQYF TRBJ2-7	TRBV17 TRBJ2-7	28
TRBV17	TRBJ2-7	CASSRGGEQYF	TGTGCTAGCAGTAGGGGGGGTGAACAGTACTTC	TRBV17 CASSRGGEQYF TRBJ2-7	TRBV17 TRBJ2-7	130
TRBV12-1	TRBJ2-4	CASSRGLGGRQNTLYF	TGTGCCAGCTCTCGCGGACTGGGGGGGCGGCAAAACACCTTGTACTTT	TRBV12-1 CASSRGLGGRQNTLYF TRBJ2-4	TRBV12-1 TRBJ2-4	162
TRBV12-1	TRBJ1-4	CASSRPNERLFF	TGTGCCAGCTCTCGCCCAAACGAAAGATTATTTTTC	TRBV12-1 CASSRPNERLFF TRBJ1-4	TRBV12-1 TRBJ1-4	572
TRBV15	TRBJ2-4	CASSRRESQNTLYF	TGTGCCAGCAGCCGCCGGGAGAGTCAAAACACCTTGTACTTT	TRBV15 CASSRRESQNTLYF TRBJ2-4	TRBV15 TRBJ2-4	138
TRBV15	TRBJ2-4	CASSRRESQNTLYF	TGTGCCAGCAGCCGCCGGGAGAGTCAAAACACCTTGTACTTT	TRBV15 CASSRRESQNTLYF TRBJ2-4	TRBV15 TRBJ2-4	2
TRBV19	TRBJ2-4	CASSRTGGQNTLYF	TGTGCCAGCAGTAGGACTGGGGGTCAAAACACCTTGTACTTT	TRBV19 CASSRTGGQNTLYF TRBJ2-4	TRBV19 TRBJ2-4	136
TRBV17	TRBJ2-4	CASSSGGGQNTLYF	TGTGCTAGCAGTTCCGGCGGGGGTCAAAACACCTTGTACTTT	TRBV17 CASSSGGGQNTLYF TRBJ2-4	TRBV17 TRBJ2-4	312
TRBV29	TRBJ1-6	CASSSGGNSPLYF	TGTGCTAGCAGTTCAGGGGGAAATTCGCCCCTCTACTTT	TRBV29 CASSSGGNSPLYF TRBJ1-6	TRBV29 TRBJ1-6	9
TRBV29	TRBJ1-6	CASSSGGNSPLYF	TGTGCTAGCAGTTCAGGGGGGAATTCGCCCCTCTACTTT	TRBV29 CASSSGGNSPLYF TRBJ1-6	TRBV29 TRBJ1-6	616
TRBV29	TRBJ1-6	CASSSGGNSTLYF	TGTGCTAGCAGTTCAGGGGGGAATTCGACCCTCTACTTT	TRBV29 CASSSGGNSTLYF TRBJ1-6	TRBV29 TRBJ1-6	58
TRBV19	TRBJ1-4	CASSSGQGSERLFF	TGTGCCAGCAGTTCGGGACAGGGAAGCGAAAGATTATTTTTC	TRBV19 CASSSGQGSERLFF TRBJ1-4	TRBV19 TRBJ1-4	24
TRBV12-1	TRBJ1-2	CASSSGTGGSDYTF	TGTGCCAGCTCTTCCGGGACAGGGGGGTCCGACTACACCTTC	TRBV12-1 CASSSGTGGSDYTF TRBJ1-2	TRBV12-1 TRBJ1-2	312
TRBV17	TRBJ2-4	CASSTGLGQNTLYF	TGTGCTAGCAGTACAGGGTTAGGTCAAAACACCTTGTACTTT	TRBV17 CASSTGLGQNTLYF TRBJ2-4	TRBV17 TRBJ2-4	412
TRBV19	TRBJ1-3	CASSWDSSGNTLYF	TGTGCCAGCAGTTGGGACAGCTCTGGAAATACGCTCTATTTT	TRBV19 CASSWDSSGNTLYF TRBJ1-3	TRBV19 TRBJ1-3	7788
TRBV31	TRBJ1-1	CAWSLRGANTEVFF	TGTGCCTGGAGTCTAAGGGGTGCAAACACAGAAGTCTTCTTT	TRBV31 CAWSLRGANTEVFF TRBJ1-1	TRBV31 TRBJ1-1	1
TRBV31	TRBJ1-1	CAWSLRGANTEVFF	TGTGCCTGGAGTCTAAGGGGTGCAAACACAGAAGTCTTCTTT	TRBV31 CAWSLRGANTEVFF TRBJ1-1	TRBV31 TRBJ1-1	432
TRBV1	TRBJ2-7	CTCSADRAGGYEQYF	TGCACCTGCAGTGCAGATAGGGCAGGGGGCTATGAACAGTACTTC	TRBV1 CTCSADRAGGYEQYF TRBJ2-7	TRBV1 TRBJ2-7	200
TRBV29	TRBJ2-7	CVSSPGTGGYGQYF	TGTGTTAGCAGTCCCGGGACAGGGGGCTATGGACAGTACTTC	TRBV29 CVSSPGTGGYGQYF TRBJ2-7	TRBV29 TRBJ2-7	2
TRBV19	TRBJ1-3	GDSSWESSGNTRYF	GGGGACAGCAGTTGGGAAAGCTCTGGAAATACGCGATATTTT	TRBV19 GDSSWESSGNTRYF TRBJ1-3	TRBV19 TRBJ1-3	2
TRBV21	TRBJ2-1	YAEQFF	TATGCTGAGCAGTTCTTC	TRBV21 YAEQFF TRBJ2-1	TRBV21 TRBJ2-1	366

Table S6. List of TMP epitopes selected in silico to bind HLA-A2 with high affinity (<50nM)

Peptide	Start	Stop	HLA	Sequence	Affinity(nM)
1	357	365	HLA-A0201	AMIEFIQGL	4.88
2	1462	1470	HLA-A0201	KMVEILEEI	7.8
3	1397	1405	HLA-A0201	RLLKYDVGV	11.55
4	765	773	HLA-A0201	TLVGVTFAI	16.94
5	1374	1382	HLA-A0201	AMQNLVAAV	17.32
6	793	801	HLA-A0201	AIMAIANGV	20.56
7	862	870	HLA-A0201	AMSMNMEEV	24.83
8	504	512	HLA-A0201	KVFGKMTSV	26.84
9	1130	1138	HLA-A0201	LLGIYQSYV	29.4
10	631	639	HLA-A0201	KLAKFASVV	29.89
11	1176	1184	HLA-A0201	KLWANMSKA	30.99
12	692	700	HLA-A0201	MLSNPITAI	32.68
13	700	708	HLA-A0201	ILVAITTTI	36.32
14	491	499	HLA-A0201	KMAALAASA	46.27
15	691	699	HLA-A0201	AMLSNPITA	49.58
16	473	481	HLA-A0201	NMAEAFASA	49.85

Table S7. Patient characteristics. Description corresponding to Figure 4E-F

Stage IIIC/IV NSCLC	**Cohort (CHUM)**	**Cohort (CGFL)**	**Cohort (validation)**
Numbers (n)	44	62	51
Age (mean, range)	65 (45-81)	65,5 (46-85)	65 (42-83)
Gender (n)			
Male	20 (45.5%)	48 (77.4%)	25 (49%)
Female	24 (54.5%)	14 (22.6%)	26 (51%)
Smokers (n)			
Yes	41 (93.2%)	54 (87.1%)	41 (80.4%)
No	3 (6.8%)	6 (9.7%)	10 (19.6%)
NA		2 (3.2%)	0 (0%)
Histology (n)			
Adenocarcinoma	32 (72.7%)	30 (48,.4%)	47 (92.2%)
Squamous cell carcinoma	8 (18.2%)	31 5(50%)	4 (7.8%)
Other	4 (9.1%)	1 (1.6%)	0 (0%)
Immunotherapy (n)			
Pembrolizumab	23 (52.3%)	0 (0%)	20 (39.2%)
Nivolumab	21 (47.7%)	62 (100%)	28 (55%)
Atezolizumab	0 (0%)	0 (0%)	3 (5.8%)
Line of therapy (n)			
1L	7 (15.9%)	0 (0%)	8 (15.7%)
2L	36 (81.8%)	62 (100%)	43 (84.3%)
NA	1 (2.3%)	0 (0%)	0 (0%)
PDL-1 status (n)			
>50%	20 (45.5%)	16 (25.8%)	14 (27.5%)
<50%	11 (25%)	33 (53.2%)	37 (72.5%)
NA	13 (29.5%)	13 (21%)	0 (0%)

Table S8. Peptide sequences

Peptide_Name	Peptide_Sequence
MART-1_A2_26-35_WT	EAAGIGILIV
MART-1_A2_26-35_Mut	ELAGIGILIV
MART-1_A2_26-35_B1	EAAGIGILAT
MART-1_A2_26-35_B2	EAAGIGFLTA
MART-1_A2_26-35_B3	FLAGIGILTV
MART-1_A2_26-35_B4	ILAGSGILTV
MART-1_A2_26-35_B5	LLAGIGILTV
MELOE-1_A2_36-44_WT	TLNDECWPA
MELOE-1_A2_36-44_B1	DLNDECSPA
MELOE-1_A2_36-44_B2	TLNDECDPT
MELOE-1_A2_36-44_B3	TLNDECINA
MELOE-1_A2_36-44_B4	TLNDEEWAA
MELOE-1_A2_36-44_B5	TLNDEEWKA
MELOE-1_A2_36-44_B6	TLNDEGYPA
MELOE-1_A2_36-44_B7	TLNDELLPA
MELOE-1_A2_36-44_B8	TLNDENWNA
MELOE-1_A2_36-44_B9	TLNDPRWPA
MELOE-1_A2_36-44_B10	TLPDECNPA
MELOE-1_A2_36-44_B11	TLTDEYWPA

Table S9. CDR3 alpha and beta sequences of MART-1-specific T-cell clones

MART-1-specific T-cell clones					
T-cell clone	TRBV	CDR3beta	TRAV	CDR3alpha	origin[1]
10C10	4-3	CASSPGTLSDTQYFG	12-2	CAVNLEGNNRLAFG	Patient PBMC
12A8	20-1	CSARD**GLG**ELFFG[2]	12-2	CAVNFDQTGANNLFFG	
24B7	4-2	CASSQDRGGAETQYFG	12-2	CAASQGFQKLVFG	
Cl12	19	CASRWGYLSNQPQHFG	35	CAGLGAQKLVFG	
10F8	20-1	CSARD**GLG**ELFFG	12-2	CAVNLEGNNRLAFG	
8A7	5-5	CASSSGEGLDTQYFG	12-2	CAVKAIYFG	HV PBMC
HA1	25-1	CASSEPYKETQYFG	12-2	CAVGTGTYKYIFG	
M77-84	6-1	CASSEEVAWGRAETQYFG	39	CAVDIVPTNDYKLSFG	TIL
M77-80	28	CASTSALLAGGEQYFG	29	CAASVNARLMFG	
M199.75	28	CASSLQ**GLG**TEAFFG	12-2	CALNQAGTALIFG	
M180.51	28	CASSFE**GLG**TEAFFG	19	CALSDNTNAGKSTFG	

[1] MART-1 specific T-cell clones were obtained either from PBMC of melanoma patients or healthy volunteers, after a step of peptide stimulation, followed by HLA-p/multimer sorting and cloning by limiting dilution, or directly from TIL spontaneously enriched in Melan-A specific T lymphocytes (Godet et al., Eur J Immunol. 2010).

[2] In bold are indicated recurrent motifs already described in the CDR3β of MART-1-specific T-cell clones (Simon et al, Front Immunol., 2018).

Table S10. CDR3 alpha and beta sequences of MELOE-1-specific T-cell clones

MELOE-1-specific T-cell clones					
T-cell clone	TRBV	CDR3beta	TRAV	CDR3alpha	origin[1]
P2.70	10-3	CAISESWGRDTEAFFG	19	CALSEAKYNQGGKLIFG	Patient PBMC
P2.45	14	CASSQPSRDRKDNEQFFG	19	**CALSGP**LLGTSYGKLTFG[2]	
P3.26	3-1	CASSQGSGTSGRRDNEQFFG	19	**CALSGP**ISGGGADGLTFG	
Cl1	10-3	CAIARTANYGYTFG	24	CAFIQGNNDMRFG	
Cl37	14	CASSQERDRGRTNEQFFG	19	**CALSGP**ILTGGGNKLTFG	
E4H	11-1	CASSVQVSGANVLTFG	17	CASRGTPLVFG	HV PBMC
DS1.33	7-2	CASSSGLAGTRNYEQYFG	19	CALRGPMDTGRRALTFG	
DS2.25	20-1	CSATSLAGIDYGYTFG	19	**CALSGP**FSGGYNKLIFG	
M170.48	3-1	CASSHKWKREPTDTQYFG	19	**CALSGP**FSDGQKLLFA	TIL
M117.35	19	CASSISEPARRDNEQFFG	19	CALRGPILTGGGNKLTFG	

[1] MELOE-1 specific T-cell clones were obtained either from PBMC of melanoma patients or healthy volunteers, after a step of peptide stimulation, followed by HLA-p/multimer sorting and cloning by limiting dilution, or directly from TIL spontaneously enriched in MELOE-1 specific T lymphocytes (Godet et al., Eur J Immunol. 2010).

[2] In bold are indicated recurrent motifs already described in the CDR3α of MELOE-1 specific –T-cell clones (Simon et al, Front Immunol., 2018).

In red are indicated T cell clones cross-reactive against at least one bacterial peptide.

Statistical Report

"Cross-reactivity between MHC class I-restricted antigens from cancer cells and an enterococcal bacteriophage"

(All tests are non-parametric, due to the absence of Gaussian distribution assumption)

---- Figure 1 ----

Fig.1B

Table Analyzed	Fig 1B

Kruskal-Wallis test

P value	0,0023
Exact or approximate P value?	Approximate
P value summary	**
Do the medians vary signif. (P < 0.05)	Yes
Number of groups	5
Kruskal-Wallis statistic	16,62

Table Analyzed	**Fig 1B**
Column B	CTX + 13144
vs.	vs,
Column A	CTX
Mann Whitney test	
P value	0,0030
Exact or approximate P value?	Exact
P value summary	**
Significantly different? (P < 0.05)	Yes
One- or two-tailed P value?	Two-tailed
Sum of ranks in column A,B	302,0 , 163,0
Mann-Whitney U	43,00
Difference between medians	
Median of column A	140,0
Median of column B	72,00
Difference: Actual	-68,00
Difference: Hodges-Lehmann	-64,25

Table Analyzed	**Fig 1B**
Column E	CTX + IGR11
vs.	vs,
Column A	CTX
Mann Whitney test	
P value	0,0202
Exact or approximate P value?	Exact
P value summary	*
Significantly different? (P < 0.05)	Yes
One- or two-tailed P value?	Two-tailed
Sum of ranks in column A,E	288,0 , 177,0
Mann-Whitney U	57,00
Difference between medians	
Median of column A	140,0
Median of column E	88,00
Difference: Actual	-52,00
Difference: Hodges-Lehmann	-52,00

Table Analyzed	**Fig 1B**
Column C	CTX + 13344
vs.	vs,
Column A	CTX
Mann Whitney test	
P value	0,1698
Exact or approximate P value?	Exact
P value summary	ns
Significantly different? (P < 0.05)	No
One- or two-tailed P value?	Two-tailed

Sum of ranks in column A,C	266,0 , 199,0
Mann-Whitney U	79,00
Difference between medians	
Median of column A	140,0
Median of column C	110,5
Difference: Actual	-29,50
Difference: Hodges-Lehmann	-26,00

Table Analyzed	**Fig 1B**
Column D	CTX + ATCC9790
vs.	vs,
Column A	CTX
Mann Whitney test	
P value	0,1512
Exact or approximate P value?	Exact
P value summary	ns
Significantly different? (P < 0.05)	No
One- or two-tailed P value?	Two-tailed
Sum of ranks in column A,D	267,5 , 197,5
Mann-Whitney U	77,50
Difference between medians	
Median of column A	140,0
Median of column D	115,0
Difference: Actual	-25,00
Difference: Hodges-Lehmann	-30,00

Table Analyzed	**Fig 1B**
Column D	CTX + ATCC9790
vs.	vs,
Column B	CTX + 13144
Mann Whitney test	
P value	0,0055
Exact or approximate P value?	Exact
P value summary	**
Significantly different? (P < 0.05)	Yes
One- or two-tailed P value?	Two-tailed
Sum of ranks in column B,D	167,0 , 298,0
Mann-Whitney U	47,00
Difference between medians	
Median of column B	72,00
Median of column D	115,0
Difference: Actual	43,00
Difference: Hodges-Lehmann	36,00

Table Analyzed	**Fig 1B**
Column C	CTX + 13344
vs.	vs,
Column B	CTX + 13144
Mann Whitney test	
P value	0,0063
Exact or approximate P value?	Exact
P value summary	**
Significantly different? (P < 0.05)	Yes
One- or two-tailed P value?	Two-tailed
Sum of ranks in column B,C	168,0 , 297,0
Mann-Whitney U	48,00
Difference between medians	
Median of column B	72,00
Median of column C	110,5
Difference: Actual	38,50
Difference: Hodges-Lehmann	39,00

Table Analyzed	**Fig 1B**
Column E	CTX + IGR11
vs.	vs,
Column D	CTX + ATCC9790
Mann Whitney test	

P value	0,0992
Exact or approximate P value?	Exact
P value summary	ns
Significantly different? (P < 0.05)	No
One- or two-tailed P value?	Two-tailed
Sum of ranks in column D,E	272,5 , 192,5
Mann-Whitney U	72,50
Difference between medians	
Median of column D	115,0
Median of column E	88,00
Difference: Actual	-27,00
Difference: Hodges-Lehmann	-23,00

Table Analyzed	**Fig 1B**
Column E	CTX + IGR11
vs.	vs,
Column C	CTX + 13344
Mann Whitney test	
P value	0,0179
Exact or approximate P value?	Exact
P value summary	*
Significantly different? (P < 0.05)	Yes
One- or two-tailed P value?	Two-tailed
Sum of ranks in column C,E	289,0 , 176,0
Mann-Whitney U	56,00
Difference between medians	
Median of column C	110,5
Median of column E	88,00
Difference: Actual	-22,50
Difference: Hodges-Lehmann	-22,50

Fig.1D

Table Analyzed	**Fig 1D - CTX**		
Kruskal-Wallis test			
P value	0,1836		
Exact or approximate P value?	Gaussian Approximation		
P value summary	ns		
Do the medians vary signif. (P < 0.05)	No		
Number of groups	5		
Kruskal-Wallis statistic	6,216		
Dunn's Multiple Comparison Test	Difference in rank sum	Significant? P < 0.05?	Summary
No peptide vs TMP1	-22,02	No	ns
No peptide vs TMP2	-11,30	No	ns
No peptide vs TMP3	-19,74	No	ns
No peptide vs Hypothetical protein	-13,89	No	ns
TMP1 vs TMP2	10,72	No	ns
TMP1 vs TMP3	2,283	No	ns
TMP1 vs Hypothetical protein	8,130	No	ns
TMP2 vs TMP3	-8,435	No	ns
TMP2 vs Hypothetical protein	-2,587	No	ns
TMP3 vs Hypothetical protein	5,848	No	ns

Table Analyzed	**Fig 1D – CTX + Eh13144**		
Kruskal-Wallis test			
P value	0,0028		
Exact or approximate P value?	Gaussian Approximation		
P value summary	**		
Do the medians vary signif. (P < 0.05)	Yes		
Number of groups	5		
Kruskal-Wallis statistic	16,17		
Dunn's Multiple Comparison Test	Difference in rank sum	Significant? P < 0.05?	Summary
No peptide vs TMP1	-31,42	Yes	**
No peptide vs TMP2	-22,03	No	ns

No peptide vs TMP3	-11,11	No	ns
No peptide vs Hypothetical protein	-7,667	No	ns
TMP1 vs TMP2	9,389	No	ns
TMP1 vs TMP3	20,31	No	ns
TMP1 vs Hypothetical protein	23,75	No	ns
TMP2 vs TMP3	10,92	No	ns
TMP2 vs Hypothetical protein	14,36	No	ns
TMP3 vs Hypothetical protein	3,444	No	ns

Table Analyzed	**Fig 1D – CTX + Eh IGR11**		
Kruskal-Wallis test			
P value	0,0131		
Exact or approximate P value?	Gaussian Approximation		
P value summary	*		
Do the medians vary signif. (P < 0.05)	Yes		
Number of groups	5		
Kruskal-Wallis statistic	12,66		
Dunn's Multiple Comparison Test	Difference in rank sum	Significant? P < 0.05?	Summary
No peptide vs TMP1	-20,90	Yes	*
No peptide vs TMP2	-18,00	No	ns
No peptide vs TMP3	-9,200	No	ns
No peptide vs Hypothetical protein	-11,40	No	ns
TMP1 vs TMP2	2,900	No	ns
TMP1 vs TMP3	11,70	No	ns
TMP1 vs Hypothetical protein	9,500	No	ns
TMP2 vs TMP3	8,800	No	ns
TMP2 vs Hypothetical protein	6,600	No	ns
TMP3 vs Hypothetical protein	-2,200	No	ns

Table Analyzed	**Fig 1D – CTX + ATCC9790**		
Kruskal-Wallis test			
P value	0,0711		
Exact or approximate P value?	Gaussian Approximation		
P value summary	ns		
Do the medians vary signif. (P < 0.05)	No		
Number of groups	5		
Kruskal-Wallis statistic	8,627		
Dunn's Multiple Comparison Test	Difference in rank sum	Significant? P < 0.05?	Summary
No peptide vs TMP1	-14,60	No	ns
No peptide vs TMP2	-12,45	No	ns
No peptide vs TMP3	-2,850	No	ns
No peptide vs Hypothetical protein	-1,350	No	ns
TMP1 vs TMP2	2,150	No	ns
TMP1 vs TMP3	11,75	No	ns
TMP1 vs Hypothetical protein	13,25	No	ns
TMP2 vs TMP3	9,600	No	ns
TMP2 vs Hypothetical protein	11,10	No	ns
TMP3 vs Hypothetical protein	1,500	No	ns

Table Analyzed	**Fig 1D – CTX + Eh13344**		
Kruskal-Wallis test			
P value	0,0149		
Exact or approximate P value?	Gaussian Approximation		
P value summary	*		
Do the medians vary signif. (P < 0.05)	Yes		
Number of groups	5		
Kruskal-Wallis statistic	12,36		
Dunn's Multiple Comparison Test	Difference in rank sum	Significant? P < 0.05?	Summary
No peptide vs TMP1	-14,40	No	ns
No peptide vs TMP2	-7,300	No	ns
No peptide vs TMP3	0,3000	No	ns
No peptide vs Hypothetical protein	6,650	No	ns
TMP1 vs TMP2	7,100	No	ns

TMP1 vs TMP3	14,70	No	ns
TMP1 vs Hypothetical protein	21,05	Yes	*
TMP2 vs TMP3	7,600	No	ns
TMP2 vs Hypothetical protein	13,95	No	ns
TMP3 vs Hypothetical protein	6,350	No	ns

Table Analyzed	**Fig 1D – CTX + Eh708**		
Kruskal-Wallis test			
P value	0,1359		
Exact or approximate P value?	Gaussian Approximation		
P value summary	ns		
Do the medians vary signif. (P < 0.05)	No		
Number of groups	5		
Kruskal-Wallis statistic	6,999		
Dunn's Multiple Comparison Test	Difference in rank sum	Significant? P < 0.05?	Summary
No peptide vs TMP1	-19,43	No	ns
No peptide vs TMP2	-8,200	No	ns
No peptide vs TMP3	-3,700	No	ns
No peptide vs Hypothetical protein	-4,833	No	ns
TMP1 vs TMP2	11,23	No	ns
TMP1 vs TMP3	15,73	No	ns
TMP1 vs Hypothetical protein	14,60	No	ns
TMP2 vs TMP3	4,500	No	ns
TMP2 vs Hypothetical protein	3,367	No	ns
TMP3 vs Hypothetical protein	-1,133	No	ns

Fig.1E

Table Analyzed	**Fig 1E**		
Kruskal-Wallis test			
P value	P<0.0001		
Exact or approximate P value?	Gaussian Approximation		
P value summary	***		
Do the medians vary signif. (P < 0.05)	Yes		
Number of groups	6		
Kruskal-Wallis statistic	50,89		
Dunn's Multiple Comparison Test	Difference in rank sum	Significant? P < 0.05?	Summary
Ctrl vs CTX	-9.000	No	ns
Ctrl vs 13144	-51.54	Yes	***
Ctrl vs CTX+13344	-15.58	No	ns
Ctrl vs CTX+ATCC9790	-3.985	No	ns
Ctrl vs CTX+IGR11	-45.88	Yes	**
CTX vs 13144	-42.54	Yes	***
CTX vs CTX+13344	-6.585	No	ns
CTX vs CTX+ATCC9790	5.015	No	ns
CTX vs CTX+IGR11	-36.88	Yes	*
13144 vs CTX+13344	35.95	Yes	*
13144 vs CTX+ATCC9790	47.55	Yes	***
13144 vs CTX+IGR11	5.654	No	ns
CTX+13344 vs CTX+ATCC9790	11.60	No	ns
CTX+13344 vs CTX+IGR11	-30.30	No	ns
CTX+ATCC9790 vs CTX+IGR11	-41.90	Yes	*

---- Figure 2 ----

Fig.2B

Longitudinal analysis

	F test (KR)	F test (S)	LR test	Wald test
Time x Treat	5.73 (d.f.=5/95.9), p<0.0001	5.73 (d.f.=5/96.2), p<0.0001	26.63 (d.f.=5), p<<0.0001	28.63 (d.f.=5), p<<0.0001
Time	195.36 (d.f.=1/101.0), p<<0.0001	195.36 (d.f.=1/101.2), p<<0.0001	109.86 (d.f.=1), p<<0.0001	195.36 (d.f.=1), p<<0.0001
Treat	9.89 (d.f.=5/95.8), p<<0.0001	10.10 (d.f.=5/95.3), p<<0.0001	38.51 (d.f.=5), p<<0.0001	50.48 (d.f.=5), p<<0.0001

Selected pairwise comparisons

P-value adjustement: **no**

Largest	Smallest	Contrast	Df	Pvalue	PvalueAdj
PBS	BMDC	1.628 [-0.587;3.844]	96.48	0.1478	0.1478
PBS	Gr1pulsedBMDC	2.523 [0.142;4.903]	96.06	0.0380	0.0380
PBS	TMPpulsedBMDC	4.508 [2.452;6.564]	96.20	<0.0001	<0.0001
PBS	13144pulsedBMDC	4.044 [1.713;6.376]	96.07	0.0009	0.0009
TMP1-mut3pulsedBMDC	PBS	0.377 [-2.378;3.131]	95.95	0.7866	0.7866
BMDC	Gr1pulsedBMDC	0.894 [-1.586;3.375]	95.92	0.4759	0.4759
BMDC	TMPpulsedBMDC	2.880 [0.709;5.050]	96.01	0.0099	0.0099
BMDC	13144pulsedBMDC	2.416 [-0.018;4.849]	95.93	0.0516	0.0516
TMP1-mut3pulsedBMDC	BMDC	2.005 [-0.836;4.846]	95.86	0.1645	0.1645
Gr1pulsedBMDC	TMPpulsedBMDC	1.985 [-0.354;4.324]	95.64	0.0953	0.0953
Gr1pulsedBMDC	13144pulsedBMDC	1.522 [-1.063;4.106]	95.64	0.2454	0.2454
TMP1-mut3pulsedBMDC	Gr1pulsedBMDC	2.899 [-0.072;5.871]	95.64	0.0557	0.0557
13144pulsedBMDC	TMPpulsedBMDC	0.464 [-1.826;2.753]	95.64	0.6885	0.6885
TMP1-mut3pulsedBMDC	TMPpulsedBMDC	4.885 [2.166;7.603]	95.64	0.0006	0.0006
TMP1-mut3pulsedBMDC	13144pulsedBMDC	4.421 [1.488;7.353]	95.64	0.0035	0.0035

Fig.2C

Table Analyzed	**Fig 2C**		
Kruskal-Wallis test			
P value	0,0002		
Exact or approximate P value?	Gaussian Approximation		
P value summary	***		
Do the medians vary signif. (P < 0.05)	Yes		
Number of groups	6		
Kruskal-Wallis statistic	23,96		
Dunn's Multiple Comparison Test	Difference in rank sum	Significant? P < 0.05?	Summary
PBS vs BMDC	4,875	No	ns
PBS vs Gr1 pulsed BMDC	18,49	No	ns
PBS vs TMP pulsed BMDC	25,84	Yes	*
PBS vs 13144 pulsed BMDC	30,21	Yes	*
PBS vs TMPmut pulsed BMDC	-3,347	No	ns
BMDC vs Gr1 pulsed BMDC	13,61	No	ns
BMDC vs TMP pulsed BMDC	20,96	No	ns
BMDC vs 13144 pulsed BMDC	25,33	No	ns
BMDC vs TMPmut pulsed BMDC	-8,222	No	ns
Gr1 pulsed BMDC vs TMP pulsed BMDC	7,354	No	ns
Gr1 pulsed BMDC vs 13144 pulsed BMDC	11,72	No	ns
Gr1 pulsed BMDC vs TMPmut pulsed BMDC	-21,83	No	ns
TMP pulsed BMDC vs 13144 pulsed BMDC	4,368	No	ns
TMP pulsed BMDC vs TMPmut pulsed BMDC	-29,19	Yes	*
13144 pulsed BMDC vs TMPmut pulsed BMDC	-33,56	Yes	*

Fig.2D

Table Analyzed	Fig 2D		
Kruskal-Wallis test			
P value	0,0003		
Exact or approximate P value?	Gaussian Approximation		
P value summary	***		
Do the medians vary signif. (P < 0.05)	Yes		
Number of groups	6		
Kruskal-Wallis statistic	23,57		
Dunn's Multiple Comparison Test	Difference in rank sum	Significant? P < 0.05?	Summary
CTX-spect vs CTX+13144	27,10	Yes	**
CTX-spect vs CTX+E.coli TMP-	10,20	No	ns
CTX-spect vs CTX+E.coli TMP+	23,43	Yes	*
CTX-spect vs CTX+E.coli TMPmut2	-0,6667	No	ns
CTX-spect vs CTX+E.coli TMPmut3	-4,667	No	ns
CTX+13144 vs CTX+E.coli TMP-	-16,90	No	ns
CTX+13144 vs CTX+E.coli TMP+	-3,667	No	ns
CTX+13144 vs CTX+E.coli TMPmut2	-27,77	No	ns
CTX+13144 vs CTX+E.coli TMPmut3	-31,77	Yes	*
CTX+E.coli TMP- vs CTX+E.coli TMP+	13,23	No	ns
CTX+E.coli TMP- vs CTX+E.coli TMPmut2	-10,87	No	ns
CTX+E.coli TMP- vs CTX+E.coli TMPmut3	-14,87	No	ns
CTX+E.coli TMP+ vs CTX+E.coli TMPmut2	-24,10	No	ns
CTX+E.coli TMP+ vs CTX+E.coli TMPmut3	-28,10	No	ns
CTX+E.coli TMPmut2 vs CTX+E.coli TMPmut3	-4,000	No	ns

Fig.2E

Table Analyzed	Fig 2E		
Kruskal-Wallis test			
P value	0,0003		
Exact or approximate P value?	Gaussian Approximation		
P value summary	***		
Do the medians vary signif. (P < 0.05)	Yes		
Number of groups	6		
Kruskal-Wallis statistic	23,68		
Dunn's Multiple Comparison Test	Difference in rank sum	Significant? P < 0.05?	Summary
CTX-spect vs CTX+13144	-19,60	Yes	*
CTX-spect vs CTX+E.coli TMP-	-8,450	No	ns
CTX-spect vs CTX+E.coli TMP+	-18,85	No	ns
CTX-spect vs CTX+E.coli TMPmut2	8,100	No	ns
CTX-spect vs CTX+E.coli TMPmut3	2,700	No	ns
CTX+13144 vs CTX+E.coli TMP-	11,15	No	ns
CTX+13144 vs CTX+E.coli TMP+	0,7500	No	ns
CTX+13144 vs CTX+E.coli TMPmut2	27,70	Yes	**
CTX+13144 vs CTX+E.coli TMPmut3	22,30	No	ns
CTX+E.coli TMP- vs CTX+E.coli TMP+	-10,40	No	ns
CTX+E.coli TMP- vs CTX+E.coli TMPmut2	16,55	No	ns
CTX+E.coli TMP- vs CTX+E.coli TMPmut3	11,15	No	ns
CTX+E.coli TMP+ vs CTX+E.coli TMPmut2	26,95	Yes	*
CTX+E.coli TMP+ vs CTX+E.coli TMPmut3	21,55	No	ns
CTX+E.coli TMPmut2 vs CTX+E.coli TMPmut3	-5,400	No	ns

---- Figure 3 ----

Fig.3B

Table Analyzed	Fig 3B		
Kruskal-Wallis test			
P value	0,0013		
Exact or approximate P value?	Gaussian Approximation		
P value summary	**		
Do the medians vary signif. (P < 0.05)	Yes		
Number of groups	4		
Kruskal-Wallis statistic	15,68		
Dunn's Multiple Comparison Test	Difference in rank sum	Significant? P < 0,05?	Summary
Ctrl vs MCA205	-8,333	No	ns
Ctrl vs TC1	-12,11	No	ns
Ctrl vs MC38	5,500	No	ns
MCA205 vs TC1	-3,778	No	ns
MCA205 vs MC38	13,83	Yes	*
TC1 vs MC38	17,61	Yes	**

Fig.3C (left panel)

Longitudinal analysis

	F test (KR)	F test (S)	LR test	Wald test
Time x Treat	95.65 (d.f.=2/21.6), p<<0.0001	95.94 (d.f.=2/22.2), p<<0.0001	51.22 (d.f.=2), p<<0.0001	191.88 (d.f.=2), p<<0.0001
Time	22.86 (d.f.=1/17.5), p<0.0002	22.86 (d.f.=1/16.6), p<0.0002	15.41 (d.f.=1), p<<0.0001	22.86 (d.f.=1), p<<0.0001
Treat	93.37 (d.f.=2/14.9), p<<0.0001	94.54 (d.f.=2/13.1), p<<0.0001	48.63 (d.f.=2), p<<0.0001	189.08 (d.f.=2), p<<0.0001

Selected pairwise comparisons

P-value adjustement: **no**

Largest	Smallest	Contrast	Df	Pvalue	PvalueAdj
WTClone1Ctrl	WTClone1CTX	12.073 [9.785;14.360]	22.53	<0.0001	<0.0001
WTClone1Ctrl	WTClone1EH	14.339 [12.052;16.627]	22.53	<0.0001	<0.0001
WTClone1CTX	WTClone1EH	2.266 [0.034;4.499]	20.08	0.0470	0.0470

Fig.3C (middle panel)

Longitudinal analysis

	F test (KR)	F test (S)	LR test	Wald test
Time x Treat	5.54 (d.f.=2/15.0), p<0.0158	5.54 (d.f.=2/15.0), p<0.0157	9.93 (d.f.=2), p<0.0070	11.09 (d.f.=2), p<0.0039
Time	48.61 (d.f.=1/17.0), p<<0.0001	48.62 (d.f.=1/16.9), p<<0.0001	24.24 (d.f.=1), p<<0.0001	48.62 (d.f.=1), p<<0.0001
Treat	9.89 (d.f.=2/14.8), p<0.0019	11.24 (d.f.=2/65.0), p<<0.0001	14.44 (d.f.=2), p<0.0007	22.48 (d.f.=2), p<<0.0001

Selected pairwise comparisons

P-value adjustement: **no**

Largest	Smallest	Contrast	Df	Pvalue	PvalueAdj
Mut2Clone1Ctrl	Mut2Clone1CTX	6.317 [2.194;10.440]	15.06	0.0052	0.0052
Mut2Clone1Ctrl	Mut2Clone1EH	4.265 [0.142;8.388]	15.06	0.0435	0.0435
Mut2Clone1EH	Mut2Clone1CTX	2.052 [-2.062;6.167]	14.89	0.3044	0.3044

Fig.3C (right panel)

Longitudinal analysis

	F test (KR)	F test (S)	LR test	Wald test
Time x Treat	2.77 (d.f.=2/15.0), p<0.0949	2.77 (d.f.=2/14.9), p<0.0952	5.64 (d.f.=2), p<0.0596	5.53 (d.f.=2), p<0.0629
Time	27.10 (d.f.=1/17.0), p<<0.0001	27.10 (d.f.=1/16.8), p<<0.0001	17.11 (d.f.=1), p<<0.0001	27.10 (d.f.=1), p<<0.0001
Treat	4.75 (d.f.=2/15.0), p<0.0252	5.38 (d.f.=2/102.0), p<0.0060	7.42 (d.f.=2), p<0.0245	10.76 (d.f.=2), p<0.0046

Selected pairwise comparisons

P-value adjustement: **no**

Largest	Smallest	Contrast	Df	Pvalue	PvalueAdj
Mut3Clone1Ctrl	Mut3Clone1CTX	4.589 [0.245;8.934]	15.02	0.0398	0.0398
Mut3Clone1Ctrl	Mut3Clone1EH	3.499 [-0.846;7.843]	15.00	0.1066	0.1066
Mut3Clone1EH	Mut3Clone1CTX	1.091 [-3.252;5.434]	14.98	0.6003	0.6003

Fig.3D

Table Analyzed	**Fig 3D – WT Polyclonal**
Column A	CTX
vs	vs
Column B	CTX + 13144
Mann Whitney test	
P value	0,0119
Exact or approximate P value?	Gaussian Approximation
P value summary	*
Are medians signif. different? (P < 0.05)	Yes
One- or two-tailed P value?	Two-tailed
Sum of ranks in column A,B	40 , 15
Mann-Whitney U	0,0000

Table Analyzed	**Fig 3D – WT Clone 1**
Column C	CTX
vs	vs
Column D	CTX + 13144
Mann Whitney test	
P value	0,0247
Exact or approximate P value?	Gaussian Approximation
P value summary	*
Are medians signif. different? (P < 0.05)	Yes
One- or two-tailed P value?	Two-tailed
Sum of ranks in column C,D	53.50 , 24.50
Mann-Whitney U	3,500

Table Analyzed	**Fig 3D – WT Clone 2**
Column E	CTX
vs	vs
Column F	CTX + 13144
Mann Whitney test	
P value	0,0823
Exact or approximate P value?	Exact
P value summary	ns
Are medians signif. different? (P < 0.05)	No
One- or two-tailed P value?	Two-tailed
Sum of ranks in column E,F	46 , 20
Mann-Whitney U	5,000

Table Analyzed	**Fig 3D – mut2 Clone 1**
Column M	CTX
vs	vs
Column N	CTX + 13144
Mann Whitney test	
P value	0,3939

Exact or approximate P value?	Exact
P value summary	ns
Are medians signif. different? (P < 0.05)	No
One- or two-tailed P value?	Two-tailed
Sum of ranks in column M,N	33 , 45
Mann-Whitney U	12,00

Table Analyzed	**Fig 3D – mut2 Clone 2**
Column O	CTX
vs	vs
Column P	CTX + 13144

Mann Whitney test	
P value	0,3095
Exact or approximate P value?	Exact
P value summary	ns
Are medians signif. different? (P < 0.05)	No
One- or two-tailed P value?	Two-tailed
Sum of ranks in column O,P	32 , 46
Mann-Whitney U	11,00

Table Analyzed	**Fig 3D – mut3 Clone 1**
Column G	CTX
vs	vs
Column H	CTX + 13144

Mann Whitney test	
P value	0,6884
Exact or approximate P value?	Gaussian Approximation
P value summary	ns
Are medians signif. different? (P < 0.05)	No
One- or two-tailed P value?	Two-tailed
Sum of ranks in column G,H	36 , 42
Mann-Whitney U	15,00

Table Analyzed	**Fig 3D – mut3 Clone 2**
Column I	CTX
vs	vs
Column J	CTX + 13144

Mann Whitney test	
P value	0,9360
Exact or approximate P value?	Gaussian Approximation
P value summary	ns
Are medians signif. different? (P < 0.05)	No
One- or two-tailed P value?	Two-tailed
Sum of ranks in column I,J	40 , 38
Mann-Whitney U	17,00

Table Analyzed	**Fig 3D – mut3 Clone 3**
Column K	CTX
vs	vs
Column L	CTX + 13144

Mann Whitney test	
P value	0,3358
Exact or approximate P value?	Gaussian Approximation
P value summary	ns
Are medians signif. different? (P < 0.05)	No
One- or two-tailed P value?	Two-tailed
Sum of ranks in column K,L	45.50 , 32.50
Mann-Whitney U	11,50

Fig.3E (left panel)

Longitudinal analysis

	F test (KR)	F test (S)	LR test	Wald test
Time x Treat	6.35 (d.f.=2/26.3), p<0.0056	6.35 (d.f.=2/26.1), p<0.0057	11.50 (d.f.=2), p<0.0032	12.69 (d.f.=2), p<0.0018
Time	80.88 (d.f.=1/28.0), p<<0.0001	80.88 (d.f.=1/27.8), p<<0.0001	39.41 (d.f.=1), p<<0.0001	80.88 (d.f.=1), p<<0.0001
Treat	0.88 (d.f.=2/26.2), p<0.4248	0.95 (d.f.=2/144.3), p<0.3882	1.93 (d.f.=2), p<0.3801	1.91 (d.f.=2), p<0.3858

Selected pairwise comparisons

P-value adjustement: **no**

Largest	Smallest	Contrast	Df	Pvalue	PvalueAdj
TC1WTPBS	TC1WTCTX	2.291 [-1.256;5.838]	26.98	0.1962	0.1962
TC1WTPBS	TC1WT13144	5.866 [2.389;9.344]	27.09	0.0018	0.0018
TC1WTCTX	TC1WT13144	3.575 [0.352;6.799]	25.22	0.0311	0.0311

Fig.3E (middle panel)

Longitudinal analysis

	F test (KR)	F test (S)	LR test	Wald test
Time x Treat	1.54 (d.f.=2/27.9), p<0.2324	1.54 (d.f.=2/28.1), p<0.2322	3.21 (d.f.=2), p<0.2006	3.08 (d.f.=2), p<0.2147
Time	126.95 (d.f.=1/30.0), p<<0.0001	126.99 (d.f.=1/30.1), p<<0.0001	51.38 (d.f.=1), p<<0.0001	126.99 (d.f.=1), p<<0.0001
Treat	0.19 (d.f.=2/27.9), p<0.8319	0.20 (d.f.=2/120.8), p<0.8200	0.34 (d.f.=2), p<0.8449	0.40 (d.f.=2), p<0.8197

Selected pairwise comparisons

P-value adjustement: **no**

Largest	Smallest	Contrast	Df	Pvalue	PvalueAdj
TC1mut3PBS	TC1mut3CTX	0.833 [-1.969;3.635]	28.54	0.5478	0.5478
TC1mut3PBS	TC1mut313144	2.369 [-0.432;5.170]	28.48	0.0942	0.0942
TC1mut3CTX	TC1mut313144	1.536 [-1.294;4.367]	26.83	0.2751	0.2751

Fig.3E (right panel)

Table Analyzed	**Fig 3E right – TC1 WT**
Mann Whitney test	
P value	0,0229
Exact or approximate P value?	Exact
P value summary	*
Significantly different? (P < 0.05)	Yes
One- or two-tailed P value?	Two-tailed
Sum of ranks in column A,B	142,0 , 89,00
Mann-Whitney U	23,00
Difference between medians	
Median of column A	195,0
Median of column B	91,00
Difference: Actual	-104,0
Difference: Hodges-Lehmann	-65,00

Table Analyzed	**Fig 3E right - TC1 mut3**
Mann Whitney test	
P value	0,4467
Exact or approximate P value?	Exact
P value summary	ns
Significantly different? (P < 0.05)	No
One- or two-tailed P value?	Two-tailed
Sum of ranks in column C,D	115,5 , 94,50
Mann-Whitney U	39,50

Difference between medians	
Median of column C	187,5
Median of column D	189,0
Difference: Actual	1,500
Difference: Hodges-Lehmann	-38,50

---- Figure 4 ----

Fig.4A (left panel)

Table Analyzed	**Fig 4A**		
Kruskal-Wallis test			
P value	P<0.0001		
Exact or approximate P value?	Gaussian Approximation		
P value summary	***		
Do the medians vary signif. (P < 0.05)	Yes		
Number of groups	3		
Kruskal-Wallis statistic	23,42		
Dunn's Multiple Comparison Test	Difference in rank sum	Significant? P < 0.05?	Summary
Ctrl vs CTX	-12,12	No	ns
Ctrl vs CTX + 13144	-24,48	Yes	***
CTX vs CTX + 13144	-12,36	Yes	*

Fig.4A (middle panel)

Table Analyzed	**Fig 4A**		
Kruskal-Wallis test			
P value	0,0015		
Exact or approximate P value?	Gaussian Approximation		
P value summary	**		
Do the medians vary signif. (P < 0.05)	Yes		
Number of groups	3		
Kruskal-Wallis statistic	13,02		
Dunn's Multiple Comparison Test	Difference in rank sum	Significant? P < 0.05?	Summary
Ctrl vs CTX	-11,17	No	ns
Ctrl vs CTX + 13144	-18,27	Yes	***
CTX vs CTX + 13144	-7,100	No	ns

Fig.4A (right panel)

Table Analyzed	**Fig 4A**		
Kruskal-Wallis test			
P value	0,0007		
Exact or approximate P value?	Gaussian Approximation		
P value summary	***		
Do the medians vary signif. (P < 0.05)	Yes		
Number of groups	3		
Kruskal-Wallis statistic	14,51		
Dunn's Multiple Comparison Test	Difference in rank sum	Significant? P < 0.05?	Summary
Ctrl vs CTX	-6,652	No	ns
Ctrl vs CTX + 13144	-18,73	Yes	***
CTX vs CTX + 13144	-12,08	Yes	*

Fig.4C

Table Analyzed	**Figure 4F – left panel**
Kruskal-Wallis test	
P value	0,0019
Exact or approximate P value?	Gaussian Approximation
P value summary	**
Do the medians vary signif. (P < 0.05)	Yes
Number of groups	5
Kruskal-Wallis statistic	17,04

Table Analyzed	**Figure 4C**
Column B	TMP1
vs.	vs,
Column D	SIINFEKL
Mann Whitney test	

P value	0,0286
Exact or approximate P value?	Exact
P value summary	*
Significantly different? (P < 0.05)	Yes
One- or two-tailed P value?	Two-tailed
Sum of ranks in column B,D	26,00 , 10,00
Mann-Whitney U	0,0
Difference between medians	
Median of column B	105,5
Median of column D	14,00
Difference: Actual	91,50
Difference: Hodges-Lehmann	90,00

Table Analyzed	**Figure 4C**
Column C	PSMB4
vs.	vs,
Column D	SIINFEKL
Mann Whitney test	
P value	0,0286
Exact or approximate P value?	Exact
P value summary	*
Significantly different? (P < 0.05)	Yes
One- or two-tailed P value?	Two-tailed
Sum of ranks in column C,D	26,00 , 10,00
Mann-Whitney U	0,0
Difference between medians	
Median of column C	35,00
Median of column D	14,00
Difference: Actual	21,00
Difference: Hodges-Lehmann	21,00

Table Analyzed	**Figure 4C**
Column D	SIINFEKL
vs.	vs,
Column E	13144
Mann Whitney test	
P value	0,0286
Exact or approximate P value?	Exact
P value summary	*
Significantly different? (P < 0.05)	Yes
One- or two-tailed P value?	Two-tailed
Sum of ranks in column D,E	10,00 , 26,00
Mann-Whitney U	0,0
Difference between medians	
Median of column D	14,00
Median of column E	38,50
Difference: Actual	-24,50
Difference: Hodges-Lehmann	-24,50

---- Figure S2 ----

Fig.S2A

Table Analyzed	Fig S2A - DC		
Kruskal-Wallis test			
P value	0,0464		
Exact or approximate P value?	Gaussian Approximation		
P value summary	*		
Do the medians vary signif. (P < 0.05)	Yes		
Number of groups	4		
Kruskal-Wallis statistic	7,981		
Dunn's Multiple Comparison Test	Difference in rank sum	Significant? P < 0.05?	Summary
Naïves vs CTX	-8,138	No	ns
Naïves vs CTX + 708	-13,60	No	ns
Naïves vs CTX + 13144	-19,65	Yes	*
CTX vs CTX + 708	-5,462	No	ns
CTX vs CTX + 13144	-11,51	No	ns
CTX + 708 vs CTX + 13144	-6,050	No	ns
Table Analyzed	Fig S2A – DC + Eh13144		
Kruskal-Wallis test			
P value	P<0.0001		
Exact or approximate P value?	Gaussian Approximation		
P value summary	***		
Do the medians vary signif. (P < 0.05)	Yes		
Number of groups	4		
Kruskal-Wallis statistic	34,98		
Dunn's Multiple Comparison Test	Difference in rank sum	Significant? P < 0.05?	Summary
Naïves vs CTX	-6,575	No	ns
Naïves vs CTX + 708	-30,68	Yes	***
Naïves vs CTX + 13144	-36,15	Yes	***
CTX vs CTX + 708	-24,10	Yes	**
CTX vs CTX + 13144	-29,58	Yes	***
CTX + 708 vs CTX + 13144	-5,475	No	ns
Table Analyzed	Fig S2A –DC + Eh708		
Kruskal-Wallis test			
P value	0,0148		
Exact or approximate P value?	Gaussian Approximation		
P value summary	*		
Do the medians vary signif. (P < 0.05)	Yes		
Number of groups	4		
Kruskal-Wallis statistic	10,49		
Dunn's Multiple Comparison Test	Difference in rank sum	Significant? P < 0.05?	Summary
Naïves vs CTX	-2,200	No	ns
Naïves vs CTX + 708	-13,58	No	ns
Naïves vs CTX + 13144	-20,63	Yes	*
CTX vs CTX + 708	-11,38	No	ns
CTX vs CTX + 13144	-18,43	No	ns
CTX + 708 vs CTX + 13144	-7,050	No	ns
Table Analyzed	Fig S2A – DC + Eh13344		
Kruskal-Wallis test			
P value	0,0987		
Exact or approximate P value?	Gaussian Approximation		
P value summary	ns		
Do the medians vary signif. (P < 0.05)	No		
Number of groups	4		
Kruskal-Wallis statistic	6,282		

Dunn's Multiple Comparison Test	Difference in rank sum	Significant? P < 0.05?	Summary
Naïves vs CTX	-10,75	No	ns
Naïves vs CTX + 708	-11,48	No	ns
Naïves vs CTX + 13144	-18,18	No	ns
CTX vs CTX + 708	-0,7250	No	ns
CTX vs CTX + 13144	-7,425	No	ns
CTX + 708 vs CTX + 13144	-6,700	No	ns

Table Analyzed	Fig S2A - DC + L.plant
Kruskal-Wallis test	
P value	0,0443
Exact or approximate P value?	Gaussian Approximation
P value summary	*
Do the medians vary signif. (P < 0.05)	Yes
Number of groups	4
Kruskal-Wallis statistic	8,082

Dunn's Multiple Comparison Test	Difference in rank sum	Significant? P < 0.05?	Summary
Naïves vs CTX	-6,200	No	ns
Naïves vs CTX + 708	13,90	No	ns
Naïves vs CTX + 13144	-0,3000	No	ns
CTX vs CTX + 708	20,10	Yes	*
CTX vs CTX + 13144	5,900	No	ns
CTX + 708 vs CTX + 13144	-14,20	No	ns

Fig.S2C (left panel)

Table Analyzed	**Fig S2C – left panel**
Kruskal-Wallis test	
P value	0,0032
Exact or approximate P value?	Approximate
P value summary	**
Do the medians vary signif. (P < 0.05)	Yes

Dunn's multiple comparisons test	Mean rank diff,	Significant?	Summary
Ctrl vs. CTX	-2,200	No	ns
Ctrl vs. 13144	-12,50	Yes	**
CTX vs. 13144	-10,30	Yes	*

Fig.S2C (right panel)

Table Analyzed	**Fig S2C – D11**
Kruskal-Wallis test	
P value	0,1939
Exact or approximate P value?	Exact
P value summary	ns
Do the medians vary signif. (P < 0.05)	No

Dunn's multiple comparisons test	Mean rank diff,	Significant?	Summary
Column A vs. Column B	-4,600	No	ns
Column A vs. Column C	-0,2000	No	ns
Column B vs. Column C	4,400	No	ns

Table Analyzed	**Fig S2C – D18**
Kruskal-Wallis test	
P value	0,4163
Exact or approximate P value?	Exact
P value summary	ns
Do the medians vary signif. (P < 0.05)	No

Dunn's multiple comparisons test	Mean rank diff,	Significant?	Summary
Column E vs. Column F	-0,6000	No	ns
Column E vs. Column G	-3,600	No	ns
Column F vs. Column G	-3,000	No	ns

Table Analyzed	Fig S2C – D25		
Kruskal-Wallis test			
P value	0,0130		
Exact or approximate P value?	Exact		
P value summary	*		
Do the medians vary signif. (P < 0.05)	Yes		
Dunn's multiple comparisons test	Mean rank diff,	Significant?	Summary
Column I vs. Column J	4,200	No	ns
Column I vs. Column K	-3,600	No	ns
Column J vs. Column K	-7,800	Yes	*

Fig.S2D

Table Analyzed	Fig S2D – D11		
Kruskal-Wallis test			
P value	0,8261		
Exact or approximate P value?	Gaussian Approximation		
P value summary	ns		
Do the medians vary signif. (P < 0.05)	No		
Number of groups	3		
Kruskal-Wallis statistic	0,3820		
Dunn's Multiple Comparison Test	Difference in rank sum	Significant? P < 0.05?	Summary
Ctrl vs CTX	0,2000	No	ns
Ctrl vs 13144	-1,400	No	ns
CTX vs 13144	-1,600	No	ns

Table Analyzed	Fig S2D – D18		
Kruskal-Wallis test			
P value	0,0131		
Exact or approximate P value?	Gaussian Approximation		
P value summary	*		
Do the medians vary signif. (P < 0.05)	Yes		
Number of groups	3		
Kruskal-Wallis statistic	8,676		
Dunn's Multiple Comparison Test	Difference in rank sum	Significant? P < 0.05?	Summary
Ctrl vs CTX	1,700	No	ns
Ctrl vs 13144	-6,200	No	ns
CTX vs 13144	-7,900	Yes	*

Table Analyzed	Fig S2D – D25		
Kruskal-Wallis test			
P value	0,0657		
Exact or approximate P value?	Gaussian Approximation		
P value summary	ns		
Do the medians vary signif. (P < 0.05)	No		
Number of groups	3		
Kruskal-Wallis statistic	5,445		
Dunn's Multiple Comparison Test	Difference in rank sum	Significant? P < 0.05?	Summary
Ctrl vs CTX	0,4000	No	ns
Ctrl vs 13144	-5,500	No	ns
CTX vs 13144	-5,900	No	ns

Fig.S2F

Table Analyzed	Fig S2F – D10
Kruskal-Wallis test	
P value	0,0177
Exact or approximate P value?	Exact
P value summary	*
Do the medians vary signif. (P < 0.05)	Yes

Number of groups	3		
Kruskal-Wallis statistic	7,246		
Dunn's multiple comparisons test	Mean rank diff,	Significant?	Summary
Ctrl vs. CTX	5,200	No	ns
Ctrl vs. CTX+13144	7,400	Yes	*
CTX vs. CTX+13144	2,200	No	ns

Fig.S2G

Table Analyzed	**Fig S2G – D14**
Kruskal-Wallis test	
P value	0,0298
Exact or approximate P value?	Exact
P value summary	*
Do the medians vary signif. (P < 0.05)	Yes
Number of groups	3
Kruskal-Wallis statistic	6,503

Dunn's multiple comparisons test	Mean rank diff,	Significant?	Summary
Ctrl vs. CTX	3,600	No	ns
Ctrl vs. CTX+13144	7,200	Yes	*
CTX vs. CTX+13144	3,600	No	ns

Fig.S2H

Table Analyzed	**Fig S2H – D17**
ANOVA summary	
F	12,86
P value	0,0010
P value summary	**
Are differences among means statistically significant? (P < 0.05)	Yes
R square	0,6819
ANOVA summary	

Dunnett's multiple comparisons test	Mean Diff,	95% CI of diff,	Significant?	Summary
Ctrl vs. CTX+13144	1,740	0,8359 to 2,644	Yes	***
CTX vs. CTX+13144	1,368	0,4639 to 2,272	Yes	**

---- Figure S4 ----

Fig.S4B

Longitudinal analysis

	F test (KR)	F test (S)	LR test	Wald test
Time x Treat	5.18 (d.f.=5/64.0), p<0.0005	5.18 (d.f.=5/64.0), p<0.0005	23.80 (d.f.=5), p<0.0002	25.92 (d.f.=5), p<<0.0001
Time	413.68 (d.f.=1/69.0), p<<0.0001	413.68 (d.f.=1/69.0), p<<0.0001	136.16 (d.f.=1), p<<0.0001	413.68 (d.f.=1), p<<0.0001
Treat	1.67 (d.f.=5/64.0), p<0.1545	1.72 (d.f.=5/64.0), p<0.1421	8.35 (d.f.=5), p<0.1382	8.61 (d.f.=5), p<0.1255

Selected pairwise comparisons

P-value adjustement: **no**

Largest	Smallest	Contrast	Df	Pvalue	PvalueAdj
CTX+S	13144	2.973 [1.302;4.644]	64.01	0.0007	0.0007
CTX+S	E.coli-EGFP	1.220 [-0.451;2.892]	64.01	0.1495	0.1495
CTX+S	E.coli-TMP	2.961 [1.289;4.632]	64.01	0.0008	0.0008
E.coli-TMPmut2	CTX+S	0.373 [-1.990;2.737]	64.00	0.7535	0.7535
E.coli-TMPmut3	CTX+S	0.455 [-1.909;2.818]	64.00	0.7019	0.7019
E.coli-EGFP	13144	1.753 [0.081;3.424]	63.99	0.0401	0.0401
E.coli-TMP	13144	0.012 [-1.659;1.684]	63.99	0.9882	0.9882
E.coli-TMPmut2	13144	3.346 [0.983;5.710]	63.99	0.0062	0.0062
E.coli-TMPmut3	13144	3.428 [1.064;5.791]	63.99	0.0051	0.0051
E.coli-EGFP	E.coli-TMP	1.740 [0.069;3.411]	63.99	0.0415	0.0415
E.coli-TMPmut2	E.coli-EGFP	1.594 [-0.770;3.957]	63.99	0.1827	0.1827
E.coli-TMPmut3	E.coli-EGFP	1.675 [-0.688;4.039]	63.99	0.1616	0.1616
E.coli-TMPmut2	E.coli-TMP	3.334 [0.970;5.697]	63.99	0.0064	0.0064
E.coli-TMPmut3	E.coli-TMP	3.415 [1.052;5.779]	63.99	0.0053	0.0053
E.coli-TMPmut3	E.coli-TMPmut2	0.082 [-2.813;2.976]	63.99	0.9552	0.9552

---- Figure S6 ----

Fig.S6A

Longitudinal analysis

	F test (KR)	F test (S)	LR test	Wald test
Time x Treat	78.75 (d.f.=2/27.1), p<<0.0001	78.99 (d.f.=2/26.8), p<<0.0001	59.80 (d.f.=2), p<<0.0001	157.98 (d.f.=2), p<<0.0001
Time	12.62 (d.f.=1/29.0), p<0.0013	12.62 (d.f.=1/28.2), p<0.0014	10.91 (d.f.=1), p<0.0010	12.62 (d.f.=1), p<0.0004
Treat	20.60 (d.f.=2/27.0), p<<0.0001	22.09 (d.f.=2/27.6), p<<0.0001	6.14 (d.f.=2), p<0.0464	44.19 (d.f.=2), p<<0.0001

Selected pairwise comparisons

P-value adjustement: **no**

Largest	Smallest	Contrast	Df	Pvalue	PvalueAdj
Ctrl	CTX	16.277 [12.721;19.834]	28.52	<0.0001	<0.0001
Ctrl	CTX+13144	20.995 [17.439;24.552]	28.52	<0.0001	<0.0001
CTX	CTX+13144	4.718 [1.277;8.159]	24.84	0.0092	0.0092

Fig.S6B

Longitudinal analysis

	F test (KR)	F test (S)	LR test	Wald test
Time x Treat	11.94 (d.f.=2/25.9), p<0.0002	11.97 (d.f.=2/26.0), p<0.0002	19.34 (d.f.=2), p<<0.0001	23.94 (d.f.=2), p<<0.0001
Time	31.62 (d.f.=1/27.9), p<<0.0001	31.64 (d.f.=1/27.2), p<<0.0001	22.08 (d.f.=1), p<<0.0001	31.64 (d.f.=1), p<<0.0001
Treat	15.25 (d.f.=2/26.0), p<<0.0001	16.42 (d.f.=2/24.4), p<<0.0001	13.97 (d.f.=2), p<0.0009	32.83 (d.f.=2), p<<0.0001

Selected pairwise comparisons

P-value adjustement: **no**

Largest	Smallest	Contrast	Df	Pvalue	PvalueAdj
Ctrl	CTX	6.951 [3.078;10.824]	26.33	0.0010	0.0010
Ctrl	CTX+13144	8.849 [4.976;12.722]	26.33	<0.0001	<0.0001
CTX	CTX+13144	1.898 [-1.814;5.611]	25.19	0.3025	0.3025

Fig.S6C

Longitudinal analysis

	F test (KR)	F test (S)	LR test	Wald test
Time x Treat	54.75 (d.f.=1/46.0), p<<0.0001	54.76 (d.f.=1/44.0), p<<0.0001	37.54 (d.f.=1), p<<0.0001	54.76 (d.f.=1), p<<0.0001
Time	129.98 (d.f.=1/47.0), p<<0.0001	129.99 (d.f.=1/46.1), p<<0.0001	63.50 (d.f.=1), p<<0.0001	129.99 (d.f.=1), p<<0.0001
Treat	0.35 (d.f.=1/44.7), p<0.5588	0.36 (d.f.=1/216.6), p<0.5473	0.15 (d.f.=1), p<0.6999	0.36 (d.f.=1), p<0.5467

Selected pairwise comparisons

P-value adjustement: **no**

Comp to MCA205WT	Contrast	Df	Pvalue	PvalueAdj
MCA205mut2	-7.321 [-9.313;-5.329]	45.98	<0.0001	<0.0001

Fig.S6D

Longitudinal analysis

	F test (KR)	F test (S)	LR test	Wald test
Time x Treat	53.16 (d.f.=1/23.0), p<<0.0001	53.16 (d.f.=1/24.3), p<<0.0001	30.07 (d.f.=1), p<<0.0001	53.16 (d.f.=1), p<<0.0001
Time	43.59 (d.f.=1/24.0), p<<0.0001	43.59 (d.f.=1/24.1), p<<0.0001	25.87 (d.f.=1), p<<0.0001	43.59 (d.f.=1), p<<0.0001
Treat	25.21 (d.f.=1/23.0), p<<0.0001	27.40 (d.f.=1/66.8), p<<0.0001	8.16 (d.f.=1), p<0.0043	27.40 (d.f.=1), p<<0.0001

Selected pairwise comparisons

P-value adjustement: **no**

Comp to TC1WT	Contrast	Df	Pvalue	PvalueAdj
TC1mut2	-10.327 [-13.257;-7.397]	23.00	<0.0001	<0.0001

Fig.S6E

Table Analyzed	**Fig S6E – MCA205 WT**
Mann Whitney test	
P value	0,0065
Exact or approximate P value?	Exact
P value summary	**
Significantly different? (P < 0.05)	Yes
One- or two-tailed P value?	Two-tailed
Sum of ranks in column A,B	55,50 , 22,50
Mann-Whitney U	1,500
Difference between medians	
Median of column A	80,00
Median of column B	54,00
Difference: Actual	-26,00
Difference: Hodges-Lehmann	-26,50

Table Analyzed	**Fig S6E – MCA205 mut3**
Mann Whitney test	
P value	0,9805
Exact or approximate P value?	Exact
P value summary	ns
Significantly different? (P < 0.05)	No
One- or two-tailed P value?	Two-tailed
Sum of ranks in column C,D	39,50 , 38,50
Mann-Whitney U	17,50
Difference between medians	
Median of column C	65,00
Median of column D	58,00
Difference: Actual	-7,000
Difference: Hodges-Lehmann	-2,000

Fig.S6G (upper panel)

Table Analyzed	**Figure 6G – upper panel**
Kruskal-Wallis test	
P value	0,0014
Exact or approximate P value?	Approximate
P value summary	**
Do the medians vary signif. (P < 0.05)	Yes
Number of groups	5
Kruskal-Wallis statistic	17,65
Data summary	
Number of treatments (columns)	5

Number of values (total)	20

Table Analyzed	**Figure 6G – upper panel**
Column G	Ctrl
vs.	vs,
Column H	TMP1
Mann Whitney test	
P value	0,0286
Exact or approximate P value?	Exact
P value summary	*
Significantly different? (P < 0.05)	Yes
One- or two-tailed P value?	Two-tailed
Sum of ranks in column G,H	10,00 , 26,00
Mann-Whitney U	0,0
Difference between medians	
Median of column G	1,000
Median of column H	5,481
Difference: Actual	-4,481
Difference: Hodges-Lehmann	-4,481

Table Analyzed	**Figure 6G – upper panel**
Column G	Ctrl
vs.	vs,
Column I	PSMB4
Mann Whitney test	
P value	0,0286
Exact or approximate P value?	Exact
P value summary	*
Significantly different? (P < 0.05)	Yes
One- or two-tailed P value?	Two-tailed
Sum of ranks in column G,I	10,00 , 26,00
Mann-Whitney U	0,0
Difference between medians	
Median of column G	1,000
Median of column I	1,818
Difference: Actual	-0,8182
Difference: Hodges-Lehmann	-0,8182

Table Analyzed	**Figure 6G – upper panel**
Column G	Ctrl
vs.	vs,
Column K	13144
Mann Whitney test	
P value	0,0286
Exact or approximate P value?	Exact
P value summary	*
Significantly different? (P < 0.05)	Yes
One- or two-tailed P value?	Two-tailed
Sum of ranks in column G,K	10,00 , 26,00
Mann-Whitney U	0,0
Difference between medians	
Median of column G	1,000
Median of column K	2,000
Difference: Actual	-1,000
Difference: Hodges-Lehmann	-1,000

Table Analyzed	**Figure 6G – upper panel**
Column H	TMP1
vs.	vs,
Column J	SIINFEKL
Mann Whitney test	
P value	0,0286
Exact or approximate P value?	Exact
P value summary	*
Significantly different? (P < 0.05)	Yes
One- or two-tailed P value?	Two-tailed
Sum of ranks in column H,J	26,00 , 10,00

Mann-Whitney U	0,0
Difference between medians	
Median of column H	5,481
Median of column J	0,7273
Difference: Actual	4,753
Difference: Hodges-Lehmann	4,675

Table Analyzed	**Figure 6G – upper panel**
Column I	PSMB4
vs.	vs,
Column J	SIINFEKL
Mann Whitney test	
P value	0,0286
Exact or approximate P value?	Exact
P value summary	*
Significantly different? (P < 0.05)	Yes
One- or two-tailed P value?	Two-tailed
Sum of ranks in column I,J	26,00 , 10,00
Mann-Whitney U	0,0
Difference between medians	
Median of column I	1,818
Median of column J	0,7273
Difference: Actual	1,091
Difference: Hodges-Lehmann	1,091

Table Analyzed	**Figure 6G – upper panel**
Column J	SIINFEKL
vs.	vs,
Column K	13144
Mann Whitney test	
P value	0,0286
Exact or approximate P value?	Exact
P value summary	*
Significantly different? (P < 0.05)	Yes
One- or two-tailed P value?	Two-tailed
Sum of ranks in column J,K	10,00 , 26,00
Mann-Whitney U	0,0
Difference between medians	
Median of column J	0,7273
Median of column K	2,000
Difference: Actual	-1,273
Difference: Hodges-Lehmann	-1,273

Fig.S6G (lower panel)

Table Analyzed	**Fig S6G - lower panel**
Kruskal-Wallis test	
P value	0,0005
Exact or approximate P value?	Exact
P value summary	***
Do the medians vary signif. (P < 0.05)	Yes
Number of groups	3
Kruskal-Wallis statistic	9,269
Data summary	
Number of treatments (columns)	3
Number of values (total)	12

Table Analyzed	**Fig S6G - lower panel**
Column B	PSMB4
vs.	vs,
Column A	SIINFEKL
Mann Whitney test	
P value	0,0286
Exact or approximate P value?	Exact
P value summary	*
Significantly different? (P < 0.05)	Yes

One- or two-tailed P value?	Two-tailed
Sum of ranks in column A,B	10,00 , 26,00
Mann-Whitney U	0,0
Difference between medians	
Median of column A	154,0
Median of column B	246,5
Difference: Actual	92,50
Difference: Hodges-Lehmann	104,0

Table Analyzed	**Fig S6G - lower panel**
Column C	TMP1
vs.	vs,
Column A	SIINFEKL
Mann Whitney test	
P value	0,0286
Exact or approximate P value?	Exact
P value summary	*
Significantly different? (P < 0.05)	Yes
One- or two-tailed P value?	Two-tailed
Sum of ranks in column A,C	10,00 , 26,00
Mann-Whitney U	0,0
Difference between medians	
Median of column A	154,0
Median of column C	176,0
Difference: Actual	22,00
Difference: Hodges-Lehmann	23,00

Table Analyzed	**Fig S6G - lower panel**
Column C	TMP1
vs.	vs,
Column B	PSMB4
Mann Whitney test	
P value	0,0571
Exact or approximate P value?	Exact
P value summary	ns
Significantly different? (P < 0.05)	No
One- or two-tailed P value?	Two-tailed
Sum of ranks in column B,C	25,00 , 11,00
Mann-Whitney U	1,000
Difference between medians	
Median of column B	246,5
Median of column C	176,0
Difference: Actual	-70,50
Difference: Hodges-Lehmann	-66,00

---- Figure S11 ----

Fig.S11A

Table Analyzed	Fig S11A – Peptide 1
Column A	No peptide
vs.	vs,
Column G	1
Mann Whitney test	
P value	0,1385
Exact or approximate P value?	Exact
P value summary	ns
Significantly different? (P < 0.05)	No
One- or two-tailed P value?	Two-tailed
Sum of ranks in column A,G	124,0 , 176,0
Mann-Whitney U	46,00
Difference between medians	
Median of column A	5,500
Median of column G	13,50
Difference: Actual	-8,000
Difference: Hodges-Lehmann	-6,000

Table Analyzed	Fig S11A – Peptide 2
Column A	No peptide
vs.	vs,
Column C	2
Mann Whitney test	
P value	0,0294
Exact or approximate P value?	Exact
P value summary	*
Significantly different? (P < 0.05)	Yes
One- or two-tailed P value?	Two-tailed
Sum of ranks in column A,C	112,5 , 187,5
Mann-Whitney U	34,50
Difference between medians	
Median of column A	5,500
Median of column C	15,50
Difference: Actual	-10,00
Difference: Hodges-Lehmann	-8,500

Table Analyzed	Fig S11A – Peptide 3
Column A	No peptide
vs.	vs,
Column D	3
Mann Whitney test	
P value	0,0229
Exact or approximate P value?	Exact
P value summary	*
Significantly different? (P < 0.05)	Yes
One- or two-tailed P value?	Two-tailed
Sum of ranks in column A,D	111,0 , 189,0
Mann-Whitney U	33,00
Difference between medians	
Median of column A	5,500
Median of column D	18,00
Difference: Actual	-12,50
Difference: Hodges-Lehmann	-10,50

Table Analyzed	Fig S11A – Peptide 4
Column A	No peptide
vs.	vs,
Column E	4
Mann Whitney test	
P value	0,1081

Exact or approximate P value?	Exact
P value summary	ns
Significantly different? (P < 0.05)	No
One- or two-tailed P value?	Two-tailed
Sum of ranks in column A,E	122,0 , 178,0
Mann-Whitney U	44,00
Difference between medians	
Median of column A	5,500
Median of column E	9,500
Difference: Actual	-4,000
Difference: Hodges-Lehmann	-4,000

Table Analyzed	**Fig S11A – Peptide 5**
Column A	No peptide
vs.	vs,
Column F	5
Mann Whitney test	
P value	0,2350
Exact or approximate P value?	Exact
P value summary	ns
Significantly different? (P < 0.05)	No
One- or two-tailed P value?	Two-tailed
Sum of ranks in column A,F	129,0 , 171,0
Mann-Whitney U	51,00
Difference between medians	
Median of column A	5,500
Median of column F	10,50
Difference: Actual	-5,000
Difference: Hodges-Lehmann	-4,000

Table Analyzed	**Fig S11A – Peptide 6**
Column A	No peptide
vs.	vs,
Column G	6
Mann Whitney test	
P value	0,1385
Exact or approximate P value?	Exact
P value summary	ns
Significantly different? (P < 0.05)	No
One- or two-tailed P value?	Two-tailed
Sum of ranks in column A,G	124,0 , 176,0
Mann-Whitney U	46,00
Difference between medians	
Median of column A	5,500
Median of column G	13,50
Difference: Actual	-8,000
Difference: Hodges-Lehmann	-6,000

Table Analyzed	**Fig S11A – Peptide 7**
Column A	No peptide
vs.	vs,
Column H	7
Mann Whitney test	
P value	0,2016
Exact or approximate P value?	Exact
P value summary	ns
Significantly different? (P < 0.05)	No
One- or two-tailed P value?	Two-tailed
Sum of ranks in column A,H	127,5 , 172,5
Mann-Whitney U	49,50
Difference between medians	
Median of column A	5,500
Median of column H	10,50
Difference: Actual	-5,000
Difference: Hodges-Lehmann	-4,000

Table Analyzed	Fig S11A – Peptide 8
Column A	No peptide
vs.	vs,
Column I	8
Mann Whitney test	
P value	0,0246
Exact or approximate P value?	Exact
P value summary	*
Significantly different? (P < 0.05)	Yes
One- or two-tailed P value?	Two-tailed
Sum of ranks in column A,I	111,5 , 188,5
Mann-Whitney U	33,50
Difference between medians	
Median of column A	5,500
Median of column I	12,00
Difference: Actual	-6,500
Difference: Hodges-Lehmann	-6,000

Table Analyzed	Fig S11A – Peptide 9
Column A	No peptide
vs.	vs,
Column J	9
Mann Whitney test	
P value	0,0281
Exact or approximate P value?	Exact
P value summary	*
Significantly different? (P < 0.05)	Yes
One- or two-tailed P value?	Two-tailed
Sum of ranks in column A,J	112,0 , 188,0
Mann-Whitney U	34,00
Difference between medians	
Median of column A	5,500
Median of column J	17,50
Difference: Actual	-12,00
Difference: Hodges-Lehmann	-10,50

Table Analyzed	Fig S11A – Peptide 10
Column A	No peptide
vs.	vs,
Column K	10
Mann Whitney test	
P value	0,0270
Exact or approximate P value?	Exact
P value summary	*
Significantly different? (P < 0.05)	Yes
One- or two-tailed P value?	Two-tailed
Sum of ranks in column A,K	112,0 , 188,0
Mann-Whitney U	34,00
Difference between medians	
Median of column A	5,500
Median of column K	17,50
Difference: Actual	-12,00
Difference: Hodges-Lehmann	-9,000

Table Analyzed	Fig S11A – Peptide 11
Column A	No peptide
vs.	vs,
Column L	11
Mann Whitney test	
P value	0,1466
Exact or approximate P value?	Exact
P value summary	ns
Significantly different? (P < 0.05)	No
One- or two-tailed P value?	Two-tailed
Sum of ranks in column A,L	124,5 , 175,5
Mann-Whitney U	46,50

Difference between medians	
Median of column A	5,500
Median of column L	10,50
Difference: Actual	-5,000
Difference: Hodges-Lehmann	-5,000

Table Analyzed	**Fig S11A – Peptide 12**
Column A	No peptide
vs.	vs,
Column M	12
Mann Whitney test	
P value	0,1918
Exact or approximate P value?	Exact
P value summary	ns
Significantly different? (P < 0.05)	No
One- or two-tailed P value?	Two-tailed
Sum of ranks in column A,M	127,0 , 173,0
Mann-Whitney U	49,00
Difference between medians	
Median of column A	5,500
Median of column M	11,50
Difference: Actual	-6,000
Difference: Hodges-Lehmann	-4,000

Table Analyzed	**Fig S11A – Peptide 13**
Column A	No peptide
vs.	vs,
Column N	13
Mann Whitney test	
P value	0,0497
Exact or approximate P value?	Exact
P value summary	*
Significantly different? (P < 0.05)	Yes
One- or two-tailed P value?	Two-tailed
Sum of ranks in column A,N	116,0 , 184,0
Mann-Whitney U	38,00
Difference between medians	
Median of column A	5,500
Median of column N	10,00
Difference: Actual	-4,500
Difference: Hodges-Lehmann	-5,500

Table Analyzed	**Fig S11A – Peptide 14**
Column A	No peptide
vs.	vs,
Column O	14
Mann Whitney test	
P value	0,2123
Exact or approximate P value?	Exact
P value summary	ns
Significantly different? (P < 0.05)	No
One- or two-tailed P value?	Two-tailed
Sum of ranks in column A,O	128,0 , 172,0
Mann-Whitney U	50,00
Difference between medians	
Median of column A	5,500
Median of column O	8,500
Difference: Actual	-3,000
Difference: Hodges-Lehmann	-3,000

Table Analyzed	**Fig S11A – Peptide 15**
Column A	No peptide
vs.	vs,
Column P	15
Mann Whitney test	
P value	0,0909

Exact or approximate P value?	Exact
P value summary	ns
Significantly different? (P < 0.05)	No
One- or two-tailed P value?	Two-tailed
Sum of ranks in column A,P	120,5 , 179,5
Mann-Whitney U	42,50
Difference between medians	
Median of column A	5,500
Median of column P	12,50
Difference: Actual	-7,000
Difference: Hodges-Lehmann	-5,000

Table Analyzed	**Fig S11A – Peptide 16**
Column A	No peptide
vs.	vs,
Column Q	16
Mann Whitney test	
P value	0,2124
Exact or approximate P value?	Exact
P value summary	ns
Significantly different? (P < 0.05)	No
One- or two-tailed P value?	Two-tailed
Sum of ranks in column A,Q	128,0 , 172,0
Mann-Whitney U	50,00
Difference between medians	
Median of column A	5,500
Median of column Q	11,50
Difference: Actual	-6,000
Difference: Hodges-Lehmann	-3,000